Università degli Studi di Salerno
Dipartimento di Chimica e Biologia "A. Zambelli"

Corso di Dottorato di Ricerca in Chimica
XIV CICLO NUOVA SERIE

Tesi di dottorato in:

"Synthesis of calixarene derivatives active towards proteic targets involved in tumor pathologies"

Tutor: **Candidato:**
Prof. Carmine Gaeta   *Stefano Tommasone*
                                   Matr.: 8880700199

Coordinatore:
Prof. Gaetano Guerra

ANNO ACCADEMICO 2014-2015

Index

Chapter 1

Chapter 2

Chapter 3

Chapter 4

Chapter 5

Chapter 1

1.   Introduction on calix[n]arenes

Calix[n]arenes[1]   are   macrocycles   belonging   to   the
[1.1.1.1.]metacyclophane   family,   in   which   *p*-substituted
phenolic units are linked together via methylene bridges. The
calixarene family consists of 17 cyclooligomers, ranging from
the tetramer to the eicosomer.
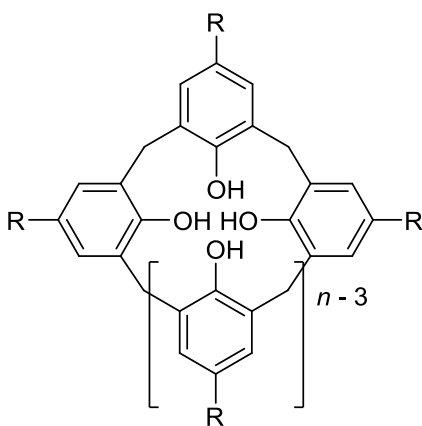

Figure 1.1

[1] (a) Vicens, J.; Harrowfield, J. *Calixarenes in the Nanoworld*, Springer: Dordrecht, **2007**; (b) Gutsche, C. D. *Calixarenes Revisited*, Royal Society of Chemistry: Cambridge, **1998**; (c) Bohmer, V. *The Chemistry of Phenols*, Wiley: Chichester, **2003**; (d) Gutsche, C. D. *Calixarenes, An Introduction*, Royal Society of Chemistry: Cambridge, **2008**.

Regarding the calix[*n*]arene nomenclature, the word "calixarene" was coined by C. David Gutsche, because the *p-t*-butylcalix[4]arene resembled the shape of a Greek vase called *calyx krater* (**Figure 1.2**), while "*n*" between square brackets indicates the number of phenolic components of the macrocycle. (**Figure 1.1**).

calyx krater   *p-t*-butylcalix[4]arene
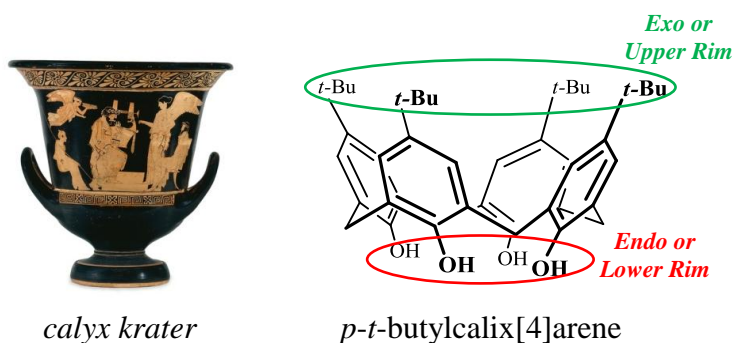
Figure 1.2

The calixarenes can exist in several conformations because the phenolic units freely rotate around the methylene bridge. Regarding the *p-tert*-butylcalix[4]arene, it adopts both in solution and in the solid state the cone conformation, with the four phenolic hydroxyl groups engaged in a cyclic network of hydrogen bonds. In this case it is possible to distinguish two regions, the *Exo or Upper Rim* and the *Endo or Lower Rim* (**Figure 1.2**).

Both the lower and upper rim can be easily functionalized, allowing the introduction of several functional groups such as ethers and esters by alkylation of the hydroxyl groups, and the introduction of halogens, $-NO_2$, $-SO_3H$, $-CHO$ and $-COOH$ by electrophilic substitution.[2]

1.1 Applications in host-guest chemistry

Together with cyclodextrins, cucurbiturils and crown ethers, calixarenes constitute the major classes of supramolecular hosts. They are bowl-shaped macrocycle and their cavity is able to host small molecules or ions. The synthetic versatility of the calixarenes enables them to act as a framework that can support a broad range of binding, signaling or other functionalities. Thus, currently many examples have been reported of calixarene-based hosts for the recognition of cations, anions and neutral molecules with the aim to develop new materials with potential applications as sensors[3] or membranes for the removal of pollutants.[4]

---

[2] (a) Gutsche, C. D.; Pagoria, P. F. *J. Org. Chem*. **1985**, *50*, 5795-5802; (b) Zhang, W. C.; Zheng, Y. A.; Huang, Z. T. *Synthetic Commun*, **1997**, 3763-3767; (c) Smith, W. E. *J. Org. Chem*. **1972**, *37*, 3972-3973. (d) Rieche, A.; Gross, H. *Chem. Ber*. **1960**, *93*, 88-94.

[3] (a) Czarnik, A. W.; Desvergne, J. P. *Chemosensors for Ion and Molecule Recognition.* Kluwer: Dordrecht, **1997**; (b) Beer, P. D.; Gale, P. A. *Angew.Chem. Int. Ed.* **2001**, *40*, 486–516.

[4] (a) Kumar, P. L.; Saxena, C.; Dubey, V. *J. Membr. Sci.* **2003**, *227*, 173–182; (b) Uragami, T.; Meotoiwa, T.; Miyata, T. *Macromolecules* **2003**, *36*, 2041–2048.

Regarding the cationic recognition, an interesting example is the *p*-sulfonatocalix[7]arene, a water soluble compound, that shows good affinity toward some organic quaternary ammonium salts of environmental relevance, such as Diquat and Paraquat.[5] Interestingly, in the solid state the dicationic Diquat guest is encapsulated in a molecular capsule constituted by two molecule of *p*-sulfonatocalix[7]arene (**Figure 1.3**).[6]

*p*-sulfonatocalix[7]arene

Diquat
(herbicide)
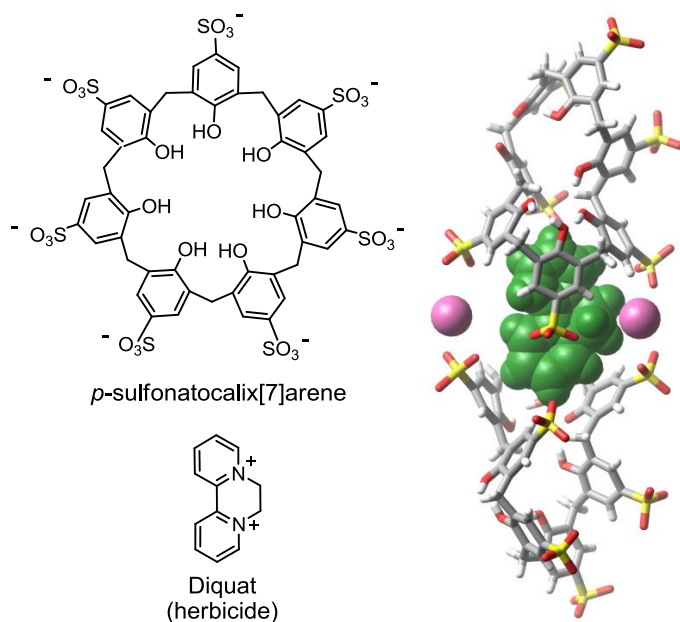
Figure 1.3

[5] Caeta, C.; Caruso, T.; Mincolelli, M.; Troisi, F.; Vasca, E.; Neri, P. *Tetrahedron*, **2008**, *64*, 5370-5378.

[6] Erra, L.; Tedesco, C.; Vaughan, G.; Brunelli, M.; Troisi, F.; Gaeta, C.; Neri, P. *CrystEngComm*, **2010**, *12*, 3463-3466.

The coordination chemistry of anions has gained more interest in the last twenty years. The design of anion receptors is really challenging. Anions are larger then isoelectronic cations, thus electrostatic binding interactions are less effective. Moreover anion species have different geometries, thus a high degree of design is required for the synthesis of suitable complementary receptors for anionic guests. Functional groups like amides, ureas, thioureas and pyrroles are very attractive for this purpose and they have recently been incorporated into macrocycle scaffolds, like calixarenes.[7]

An example is the study of the binding properties toward anionic guest by pyrrolamidocalix[4]arene hosts (**Figure 1.4**).[8]


R = H or NO$_2$
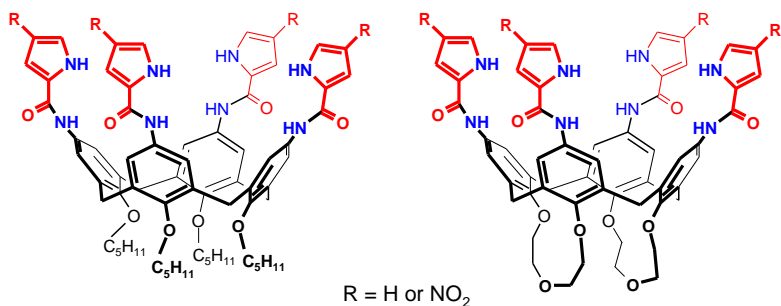
Figure 1.4

[7] Matthews, S. E.; Beer, P. D. *Supramol. Chem.* **2005**, *17*, 411-435.
[8] Troisi, F.; Gaeta, C.; Pierro, T.; Neri, P *Tetrahedron Lett.* **2009**, *50*, 5113-5115.

The derivatives shown in **Figure 1.4** are able to bind anions such as dihydrogen phosphate, fluoride, acetate and benzoate. Particularly, these derivatives are able to discriminate efficiently the $H_2PO_4^-$ anion, with a selectivity more than 38-fold higher than those for the acetate and benzoate anions. This selectivity can be explained by the planar trigonal arrangement of NHs groups of three amidopyrrole units, that are complementary to three H-bonding acceptor sites of $H_2PO_4^-$ anion.

Calixarenes have the characteristic to organize themselves in the solid state through weak interactions. They form supramolecular frameworks with lattice voids that can be occupied by guest molecules.[9] Thus, *p*-H-calix[4]arene (**Figure 1.5a**) is able to form crystal structures in which three calixarene units adopt a cyclic arrangement, with an approximately spherical shape, held together only by van der Walls interactions (**Figure 1.5b**).[10]

[9] Atwood, J. L.; Barbour, L. J.; Jerga, A. *Chem. Comm.* **2001**, *22*, 2376-2377.

[10] Atwood, J. L.; Barbour, L. J.; Jerga, A. *Science* **2002**, *296*, 2367-2369.
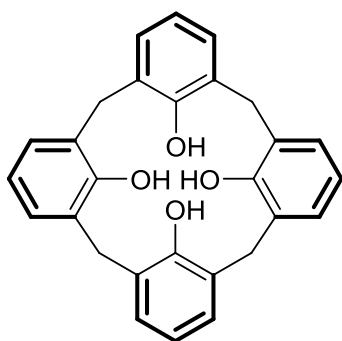
a)

b)
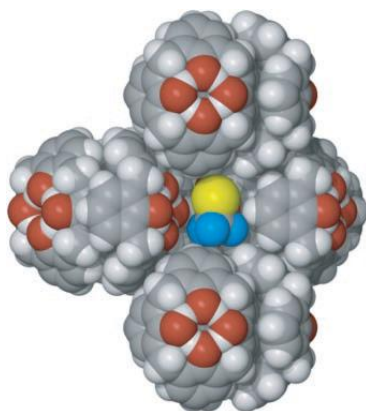
c)

Figure 1.5 a) *p*-H-calix[4]arene; b) trimeric arrangement of *p*-H-calix[4]arene; c) space filling representation of *p*-H-calix[4]arene@CF$_3$Br.

These trimers form a hexagonal close-packed (hcp) lattice with interstitial voids that are occupied by gases such as CCl$_4$,

freons and also methane (**Figure 1.5c**). The gases are retained even at relatively high temperatures and low pressures. Thus, this solid-state self-assembly of calix[4]arenes reported in 2002 by Atwood and coworkers,[9] results in a supramolecular system with potential application in gas storage.

1.2   Biological applications of calix[*n*]arenes

Over the last 30 years a growing interest has been direct toward the biomolecular recognition of calixarene derivatives and more in particular to the interaction with druggable target(s).[11,12] At this regard one of the first report by Cornforth and coworkers in 1955 showed that the *p*-octyl-calix[8]arene bearing polyoxyethylene units at the lower rim was active as anti-tuberculosis agent.[13]

More recently, *p*-sulfonatocalix[*n*]arenes have interesting antiviral activity and they find potential use in the treatment

[11] (a) de Fátima, A.; Fernandes, S. A.; Sabino, A. A. *Curr. Drug. Discov. Technol.* **2009**, *6*, 151-170. (b) Giuliani, M.; Morbioli, I.; Sansone, F.; Casnati, A. *Chem. Commun.* **2015**, *51*, 14140-14159; (c) Park, H. S.; Lin, Q.; Hamilton, A. D. *Proc. Natl. Acad. Sci. USA* **2002**, *99*, 5105-5109; (d) Baldini, L.; Casnati, A.; Sansone, F.; Ungaro, R. *Chem. Soc. Rev.* **2007**, *36*, 254-266; (e) Schrader, T. *Nat. Chem.* **2012**, *4*, 41529-41542.

[12] Da Silva, E.; Lazar, A. N.; Coleman, A. W. *J. Drug. Del. Sci. Tech.* **2004**, *14*, 3-20.

[13] (a) Cornforth, J. W.; D'Arcy Hart, P.; Nicholls, G. A.; Rees, R. J. W.; Stock, J. A. *Brit. J. Pharmacol.* **1955**, *10*, 73-86; (b) D'Arcy Hart, P.; Armstrong, J. A.; Brodaty, E. *Infetc. Immun.* **1996**, *64*, 1491-1493.

of viruses such as AIDS and Herpes.[14,15]

Some of the most fascinating results in the biological activity of calixarenes have been achieved by Hamilton and his co-workers, that described a series of peptidocalix[4]arene derivatives active as antiangiogenic and anticancer agents.[16] In this report Hamilton and coworkers studied a series of protein surface binders constituted by a calix[4]arene backbone adorned to the upper rim with four peptide loops (**Figure 1.6**).

GFB107: $AA_1 = AA_3 = Gly$; $AA_2 = AA_4 = Asp$
GFB111: $AA_1 = AA_3 = Gly$; $AA_2 = Asp$; $AA_4 = Tyr$
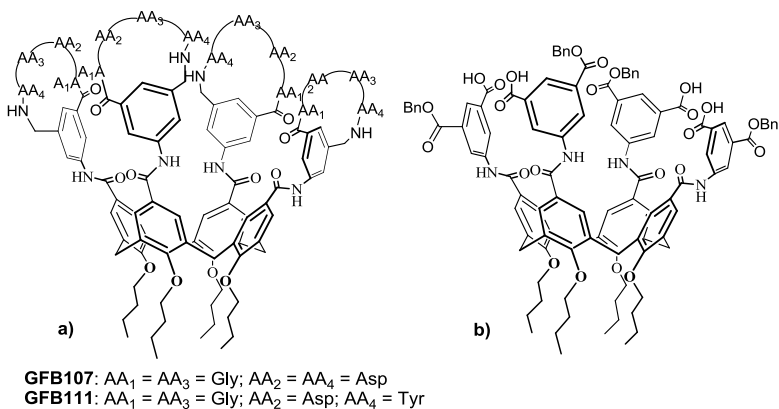
Figure 1.6 growth factor binders functionalized with: a) peptide loops; b) isophthalate groups.

[14] Hwang, K. M.; Qi, Y. M.; Liu, S. Y; Choy, W.; Chen, J.: WO9403164 (**1994**); (b) Harris, S. J.: WO200244141 (**2002**); (c) Coveney, D.; Costello, B.: US2005113454 (**2005**); (d) Wang, K.; Guo, D. S.; Zhang, H. Q.; Li, D.; Zheng, X. L.; Liu, Y. *J. Med. Chem.* **2009**, *52*, 6402-6412

[15] Motornaya, A. E.; Alimbarova, L. M.; Shokova, E. A.; Kovalev, V. V. *Pharm. Chem. J.* **2006**, *40*, 68-72.

[16] (a) Sebti, S. M.; Hamilton, A. D. *Oncogene*, **2000**, *19*, 6566-6573; (b) Blaskovich, M. A.; Lin, Q.; Delarue, F. L.; Sun, J.; Park, H. S.; Coppola, D.; Hamilton, A. D.; Sebti, S. M. *Nat. Biotechnol.* **2000**, *18*, 1065-1070; (c) Zhou, H.; Wang, D.; Baldini, L.; Ennis, E.; Jain, R.; Carie, A.; Sebti, S. M.; Hamilton, A. D. *Org. Biomol. Chem.* **2006**, *4*, 2376-2386.

These compounds were able to bind the surface of the platelet-derived growth factor (PDGF), which is a potent inducer of growth and mobility in a large number of cell types such as endothelium, fibroblasts and smooth muscle.[17] This growth factor plays a central role in cell proliferation, angiogenesis and apoptosis inhibition.[18] PDGF or PDGF receptors are implicated in the development of many malignant diseases such as cancer, and their overexpression is responsible for the uncontrolled cell proliferation and tumor growth.[19]

The growth factor binders (GFBs in **Figure 1.6**) reported by Hamilton are able to disrupt the interactions between PDGF and its cell surface receptor, a tyrosine kinase. Particularly, GFB-111 (**Figure 1.6**) binds the regions of PDGF that are involved in binding to its receptor (IC_{50} = 250 nM). The treatment of nude mice bearing human tumors with GFB-111 resulted in significant inhibition of tumor growth and angiogenesis. Human glioblastoma (U87MG)-implanted in nude mice treated with GFB-111 at 50, 100 and 200 mg/kg per day were subject to a tumor growth inhibition of 56, 81 and 88% respectively after a few weeks (**Figure 1.7**).

[17] Hannink, M.; Donoghue, D. J. *Biochim. Biophys. Acta*, **1989**, *989*, 1-10.
[18] (a) Jones, S. M.; Kazlauskas, A. *FEBS Lett*. **2001**, *490*, 110-116; (b) Heldin, C. H.; Ostman, A.; Ronnstrand, L. *Biochim. Biophys. Acta* **1998**, *1378*, F79-F113.
[19] (a) Seymour, L.; Dajee, D.; Bezwoda, W. R. *Breast Cancer Res. Treat.* **1993**, *26*, 247-252 ; (b) Dunn, I. F.; Heese, O.; Black. P. M. *J. Neuro-Oncol.* **2000**, *50*, 121-137.
.
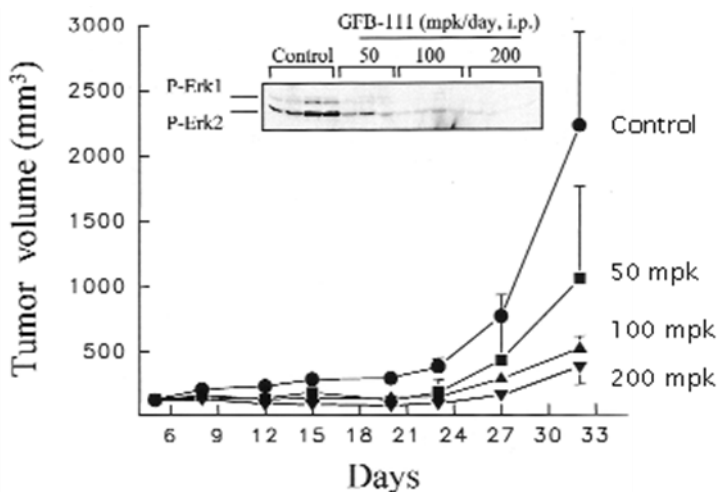
Figure 1.7 Inhibition of tumor growth in nude mice by GFB-111.

However GFB-111 has some limitations due to the difficulty of their synthesis and their low solubility that causes aggregation in water. These drawbacks were overcome with the synthesis of a second generation of GFBs in which the peptide loops at the upper rim of the calix[4]arene were replaced by acyclic isophthalate groups (**Figure 1.6**). With these modifications the molecular weight was significantly reduced without compromising the biological activity ($IC_{50} = 190$ nM).

The derivatives previously reported prevents the binding of PDGF to its receptor and consequently the biological activity of the growth factor (PDGF) is disrupted, resulting in a significant inhibition of the tumor growth. Hence, these

11

results suggest that the disruption of protein-protein interactions can be considered a promising approach for anticancer therapy.

There have been several studies on the biomolecular recognition abilities of calixarenes towards drugguble enzymes, such as α-chimotripsin[20], cholinesterase[21] and alkaline phosphatases[22].

A series of *N*-linked tetrapeptidocalix[4]arenes (**Figure 1.8**) were found to be able to inhibit the activity of transglutaminases.[23] These enzymes catalyze an acyl transfer reaction between the γ-carboxamide group of the protein-bound glutamine residue and the primary amino group of the protein-bound lysine residue or biogenic polyamines.[24]

[20] Park, H. S.; Lin, Q.; Hamilton, A. D. *J. Am. Chem. Soc.* **1999**, *121*, 8-13.

[21] Stoikova, E. E.; Evtugyn, G. A.; Belyakova, S. V.; Khrustalev, A. A.; Stoikov, I. I.; Antipin, I. S.; Budnikov, H. C.; Konovalov, A. I. *J. Inclusion Phenom. Macrocycl. Chem.* **2001**, *39*, 339-346.

[22] Vovk, A. I.; Kalchenko, V. I.; Cherenok, S. A.; Kukhar, V. P.; Muzychka, O. V.; Lozynsky, M. O. *Org. Biomol. Chem.* **2004**, *2*, 3162-3166.

[23] Francese, S.; Cozzolino, A.; Caputo, I.; Esposito, C.; Martino, M.; Gaeta, C.; Troisi, F.; Neri, P. *Tetrahedron Letters* **2005**, *46*, 1611-1615.

[24] Folk, J. E.; Finlayson, J. S. *Adv. Protein Chem.* **1977**, *31*, 1-133.
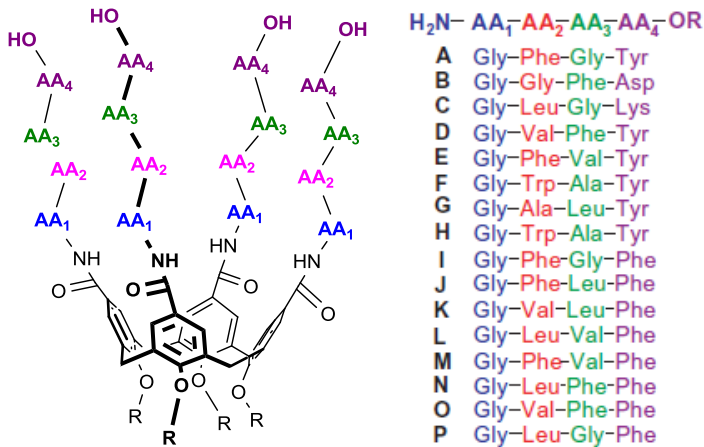
Figure 1.8 Tetrapeptidocalix[4]arenes

When overexpressed, transglutaminases may be involved in a series of pathologies such as celiac disorders and neurological Huntington diseases.[25]

The tetrapeptidocalix[4]arenes showed in vitro inhibition activity against tissue and microbial transglutaminase by means of protein surface recognition on a region noncomprising the enzyme active site.

Hystone deacetylases are enzymes involved in the epigenetic regulation of gene expression as they are responsible for the removal of acetyl groups from lysine residues in hystones. Their dysfunctions or overexpressions are involved in

---

[25] Kim, S. Y.; Jeitner, T. M.; Steinert, P. M. *Neurochem. Int.* **2002**, *40*, 85-103.

13

carcinogenesis and tumor progression.[26] Thus HDAC inhibition could be a promising approach in anticancer therapy.

Alkyl and arylamidocalix[4]arenes were synthesized and tested as hystone deacetylase inhibitors (**Figure 1.9**).[27]
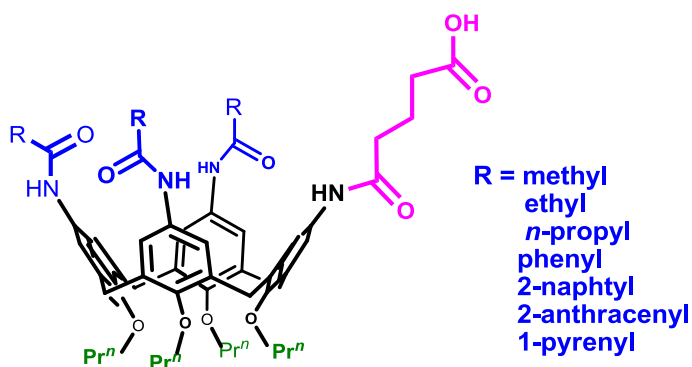
Figure 1.9 Calixarene-based hystone deacetylase inhibitors.

They are in a cone conformation, with three hydrophobic residues at the exo rim as well as a carbon aliphatic chain with a terminal carboxylic acid. Moreover the hydrophobic groups at the exo rim (especially the aromatic ones) can establish hydrophobic interactions with the pockets on the enzyme surface (**Figure 1.10**).

[26] Baylin, S. B.; Ohm, J. E. *Nat. Rev. Cancer* **2006**, *6*, 107-116.

[27] Chini, M. G.; Terracciano, S.; Riccio, R.; Bifulco, G.; Ciao, R.; Gaeta, C.; Troisi, F.; Neri, P. *Org. Lett.* **2010**, *12*, 5382-5385.
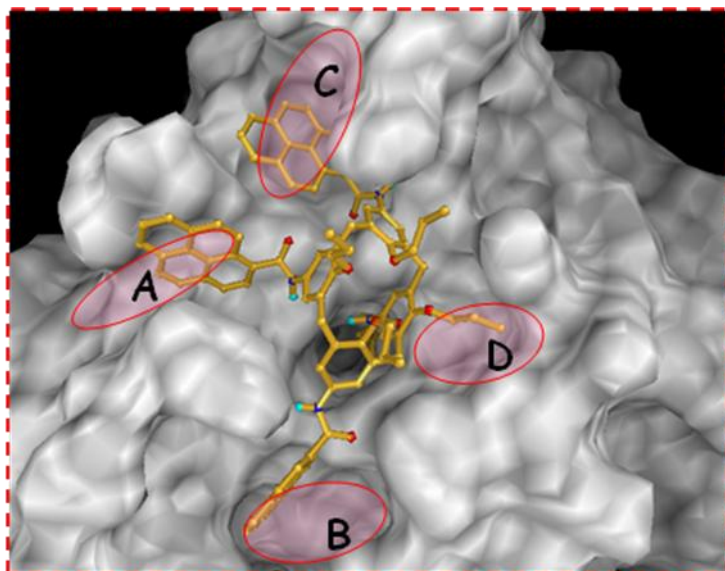
Figure 1.10 3D model of the binding mode of
amidocalixarenes and the enzyme binding site.

The inhibition of HDAC activity was evaluated in vitro.
Particularly the derivative bearing 2-naphtyl residues showed
a high inhibitory activity (IC_{50} = 0.14 µM), a value that is
comparable (only seven-fold higher) to the activity of
Trichostatin A, a well-known HDAC inhibitor (IC_{50} = 0.02
µM).

All the studies reported above show the potential and actual applications of calix[*n*]arenes in the biomolecular recognition. The synthetic and conformational versatility, together with the ability of establishing multiple interactions with biomolecules, make calixarenes a class of compounds suitable for potential applications in the field of biopharmaceutical science.

Chapter 2

2. DNA intercalators in anticancer therapy

DNA-Intercalators[28] are molecules able to interact reversibly with the DNA double helix. Many of them are currently used as drug for the treatment of ovarian and breast cancers.[29] Regarding the structure of the DNA-intercalating agents they show common structural features such as the presence of planar polyaromatic systems[30] (**Figure 2.1**) which intercalate between DNA base-pairs, with a selectivity for 5'-pyrimidine-purine-3' steps.[31]

Currently it is well known that the antitumor activity of the intercalator-based drugs is due to their ability to stabilize the DNA-intercalator-topoisomerase II ternary complex,[32] causing thus the inhibition of cellular DNA-dependent replication and transcription processes.

Nucleic acids interact reversibly with a broad range of chemical species that include, metal ions and their complexes,

[28] Martinez, R.; Chacon-Garcia, L. *Curr. Med. Chem.* **2005**, *12*, 127-151.

[29] Zhang, N.; Yang, Q. *Med. Hypotheses* **2009**, *73*, 1058-1059.

[30] Lown, J. W. *Anthracyclines and Anthracenedienone-Based Anticancer Agents*, Elsevier Science: Amsterdam **1988**.

[31] Neidle, S. *Principles of Nucleic Acid Structure*, Academic Press, Elsevier Inc.: London, **2008**.

[32] Ioanoviciu A., Antony S., Pommier Y., Staker B. L., Stewart L., Cushman M. *J. Med. Chem.* **2005**, *48*, 4803-4814.

small organic molecules and proteins. There are generally three mechanism for DNA interaction: a) binding along the exterior of the helix through non specific and primarily electrostatic interactions;[33] b) specific groove-binding interactions of the bound molecule with the edges of the base-pairs in the major or minor grooves of nucleic acids;[34] c) intercalation of planar or approximately planar aromatic ring systems between the base-pairs.[35]

This last mode of binding is very common for a large number of polycyclic aromatic hydrocarbons (PAHs). Intercalation requires changes in the sugar-phosphate torsional angles in order to accommodate the aromatic compound.[36] The creation of an intercalation site causes the separation of the base-pairs with a lengthening of the double helix and a decrease in the helical twist at the intercalation site (unwinding).

Initially all the spaces between the base-pairs are potential binding sites. However intercalators can bind at alternate base-pairs sites, thus when an intercalator binds at one particular site, the binding of another molecule at the adjacent site is inhibited.

[33] Such, D.; Chaires, J. B. *Bioorg. Med. Chem.* **1995**, *3*, 723-728.

[34] Wilson, W. D. *Nucleic Acids in Chemistry and Biology*, IRL Press: Oxford, **1990**

[35] Braña, M. F.; Cacho, M.; Gradillas, A.; de Pascual-Teresa, B.; Ramos, A. *Current Pharmaceutical Design,* **2001**, *7,* 1745-1780.

[36] Waring, M. J. *Ann. Rev. Biochem.* **1981**, *50*, 159-192.

In the last years many intercalation compounds have been developed, such as doxorubicin, mitoxantrone and camptothecin (**Figure 2.1**).[37]
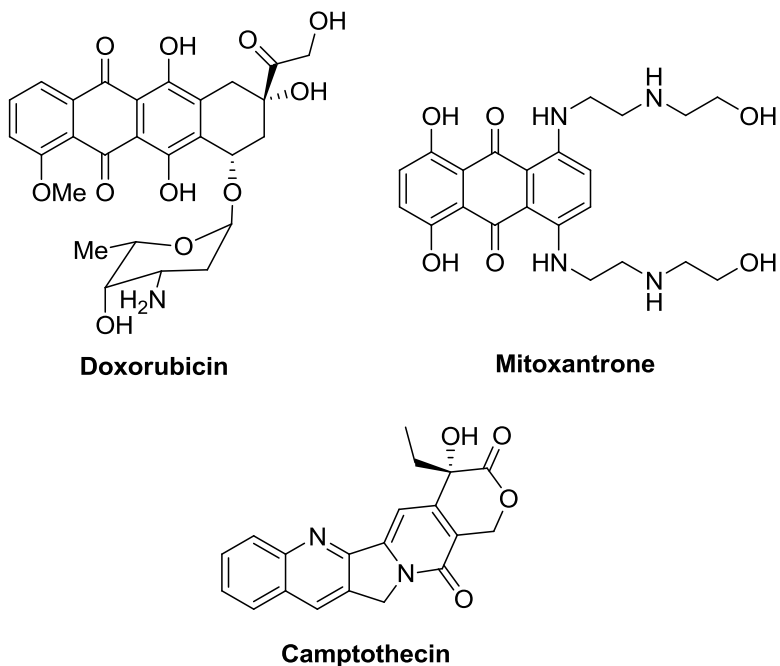

Figure 2.1 Examples of intercalators.

[37] (a) Henry, D. W *Cancer Treat. Rep.***1979**, *63*, 845-854; (b) Hsiang, Y. H.; Liu, L. F.; Wall, M. C.; Nicholas, A. W.; Manikumar, G.; Kirshenbaum, S.; Silber, R.; Potmesil, M. *Cancer Res.*, **1989**, *49*, 4385-4389.

Many classical intercalators such as those described above are inhibitors of *topoisomerase II*.

Topoisomerases are enzymes responsible for the unwinding and overwinding of DNA during the replication and transcription processes.[38] *Topoisomerase II* is highly expressed in rapidly proliferating cells and is therefore an attractive target for antitumor drugs.

The antitumor activity of intercalator agents is closely related to the ability of interacting with the DNA-*topoisomerase II* complex. Upon intercalation with DNA they form a stable ternary complex drug-DNA-*topoisomerase*, preventing the reconnection of the DNA strands.[39] As a consequence the cell replication process is inhibited, causing cell death.

Several studies have focused on bisintercalating compounds,[40] which generally consist of two aromatic units connected together by a linker which can vary in length and rigidity in order to modify the binding affinity or specificity.[35] Bisintercalators show higher DNA binding affinities and slower dissociation rates, as well as a greater potential for sequence selectivity. Several bisintercalators have been

[38] Champoux, J. J. *Annu. Rev. Biochem.* **2001**, *70*, 369-413.

[39] (a) Ross, W. E.; Bradley, M. O. *Biochim. Biophys. Acta*, **1981**, *654*, 129-134; (b) Tewey, K. M.; Rowe, T. C.; Yang, L.; Halligan, B. D.; Liu, L. F. *Science* **1984**, *226*, 466-468.

[40] (a) Braña, M. F.; Castellano, J. M.; Moran, M.; Perez de Vega, M. J.; Romerdahl, C. A.; Qian, X.D.; Bousquet, P. F.; Emling, F.; Schlick, E.; Keilhauer, G. *Anticancer Drug Des.* **1993**, *8*, 257-268; (b) Braña, M. F.; Castellano, J. M.; Moran, M.; Perez de Vega, M. J.; Perron, D.; Conlon, D.; Bousquet, P. F.; Romerdhal, C. A.; Robinson, S. P. *Anticancer Drug Des.* **1996**, *11*, 297-309.

developed as potential anticancer drugs, such as bispnaphtalimides, bisacridinecarboxamides and bisimidazoacridones (**Figure 2.2**).[41]

bispnaphtalimide

bisacridinecarboxamide

bisimidazoacridone
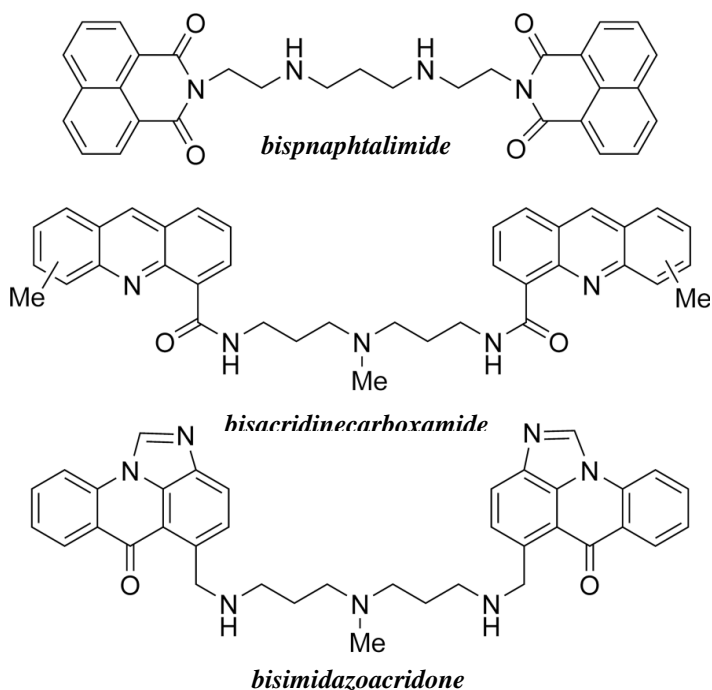
Figure 2.2 Examples of bisintercalators.

[41] (a) Cholody, W. M.; Hernández, L.; Hassner, L.; Scudiero, D. A.; Djurickovic, D. B.; Michejda, C. J. *J. Med. Chem.* **1995**, *38*, 3043-3052; (b) Wakelin, L. P. G. *Med. Res. Rev.* **1986**, *6*, 275-340; (c) Bousquet, P. F.; Braña, M. F.; Conlon, D.; Fitzgerald, K. M.; Perron, D.; Cocchiaro, C.; Miller, R.; Moran, M.; George, J.; Qian, X.-D.; Keilhauer, G.; Romerdahl, C. A. *Cancer Res.* **1995**, *55*, 1176-1180.

Recently Rescifina and his co-workers reported the synthesis of isoxazolidinyl polycyclic aromatic hydrocarbons (isoxazolidinyl-PAH) as potential DNA intercalators.[42] These derivatives have been obtained by 1,3-dipolar cycloaddition between an appropriate nitrone and allyl alcohol.

The cycloaddition reactions were performed by microwave irradiation and gave the desired products in good yields (**Figure 2.3**).


R_1 = methyl, benzyl
R_2 = 1-pyrenyl, 9-phenanthryl, 9-anthryl

y = 39-85%
cis/trans = 1.5-1.1:1.0
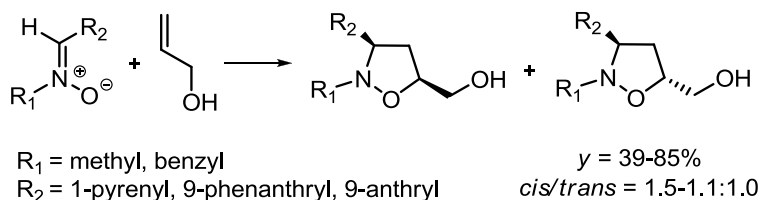
Figure 2.3

The ability of isoxazolidinyl-PAHs to interact with DNA was then investigated. Binding studies have shown that all the derivatives bind to some extent to DNA by intercalation and have IC_{50} values in the low micromolar range (**Table 2.1**).

[42] (a) Rescifina, A.; Zagni, C.; Romeo, G.; Sortino, S. *Bioorg. Med. Chem.* **2012**, *20*, 4978-4984; (b) Rescifina, A.; Chiacchio, U.; Corsaro, A.; Piperno, A.; Romeo, R. *Eur. J. Med. Chem.* **2011**, *46*, 129-136; (c) Rescifina, A.; Chiacchio, M. A.; Corsaro, A.; De Clercq, E.; Iannazzo, D.; Mastino, A.; Piperno, A.; Romeo, G.; Romeo, R.; Valveri, C. *J. Med. Chem.* **2006**, *49*, 709-715.

Cell Line	IC$_{50}$ (μM)			
	R$_1$=Me R$_2$=9-phenant *cis*	R$_1$=Me R$_2$=9-phenant *trans*	R$_1$=Me R$_2$=1-pyr *cis*	R$_1$=Bn R$_2$=1-pyr *cis*
Molt-3 (leukemia)	125	128	112	127
THP-1 (leukemia)	169	148	107	192
U937 (lymphoma)	153	154	111	193

IC$_{50}$ is the concentration of the drug required to cause 50% reduction in absorbance value in comparison with cells exposed to control medium.

Table 2.1 Evaluation of cytotoxicity by MTS Assay.

2.1 Calixarene based DNA intercalators – Results and discussion

The first topic of this PhD thesis has been inspired by the results reported by Rescifina and co-workers. In particular, we have designed and synthesized the calixarene based DNA-intercalators in **Figure 2.4** bearing isoxazolidinyl-polycyclic aromatic hydrocarbon units at the exo rim.

Several calixarene conjugates presenting polycyclic aromatic hydrocarbons (PAH) can be designed. A schematic representation is shown in **Figure 2.4**, in which a

calix[4]arene scaffold presents isoxazolidinyl-PAH units at the exo rim. The nature of the bond between the calixarene and the isoxazolidinyl unit can be of different types, such as an ester, urethane or even a direct bond.
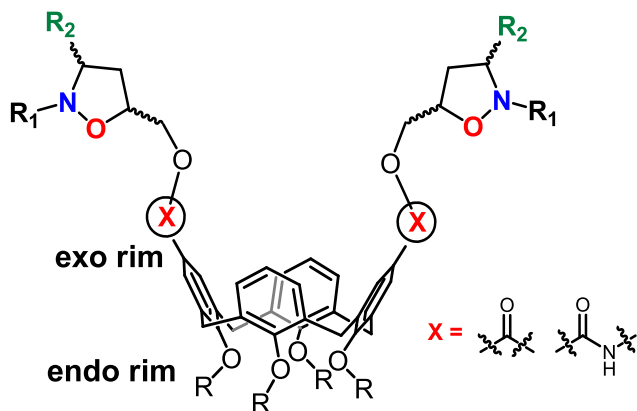

Figure 2.4 Designed isoxazolidinyl-PAH-calixarene conjugates.

Among the different possibilities, a first class of derivatives was synthesized by esterification of a cone-shaped calix[4]arene-diacyl chloride **1** with *trans-* or *cis-*pyrenylisoxazolidinyl alcohols **2a-b** (**Figure 2.5**).[43] These compounds could act as potential DNA intercalators. Their

[43] Rescifina, A.; Zagni, C.; Mineo, P. G.; Giofrè, S. V.; Chiacchio, U.; Tommasone, S.; Talotta, C.; Gaeta, C.; Neri, P. *Eur. J. Org. Chem.* **2014**, 7605-7613.

synthesis, binding studies and biological activity will be described.
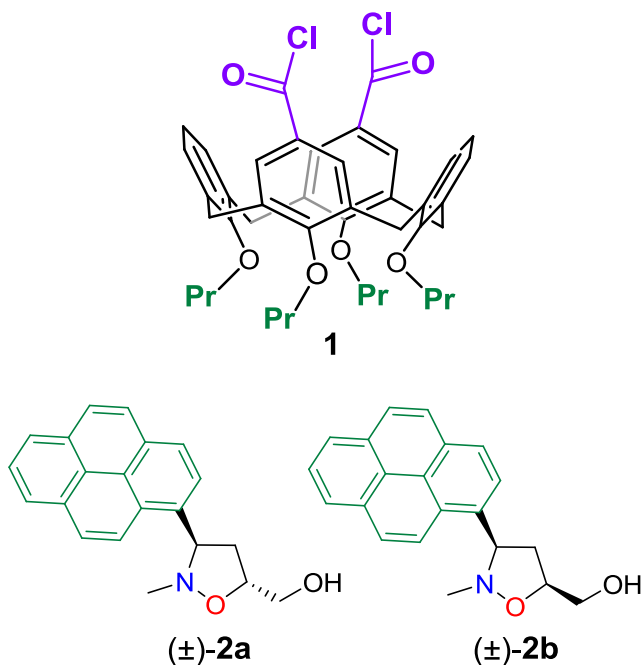
Figure 2.5

### 2.1.1 Synthesis of the calixarene conjugates

The diacyl chloride calixarene **1** was obtained by conversion of the calix[4]arene-dicarboxylic acid[44] with thionyl chloride. The synthesis of **1** is illustrated in **Scheme 2.1**.

---

[44] Sansone, F.; Barboso, S.; Casnati, A.; Fabbi, M.; Pochini, A.; Ugozzoli, F, Ungaro, R. *Eur. J. Org. Chem.* **1998**, 897-905.
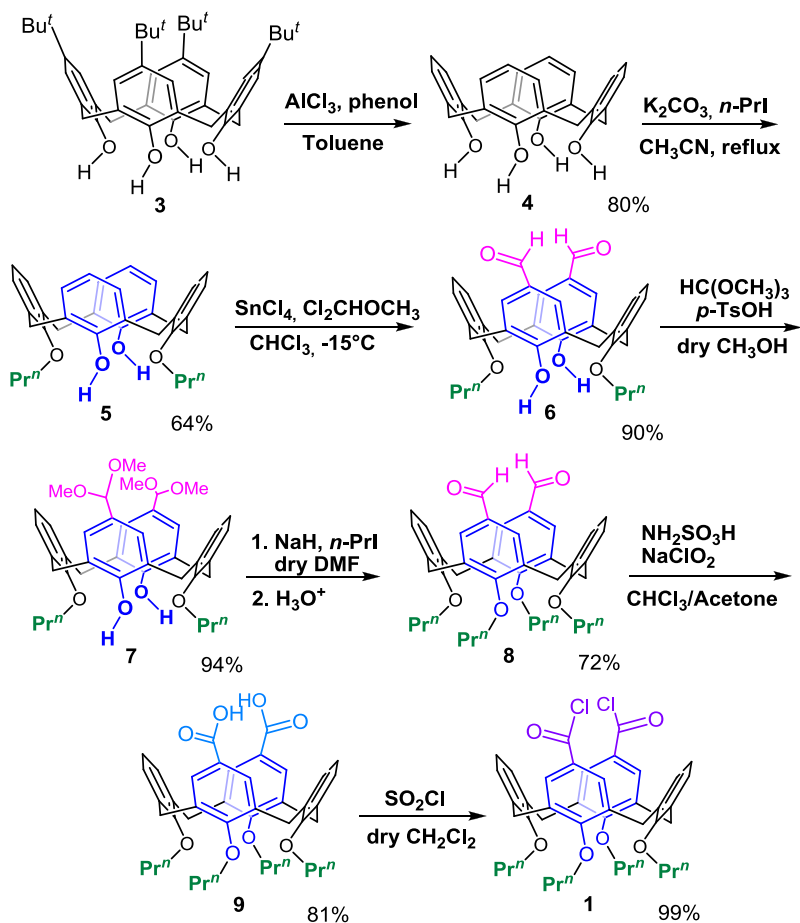
Scheme 2.1 Synthesis of diacyl chloride calix[4]arene **1**.[45]

Starting from *p-t*-Bu-calix[4]arene **3**, the *tert*-butyl groups at the exo rim were removed via retro Friedel-Crafts reaction, in

---

[45] Casnati, A.; Di Modugno, E.; Fabbi, M.; Pelizzi, N.; Pochini, A.; Sansone, F.; Tarzia, G.; Ungaro, R. *Bioorg. Med. Chem. Lett.* **1996**, *6*, 2699–2704.

presence of AlCl$_3$ and phenol.[46] Then the lower rim was selectively alkylated with K$_2$CO$_3$ and *n*-PrI in acetonitrile at reflux.[47] This was possible thanks to the different acidity of the hydroxyl groups. Indeed, after the first alkylation, the removal of the second phenolic proton takes place at the distal position, because the resulting anion is stabilized by two hydrogen bonds with the proximal hydroxyl groups. (**Figure 2.6**).
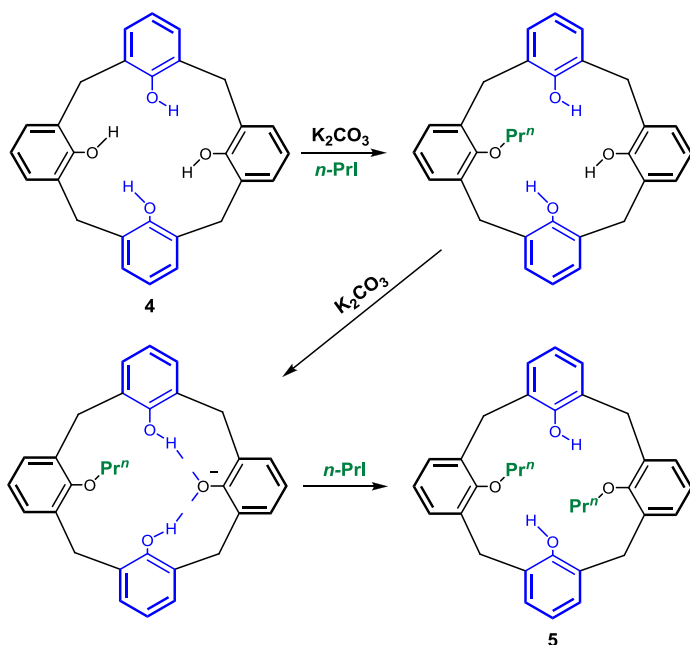

Figure 2.6 Selective dialkylation of **4**.

[46] Böhmer, V.; Rathay, D.; Kämmerer, H. *Org. Prep. Proced. Int.* **1978**, *10*, 113.

[47] Groenen, L. C.; Ruël, H. M.; Casnati, A.; Verboom, W.; Pochini, A.; Ungaro, R.; Reinhoudt, D. N. *Tetrahedron* **1991**, *47*, 8379-8384.

Following a procedure reported by Ungaro and coworkers,[48] two formyl groups were then introduced at the calixarene upper rim by Gross formylation reaction,[2d] affording product **6**. In this case the formylation occurs on the aromatic rings bearing the free hydroxyl groups. To perform an exhaustive alkylation of the lower rim a protection of the formyl groups with trimethyl orthoformate was necessary. After removal of the protective groups via acid treatment, the aldehyde groups of **8** were oxidized to carboxylic acids with NaClO and NH_2SO_3H in $CHCl_3$/Acetone.[44] Finally the treatment of **8** with thionyl chloride in dry CH_2Cl_2 led to the desired product **1**.[45]

PAH-calixarenes derivatives **10-12** in **Figure 2.7** were finally obtained by coupling of the diacyl chloride **1** with the corresponding racemic alcohols (±)-**2a** or (±)-**2b** using pyridine or triethylamine as base.[43] After a standard work-up the calixarene/pyrenylisoxazolidinyl conjugates were isolated by silica gel column chromatography. In particular, starting by the alcohol (±)-**2a**, a monosubstituted derivative (±)-**10a** the derivative with C_2 symmetry (±)-**11a**, and a *meso* compound **12a** were obtained in 15%, 10% and 8% yields respectively. Starting by the alcohol (±)-**2b**, then a monosubstituted derivative (±)-**10b** and the derivative with C_2

---

[48] Arduini, A.; Fanni, S.; Manfredi, G.; Pochini, A.; Ungaro, R.; Sicuri, A. R.; Ugozzoli, F. *J. Org. Chem.* **1995**, *60*, 1448-1453.

symmetry (±)-**11b**, were isolated in 10% and 11% yields respectively (**Figure 2.7**).

(±)-**10a**   15%

(±)-**10b**   10%

(±)-**11a**   10%

(±)-**11b**   11%

12a   8%

R =
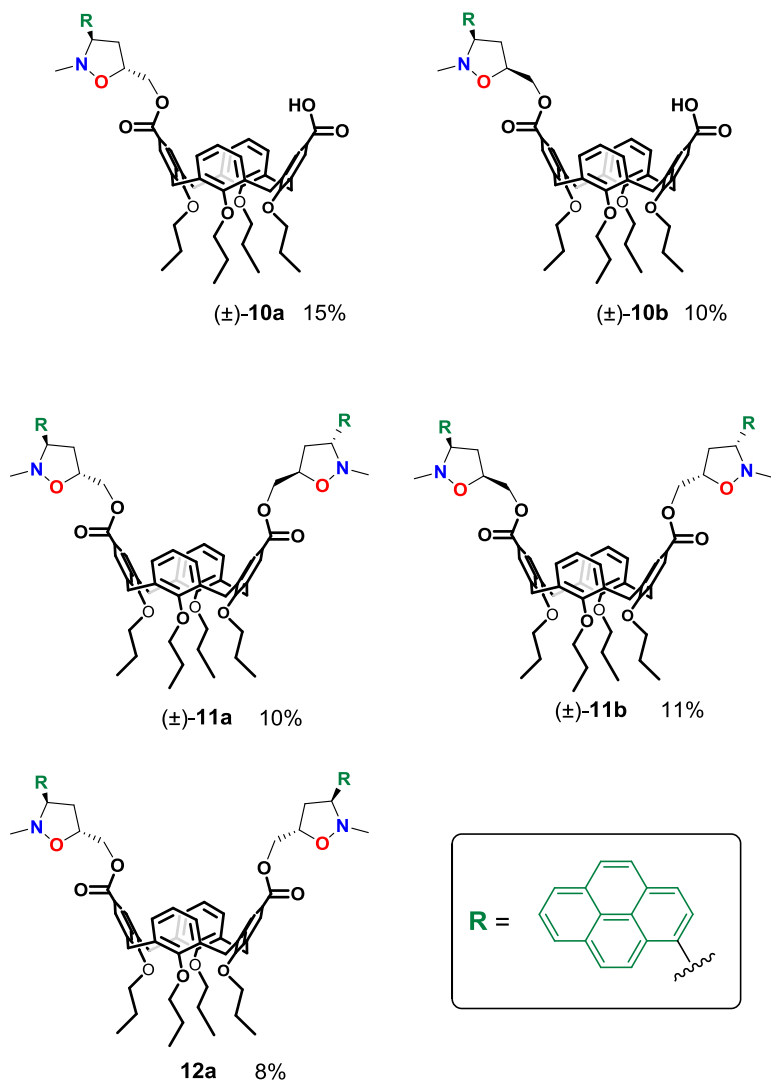
Figure 2.7 Pyrenylisoxazolidinylcalix[4]arene conjugates **10-12**.

Concerning the stereochemistry of the bis-derivatives **11**-**12**, the symmetry was assigned on the basis of the number of NMR resonances. For instance the ^{1}H NMR spectrum of **11a** showed two triplets at $\delta = 3.69$ ($J = 6.3$ Hz, 4H) and 4.04 ppm ($J = 7.6$ Hz, 4H) and two triplets at $\delta = 0.91$ and 1.07 ppm regarding the OCH_2 and terminal CH_3 of the propyl chains respectively (**Figure 2.8**).
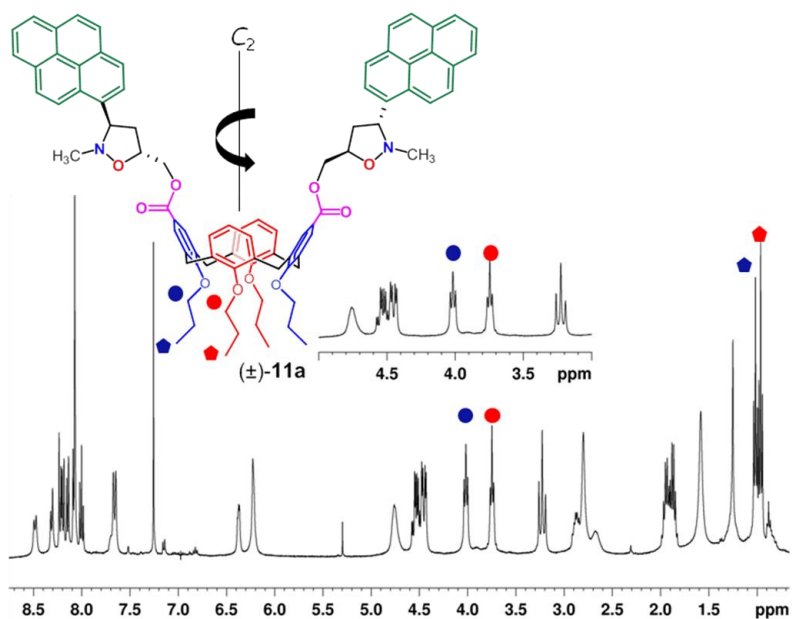

Figure 2.8 ^{1}H NMR spectrum of **11a** (400 MHz, CDCl$_3$, 298K).

Besides, the 2D HSQC spectrum showed two cross-peaks at δ = 3.69/76.9 and 4.04/76.7 ppm relative to a direct C-H

correlation between the OCH$_2$ protons and their respective carbons (**Figure 2.9**). At last, to support the C_2 symmetry, the ^{13}C NMR spectrum showed only one signal related to the carbonyl group of the ester bond and two signals for the oxygenated quaternary carbons of the calixarene (**Figure 2.10**).
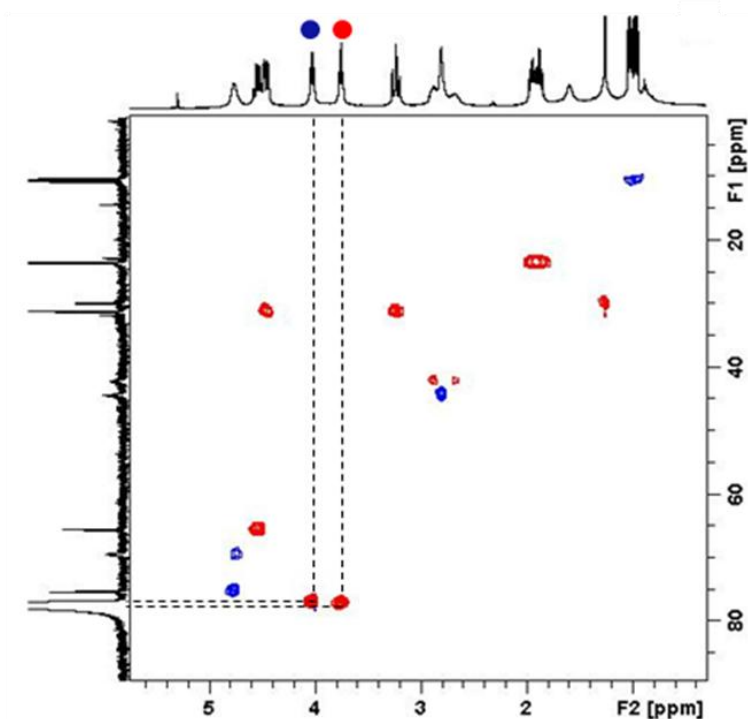
Figure 2.9 Expansion of 2D HSQC spectrum of **11a** (400 MHz, CDCl$_3$, 298 K).
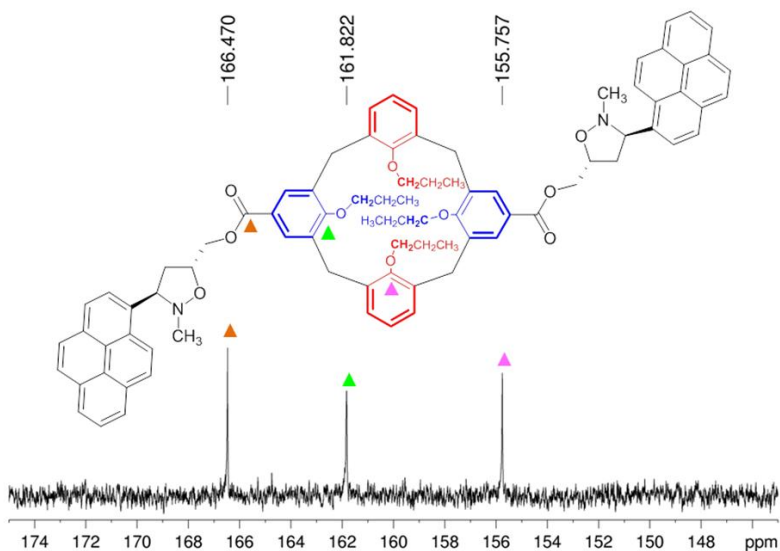
Figure 2.10 Expansion of ^{13}C NMR spectrum of **11a** (100 MHz, CDCl$_3$, 298K).

Similarly, the stereochemistry of **12a** was evident from the ^{1}H NMR spectrum in C$_6$D$_6$, in which were found three OCH$_2$ signals at δ = 3.86, 3.70 and 3.69 ppm (4H, 2H and 2H respectively). These observations were characteristic of the presence of a σ_h symmetry plane bisecting the unsubstituted aromatic rings, confirming that **12a** is a *meso* compound (**Figure 2.11**).
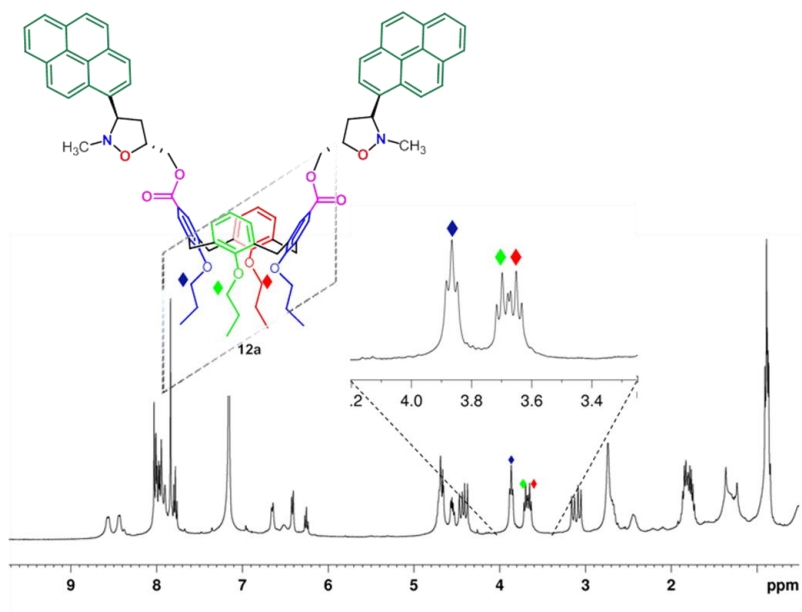
Figure 2.11 ^{1}H NMR spectrum of **12a** (400 MHz, C_6D_6, 298K).

As expected, the ^{1}H NMR spectra of the monosubstituted derivatives (±)**10a** and (±)**10b** were complex due to the lack of any symmetry element. For instance, the ^{1}H NMR spectrum of **10b** showed four AX systems for the methylene bridges in the region between 3.10-3.18 ppm and 4.40-4.53 ppm. A similar set of signals was found for **10a**.

The characterization of all these compounds was confirmed by ESI(+)-MS analysis.

2.1.2 Biological studies[49]

At this point the ability of compounds **10**-**12** to inhibit in vitro the proliferation of cancer cells was evaluated.[49] These studies were performed by Rescifina's group. Compounds **10**-**12** were tested against three different human tumor cell lines: FTC133 (follicular thyroid carcinoma), 8305C (undifferentiated thyroid carcinomas) and U87MG (glioblastoma). The cell cultures were incubated with **10**-**12** for 24h and the cell growth rates were evaluated by MTT reduction assays. The calixarenes were prepared as dimethyl sulfoxide stock solutions at 10 and 100 μM concentrations. The results of the inhibitory activities of **10**-**12** are shown in **Table 2.2** and are compared to the activities of the pyrenylisoxazolidinyl alcohols **2a-b**.

---

[49] In collaboration with Prof. Rescifina, Dipartimento di Scienze del Farmaco e dei Prodotti per la Salute, Università di Messina.

Compound	FTC133	8305C	U87MG
2a	5.88	-	5.55
2b	5.22	-	5.36
10a	>100	>100	>100
10b	0.095	0.130	57
11a	>100	>100	>100
11b	55	55	>100
12a	>100	>100	>100

Table 2.2 The results are expressed as IC_{50} [μM] (the concentration of compound at which 50% of cells are viable) and determined by MTT assay.

The most cytotoxic compound was the monosubstituted calixarene with *cis* stereochemistry **10b**, which exhibited an IC_{50} value of 95 nM toward FTC133 cells (for this cell line Doxorubicin shows $IC_{50} = 9650$ nm)[50]. The bis-substituted compound **11b** showed an IC_{50} value of 55 μM, which was ca. 580-fold less cytotoxic than **10b**. The other monosubstituted calixarene **10a** showed a low cytotoxicity, with IC_{50} values higher than 100 μM, thus stereochemistry plays a fundamental role in the activity of these compounds, as the *cis* derivative **10b** was more active than its *trans* isomer **10a**.

[50] Massart, C.; Barbet, R.; Genetet.; N.; Gibassier, J. *Thyroid* **2004**, *14*, 263.

A lack of activity was found for the bis-substituted compounds **11a** and **12a**. These unexpected results could be explained considering the low solubility of the derivatives in the culture medium. The IC_{50} values probably result from lower ligand concentrations with respect to those actually used. In contrast, the deprotonation of the carboxylic group of **10b** under physiological conditions could increase its solubility. However the hydrolysis of the carboxylic acid cannot be the only explanation for the high cytotoxcity of **10b**. The calixarene derivative is 58-fold more potent than the precursor **2b**, thus the calixarene core must clearly have a prominent implication in the biological activity.

2.1.3   Circular Dichroism[49]

The pyrenylisoxazolidinylcalix[4]arene conjugates above described were designed as potential DNA intercalators. To prove the intercalation between base pairs some studies of circular dichroism (CD) were performed. Particularly the attention was focused on the behavior of **10b** and **11b** which, as previously described, turned out to be the most cytotoxic compounds. The studies were performed on a poly(dA)-poly(dT) duplex, which is a duplex of poly(deoxyadenylic-deoxythymidinic) acid, a repetitive synthetic double-stranded

DNA sequence and a synthetic analog of B-DNA.[43]

The CD spectrum of poly(dA)-poly(dT) displayed a negative peak at λ = 248 and a positive one at λ = 260 nm, due to the right-handed helicity and to base stacking respectively.[51]

In **Figure 2.12** the CD tritation spectra of poly(dA)-poly(dT) duplex in the presence of increasing amount of **10b** are shown.
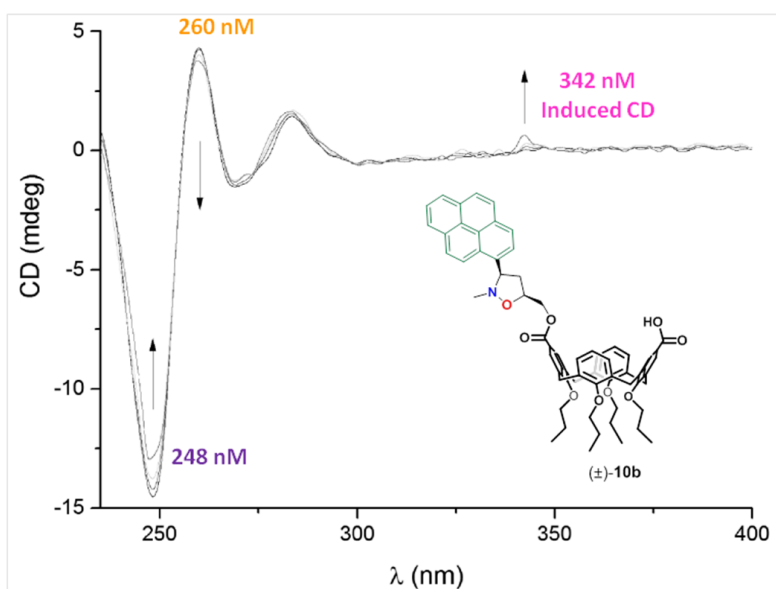

Figure 2.12 CD tritation spectra at 25 °C:
[poly(dA)–poly(dT)] = 19.7 μm in base pair; [**10b**] = 0–32 μm

Increasing concentration of **10b** led to decreases in the

[51] Palumbo, M.; Capasso, L.; Palù, G.; Marcianimagno, S. *Proc. Int. Symp. Biomol. Struct. Interactions, Suppl. J. Biosci*. **1985**, *8*, 689-697.

intensities of the signals at $\lambda = 248$ and 260 nm, together with the appearance of a positive induced CD signal at 342 nm. These observations were typical of an intercalative binding mode. The changes in the intensities of the CD spectra were due to helix unwinding as a result of the distortion of DNA upon intercalation. The small positive induced CD signal at $\lambda = 342$ nm confirmed the intercalation phenomenon, with the pyrene moiety perpendicular to the DNA axis.

Similar CD spectra were observed with the **11b**-poly(dA)-poly(dT) system, but with reduced changes in intensity.

2.1.4 Molecular Modeling[49]

To gain a deeper comprehension of the interaction of the calixarene derivatives **10**-**12** and DNA, a study of molecular modeling was performed by Prof. Rescifina and co-workers.[49] The compounds with a (3*R*) configuration for the isoxazolidine ring possess the best intercalating properties[42], thus, although the calixarene conjugates are racemates, all molecular docking calculations were performed for the (3*R*) stereoisomers. Poly(dA–dT)₂, poly(dG–dC)₂, and poly(dA)– poly(dT) were simulated as double-stranded dodecamer fragments, (dA–dT)₂, (dG–dC)₂ and poly(dA)–poly(dT), respectively. They were constructed in the B-DNA

conformation with the nucleic acids macro implemented in the YASARA software[52] and minimized with the Amber03 force field.[53] The simulations of the intercalation were performed by the docking methodology.[54] Each intercalator was manually inserted into the middle base-step of each fragment from the minor or major groove. Particularly for monointercalations the compounds were inserted between the sixth and seventh base pairs, while for bisintercalation between the fifth and sixth as well as the seventh and eighth base pairs, simultaneously. The atom positions of each compound were fixed, however the remaining molecules were minimized to suitably accommodate the ligand. To obtain the best and most reliable docking results, a coarse docking simulation was first performed for each complex by applying the Lamarckian Genetic Algorithm (LGA) implemented in AutoDock 4.2.5.1,[55] which has been recently demonstrated to accurately reproduce the complex crystallographic structures of a collection of DNA-binding small ligands.[56] The best ligand position was further subjected to an MD simulation of 5 ns in a physiological environment (pH = 7.2, H_2O, NaCl

[52] Krieger, E. *YASARA*, 13.9.8 ed., YASARA Biosciences GmbH: Vienna, **2013**.

[53] Duan, Y.; Wu, C.; Chowdhury, S.; Lee, M. C.; Xiong, G. M.; Zhang, W.; Yang, R.; Cieplak, P.; Luo, R.; Lee, T.; Caldwell, J.; Wang, J. M.; Kollman, P. *J. Comput. Chem.* **2003**, *24*, 1999-2012.

[54] Santos-Filho, O. A.; Figueroa-Villar, J. D.; Araujo, M. T. *Bioorg. Med. Chem. Lett.* **1997**,*7*, 1797-1802.

[55] Morris, G. M.; Huey, R.; Lindstorm, W.; Sanner, M. F.; Belew, R. K.; Goodsell, D. S.; Olson, A. J. *J. Comput. Chem.* **2009**, *30*, 2785-2791.

[56] Holt, P. A.; Chaires, J. B.; Trent, J. O. *J. Chem. Inf. Model.* **2008**, *48*, 1602-1615.

0.9%) to allow the ligand to be better accommodated in the pocket and model the interactions with the groove. At last, each ligand was well docked by the LGA with the system obtained by MD. Under physiological conditions the carboxylic acid moiety in compounds **10** is completely dissociated, thus, only the carboxylate form was considered. The possibility that the complexation between **10**-**11** with DNA may occur by binding along the grooves was also taken into account. The calculated binding energies after 5 ns of MD simulation are reported in **Table 2.3**.

Compound	(dA-dT)$_2$ dodecamer from major groove	(dA-dT)$_2$ dodecamer from minor groove
2a (intercalated)	-9.11	-9.03
2b (intercalated)	-9.68	-9.39
10a (intercalated)	-6.53	-8.83
10b (intercalated)	-6.69	-10.19
11a (intercalated)	-9.22 after 1 ns, -7.36	-9.81
11b (intercalated)	-11.16 after 1 ns, -8.13	-15.51
10a (groove-bound)	-4.66	-7.79
10b (groove-bound)	-4.35	-8.16
11b (groove-bound)	-8.35	-8.79
	(dG-dC)$_2$ dodecamer from major groove	(dG-dC)$_2$ dodecamer from minor groove
2a (intercalated)	-9.28	-9.09
2b (intercalated)	-9.35	-9.23
10a (intercalated)	-6.76	-7.33
10b (intercalated)	-8.91	-10.88
11a (intercalated)	-8.48	-9.05
11b (intercalated)	-10.55	-13.09
10a (groove-bound)	-5.13	-7.54
10b (groove-bound)	-4.41	-8.65
11b (groove-bound)	-8.15	-8.98
	poly(dA)-poly(dT) from major groove	poly(dA)-poly(dT) from major groove
10b (intercalated)	-6.43	-9.92
10b (groove-bound)	-5.72	-6.57

Table 2.3 Calculated binding energies [Kcal/mol] after 5 ns of MD simulation.

Intercalation from the major groove and both minor and major groove binding can be ruled out on the basis of their lower binding energies. The compounds can act as mono or bisintercalators that interact preferentially with AT base pairs,

41

penetrating into the DNA double helix from the minor groove. The lower cytotoxic activity of the *trans* stereoisomer **10a** compared to the *cis* one **10b** could be ascribable to the steric hindrance of the *N*-Me group of the isoxazolidine ring. This hypothesis is supported by the lower binding energies of **10a** compared to **10b** (see **Table 2.3**).

A graphical representation of **10a** and **10b** intercalated from the minor groove in the (dA-dT)$_2$ dodecamer is shown in **Figure 2.13**. The *N*-methyl group in the *trans* compound **10a** (**Figure 2.13**, left) is oriented towards the base pairs of the DNA fragment. Conversely in the *cis* isomer **10b** the methyl points outward, producing a lower steric hindrance (**Figure 2.13**, right).
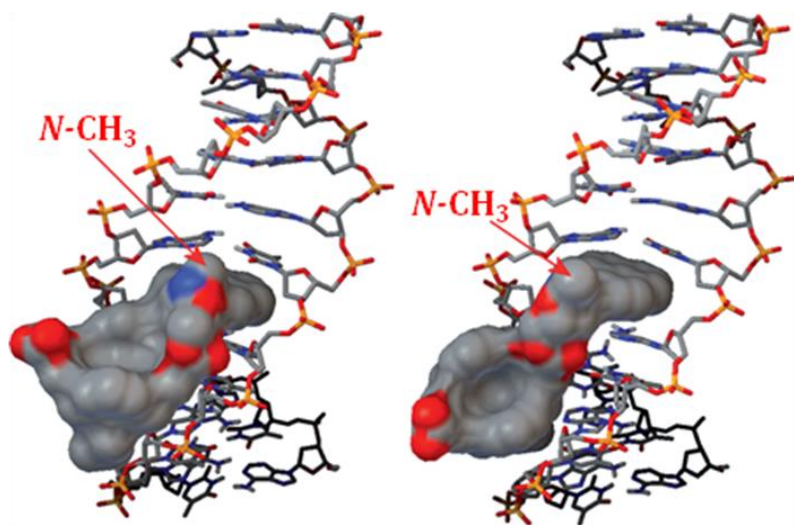

Figure 2.13 10a (left) and **10b** (right) intercalated from the minor groove in the (dA-dT)$_2$ dodecamer.

According to the binding energies in **Table 2.3**, compounds **11a** and **11b** could behave as bisintercalators. In particular, the calculate binding energy of -15.51 Kcal/mol for **11b** presupposes a strong interaction with the DNA, which should lead to a biological activity in the submicromolar range. Probably the low activity measured (IC_{50} = 55 µM for FTC133) could be ascribable to the low solubility of the compound.

An interesting behavior was observed for both **11a** and **11b** when intercalated from the major groove of poly(dA-dT)$_2$. In fact, the examination of the MD simulation trajectories revealed that they can act only as monointercalators. After 1 ns both compounds **11** are bisintercalated into the dodecamer. Subsequently one pyrene moiety deintercalates and becomes perpendicular to the calixarene exo rim. After 5 ns simulation **11** is uniquely monointercalated. A representation of the intercalation of **11b** at 1 and 5 ns are shown in **Figure 2.14**.
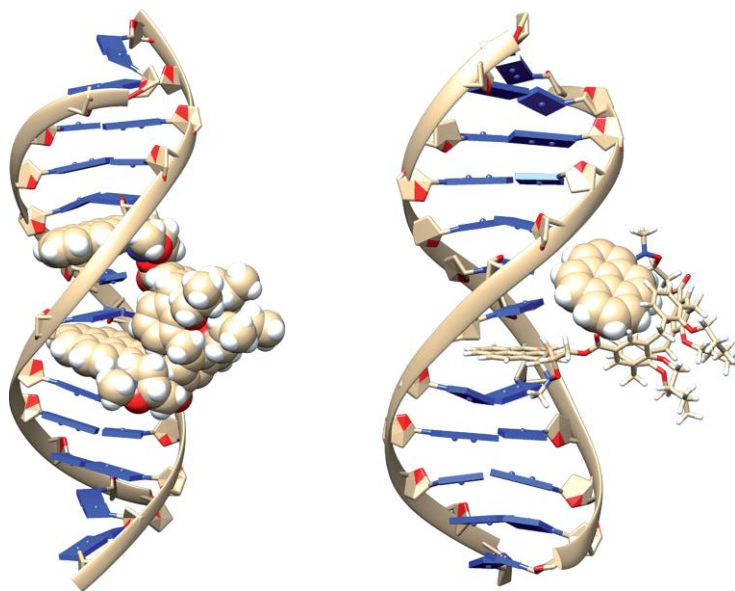
Figure 2.14 Representation of **11b** intercalated into the (dA-dT)$_2$ dodecamer from the major groove. After 1 ns of MD simulation the compound is bisintercalated (left); after 5 ns only one pyrene unit is intercalated and the other is completely deintercalated.

Nevertheless, the binding energies for these two MD periods are smaller than those observed for the intercalation of the compounds from the minor groove. Conversely, for the interaction with the (dG-dC)$_2$ dodecamer, the bisintercalate complexes are stable up to 5 ns of MD simulation (**Table 2.3**).

Finally, in **Figure 2.15** is shown the arrangement of **10b** into the pocket of poly(dA)-poly(dT) from the minor groove.
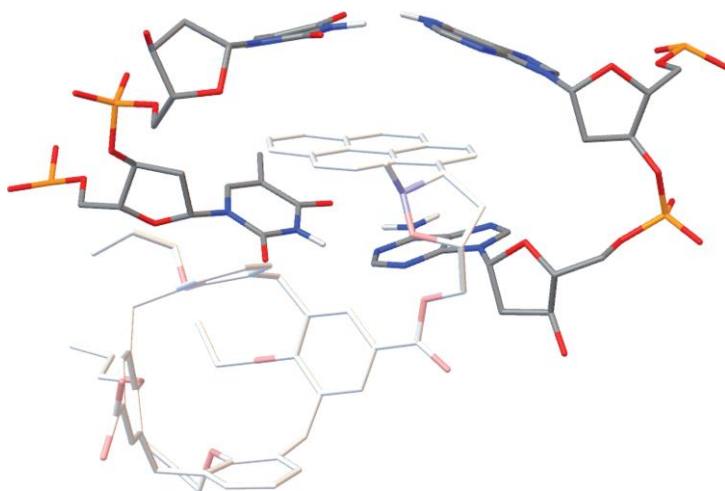

Figure 2.15 Plot representing **10b** intercalated into the poly(dA)–poly(dT) dodecamer from the minor groove.

The pyrenyl unit of **10b** is parallel to the long axis of the base pairs. This arrangement is in good agreement with the induced CD signal at λ = 342 nm observed (**Figure 2.12**), thus confirming the intercalation binding mode.

2.2 Conclusions

In this work we have obtained new PAH-presenting calix[4]arene conjugates bearing pyrenylisoxazolidine moieties at the exo rim.[43] The in vitro cytotoxic activity against three different human tumor cell lines was tested and the most active compound **10b** showed an IC_{50} of 95 nM toward FTC133 cell lines (follicular thyroid carcinoma).[43] Compared to the pyrenylisoxazolidinyl alcohols **2a-b** a 58-fold increase in activity was observed. Both CD and docking studies indicated that these calixarene derivatives are able to intercalate DNA from its minor groove.[43]

Unfortunately the bis-substituted compounds did not show the expected results, probably because of their low solubility in the cell culture medium. With no doubt the results herein reported and the information obtained during these studies can be used to design and synthesize new DNA-intercalating agents with improved antitumor activity.

Chapter 3

3. Chemical proteomics and drug discovery

Drug discovery is a research process that consists of the identification and development of a molecule that produces a desired effect in a living organism. Understanding the mechanism of action is a main requirement to find a new drug. However this request can only be satisfied provided that the biomolecular targets of the new potential drug are known.[57] In the last decades the identification of calixarenes able to bind a known biomolecular target, has been carried out by using two principal strategies: the screening of a library of potential candidates[11(c,d),16b] and the virtual screening with molecular docking.[27,58]

Recently mass spectrometry-based chemical proteomics has gained relevance as a novel strategy for the identification of possible biological targets.[59] The interest in this emerging approach has grown rapidly thanks to the remarkable

[57] Lindsay, M. A. *Nat. Rev. Drug Discovery* **2003**, *2*, 831-838.

[58] (a) Gordo, S.; Martos, V.; Santos, E.; Mendez, M.; Bo, C.; Giralt, E.; de Mendoza, J. *Proc. Natl. Acad. Sci. USA* **2008**, *105*, 16426-16431; (b) Martos, V.; Bell, S. C.; Isacoff, E. Y.; Trauner, D.; de Mendoza, J. *Proc. Natl. Acad. Sci. USA* **2009**, *106*, 10482-10486.

[59] a) Rix, U.; Superti-Furga, G. *Nat. Chem. Biol.* **2009**, *5*, 616-624; (b) Veenstra, T. D. *Drug Discovery Today: Technologies* **2006**, *4*, 433-440.

technological advances in mass spectrometry.[60] One of the principal chemical-proteomics approaches uses immobilized compounds and combines drug affinity chromatography with high-resolution mass spectrometry analysis and bioinformatics.[59]

A typical chemical proteomics experiment starts with the immobilization of a potential bioactive compound on a solid support. There are several commercially available activated resins, usually based on sepharose or agarose, that allow the attachment of chemical groups such as amino, hydroxyl or carboxyl groups.

A cell extract is then prepared either from cells or tissue and this lysate is incubated with the affinity matrix and washed extensively before the elution. For nonspecific elution, detergents, salts or denaturing agents are used. The specific elution can be achieved via the specific cleavage of an engineered linker. Subsequently, processing by SDS-PAGE and protein digestion with a protease (generally trypsin) generates a complex peptide mix, which is analyzed by nanoHPLC coupled to nanoESI/MS.

Finally the results are searched against a protein database to identify the proteins bound to the bioactive compound.

The whole chemical proteomics experiment is described in **Figure 3.1**.

[60] Domon, B.; Aebersold, R. *Science* **2006**, *12*, 212-217.
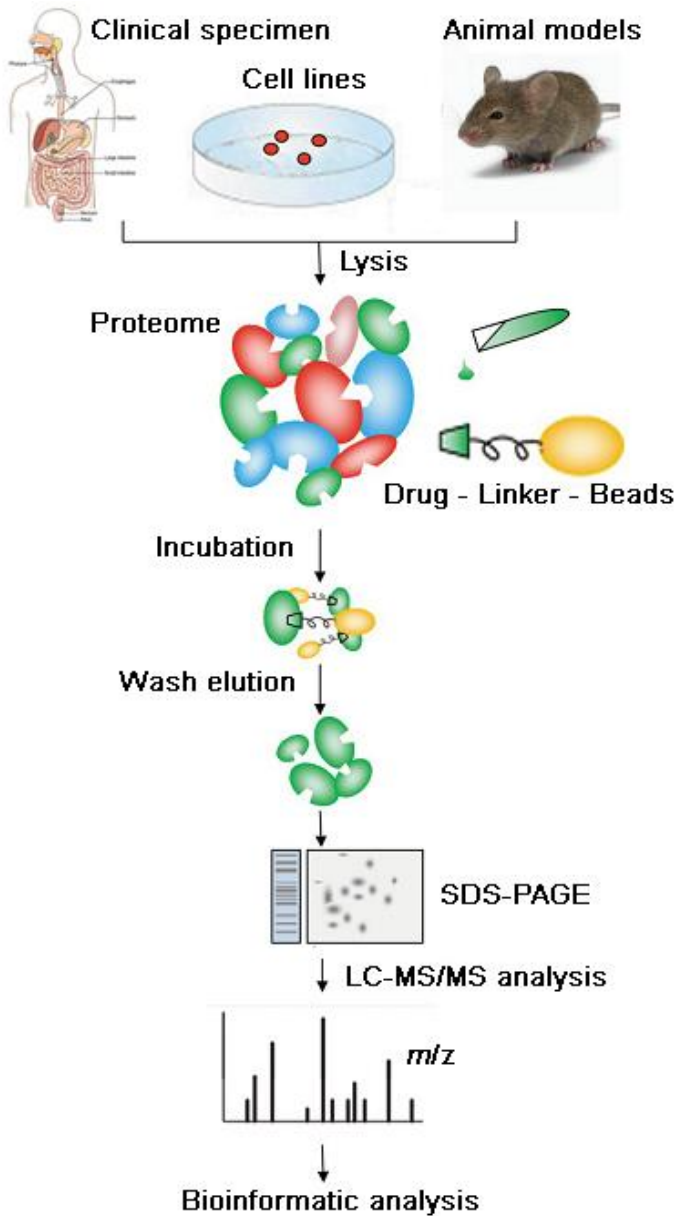
Figure 3.1 Chemical proteomics experiment

49

A great advantage of this technique is that it can be used to probe the whole proteome. Proteins are encountered in their natural state, which includes endogenous abundance levels and post translational modifications. Besides it is possible to use any cell type or tissue, from microorganism to humans.

Unfortunately chemical proteomics does not provide information about functional implications, as there is no correlation with the IC_{50}. Thus, although it can give indication about specific physical interactions between a compound and its target, the biological relevance must be validated by other techniques.
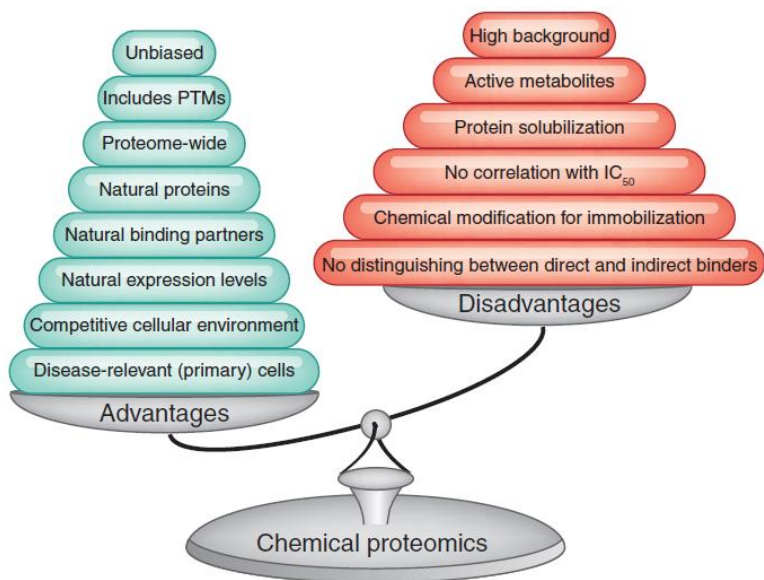

Figure 3.2 Advantages/disadvantages of chemical proteomics.

3.1 Application of chemical proteomics

The use of this technique has led to the discovery of a variety of compound targets, particularly the kinase inhibitors based on natural products. The identification of kinase targets has been investigated in various diseases such as cancer and autoimmune disorders.[61] Protein kinases are among the most investigated drug target classes, so that several kinase inhibitors have entered clinical trials in the recent years. Chemical proteomics is widely applied to identify possible targets of kinase inhibitors through affinity purification from cellular extracts. In fact, the advantage of performing the experiment using disease-relevant cells enables to study more directly the mechanism of action of a particular kinase inhibitor.[62]

Interestingly chemical proteomics is widely applied for the identification of the biomolecular targets of natural products. Due to the low abundance, the testing for the biological activity of most of the newly discovered natural products is limited. Most of these tests are focused on the antibacterial and anticancer activity, thus the potential of most natural products as drugs and their ability to interfere with biological

[61] (a) Bach, S. *et al. J. Biol. Chem.* **2005**, *280*, 31208-31219; (b) Rix, U. *et al. Blood* **2007**, *110*, 4055-4063.
[62] (a) Godl, K. *Et al. Proc. Natl. Acad. Sci.* **2003**, *100*, 15434-15439; (b) Wissing, J. *et al. Mol. Cell. Proteomics* **2004**, *3*, 1181-1193.

pathways is unexplored. Therefore the use of natural products in chemical proteomics experiments is highly worthwhile.[63] For instance, this approach was used to investigate the molecular mechanism of action of the antimitotic compound diazonamide A, a marine natural product. Chemical proteomics led to the discovery that its target, ornithine δ-amino transferase, plays a fundamental role in mitotic spindle assembly and cell division.[64]

Casapullo and co-workers paid much attention to the identification of the macromolecular targets of small bioactive compounds.[65] They disclosed the proteasome inhibitory activity of Petrosaspongiolide M (PM), an anti-inflammatory marine sesterpene.[65a] The bioactive compound was covalently linked to an activated agarose matrix, which was modified with a spacer to avoid steric interference between the ligand-bearing matrix and the targets (**Figure 3.3**).

---

[63] Piggott, A. M.; Karuso, P. *Comb. Chem. High Throughput Screen* **2004**, *7*, 607-630.

[64] Wang, G.; Shang, L.; Burgett, A. W.; Harran, P. G.; Wang, X. *Proc. Natl. Acad. Sci.* **2007**, *104*, 2068-2073.

[65] (a) Margarucci, L.; Monti, M. C.; Tosco, A.; Riccio, R.; Casapullo, A. *Angew. Chem. Int. Ed.* **2010**, *49*, 3960-3963; (b) Margarucci, L.; Monti, M. C.; Cassiano, C.; Mozzicafreddo, M.; Angeletti, M.; Riccio, R.; Tosco, A.; Casapullo, A. *Chem. Commun.* **2013**, *49*, 5844-5846; (c) Margarucci, L.; Monti, M. C.; Mencarelli, A.; Cassiano, C.; Fiorucci, S.; Riccio, R.; Zampella, A.; Casapullo, A. *Mol. BioSyst.* **2012**, *8*, 1412-1417; (d) Cassiano, C.; Monti, M. C.; Festa, C.; Zampella, A.; Riccio, R.; Casapullo, A. *ChemBioChem* **2012**, *13*, 1953-1958.
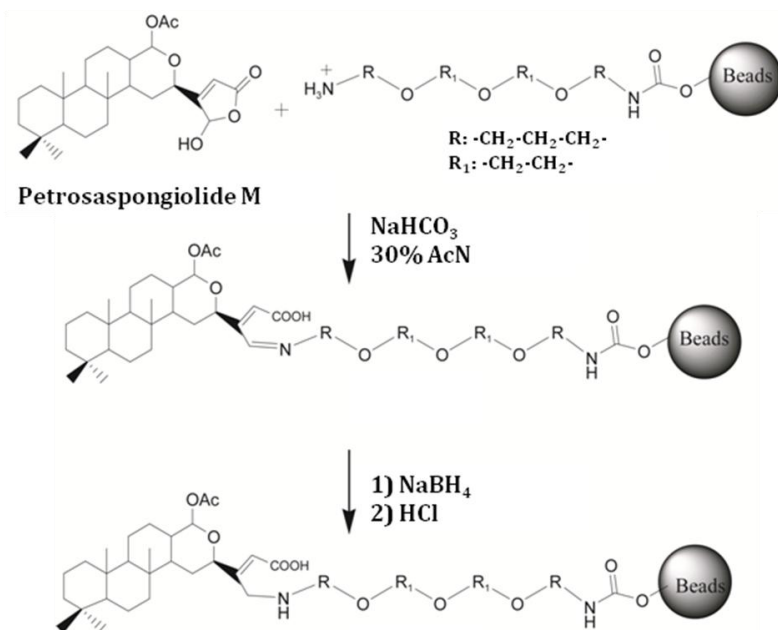
Figure 3.3 Preparation of PM-modified beads.

The PM-modified matrix was then incubated with human-macrophage-derived THP-1 cell extracts. Chemical proteomics revealed the ability of Petrosaspongiolide M to interact with several components of the proteasome enzymatic machinery. Thus the activity of PM on the 20S proteasome was tested in vitro by detecting its ability to modulate the proteasome-mediated proteolysis of three fluorogenic peptide substrates. PM was found to inhibit the proteasomal activity, particularly in the chymotrypsin-like site, with an effectiveness comparable to MG132, a well-known

proteasome inhibitor. Two proteasome inhibitors, Bortezomib[66] and MLN-519[67] have already entered clinical trials for the treatment of cancer and stroke patients respectively. The proteasome activity of PM, disclosed thanks to chemical proteomics, suggests that this molecule could be considered as a new lead compound.

Although its limitations, there is no doubt that chemical proteomics is a very powerful approach for the investigation of new drug targets and the elucidation of the mechanism of action of potential drugs. This is particularly relevant when the drug candidate is a low abundant compound, such as a natural product. Instead of performing a screening of several targets for the evaluation of the biological activity of a given compound, through a chemical proteomics experiment the potential partners can be identified simultaneously.

Chemical proteomics, in combination with other techniques and the recent and continuing technological improvements, will find more applications in the coming future and will be a even more powerful tool in drug discovery.

---

[66] Crawford, L. J.; Walker, B.; Ovaa, H.; Chaunhan, D.; Anderson, K. C.; Morris, T. C. *Cancer Res.* **2006**, *66*, 6379-6386.

[67] Shah, I. M.; Di Napoli, M. *Cardiovasc. Hematol. Disord. Drug Targets* **2007**, *7*, 250-273.

3.2 Biomolecular recognition abilities of calixarenes through the chemoproteomic approach - Results and discussion

During this PhD research project, chemical proteomics was used to study the biomolecular recognition abilities of calix[4]arene derivative bearing acetamido groups at the exo rim. This study was performed in collaboration with Prof. Casapullo (DIFARMA, University of Salerno) and his research group.

Calix[4]arenes bearing amido, urea or thiourea functionalities have the potential to establish intermolecular interactions with biological compounds, due to their hydrogen-bond donor acceptor groups. To evaluate the biomolecular recognition abilities through a chemical proteomics approach, the calixarene must be functionalized to introduce a suitable linker for the subsequent immobilization on the solid support. The first derivative to be investigated through this approach was the *p*-acetamidocalix[4]arene **13** (**Figure 3.4**).[68] This compound combines the hydrogen-bond donor/acceptor

---

[68] Tommasone, S.; Talotta, C.; Gaeta, C.; Margarucci, L.; Monti, M. C.; Csapullo, A.; Macchi, B.; Prete, S.; De Araujo, A. L.; Neri, P. *Angew. Chem. Int. Ed.* **2015**, *54*, 15405-15409.

abilities of the acetamido groups at the *exo* rim and the hydrophobicity of the calixarene backbone, which should promote the formation of protein-calixarene interactions.
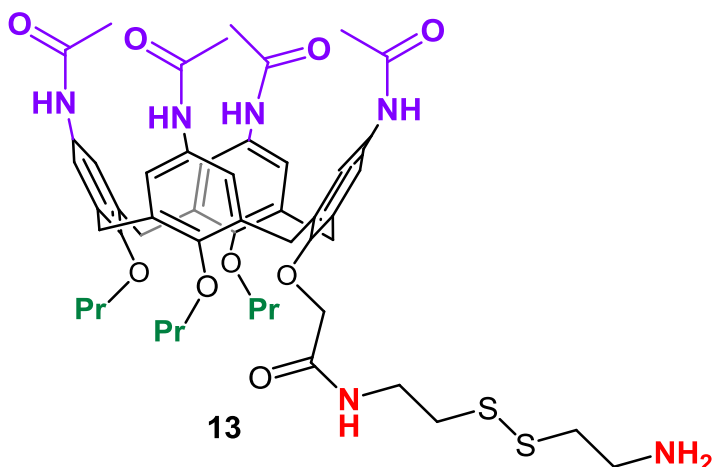

Figure 3.4 *p*-acetamidocalix[4]arene **13**.

The *p*-acetamidocalix[4]arene **13** also presents a spacer arm at the *endo* rim, 2-(2-aminoethyldisulfanyl)ethylamine, for the immobilization on the solid support. The spacer is necessary to minimize the steric hindrance between the calixarene on the matrix and its potential targets during the affinity purification step.

3.2.1 Synthesis of compound 13

The synthesis of the *p*-acetamidocalix[4]arene **13** (*p*AC **13**) is outlined in **Scheme 3.1a-b**.

The derivative **14** bearing three propyl chains at the endo rim was obtained by alkylation of *p-t*-Bu-calix[4]arene **3** with 1-iodopropane, BaO and Ba(OH)$_2$.[69] The free phenol ring was alkylated with α-bromo-ethylacetate, using NaH as base in dry DMF.[70] The ester group of **15** was then hydrolyzed with NaOH in a mixture of THF/H$_2$O at reflux, affording to derivative **16**.[71] Derivative **16** was exhaustively nitrated to the exo rim by treatment with HNO$_3$ in presence of CH$_3$COOH in dry CH$_2$Cl$_2$ as solvent. Compound **17**[71] was purified by flash column chromatography. The four nitro groups of **17** were then reduced to amino groups via catalytic hydrogenation with Nickel Raney in DMF.[71] Subsequently the tetracetamido calix[4]arene **19** was obtained by treatment of the tetramino compound **18**[71] with acetyl chloride in dry THF.

The structure of **19** was assigned by spectral analysis. In particular, the presence of a molecular ion peak at *m/z* 859.5 (M+Na$^+$) in the ESI(+) mass spectrum confirmed the

[69] Gutsche, C. D.; Dhawan, B.; Levine, J. A.; No, K. H.; Bauer, L. J. *Tetrahedron*, **1983**, *39*, 409-426.

[70] Geraci, C.; Consoli, G. M. L.; Galante, E.; Bousquet, E.; Pappalardo, M.; Spadaro, A. *Bioconjugate Chem.* **2008**, *19*, 751-758.

[71] Mattiuzzi, A.; Jabin, I.; Mangeney, C.; Roux, C.; Reinaud, O.; Santos, L.; Bergamini, J. F.; Hapiot, P.; Lagrost, C. *Nat. Commun.* **2012**, *3*, 2121/1-2121/8.

molecular formula. The ^{1}H NMR spectrum of **19** DMSO-d$_6$ showed the –NH signals of the amido moieties between δ = 9.30-9.59 ppm as well as the three singlets for the aromatic protons at δ = 6.68 (2H), 6.75 (2H) and 7.04 (4H) ppm. (**Figure 3.5**) The protons of the methylene bridges showed signals at δ = 3.06 (d, ArCH_2Ar, J = 12.8 Hz, 4H), and 4.29-4.34 (overlapped, 4H) ppm, while the ^{13}C NMR spectrum (100 MHz, MeOD, 298K) showed a signal at δ = 154.82 ppm for the COOH.
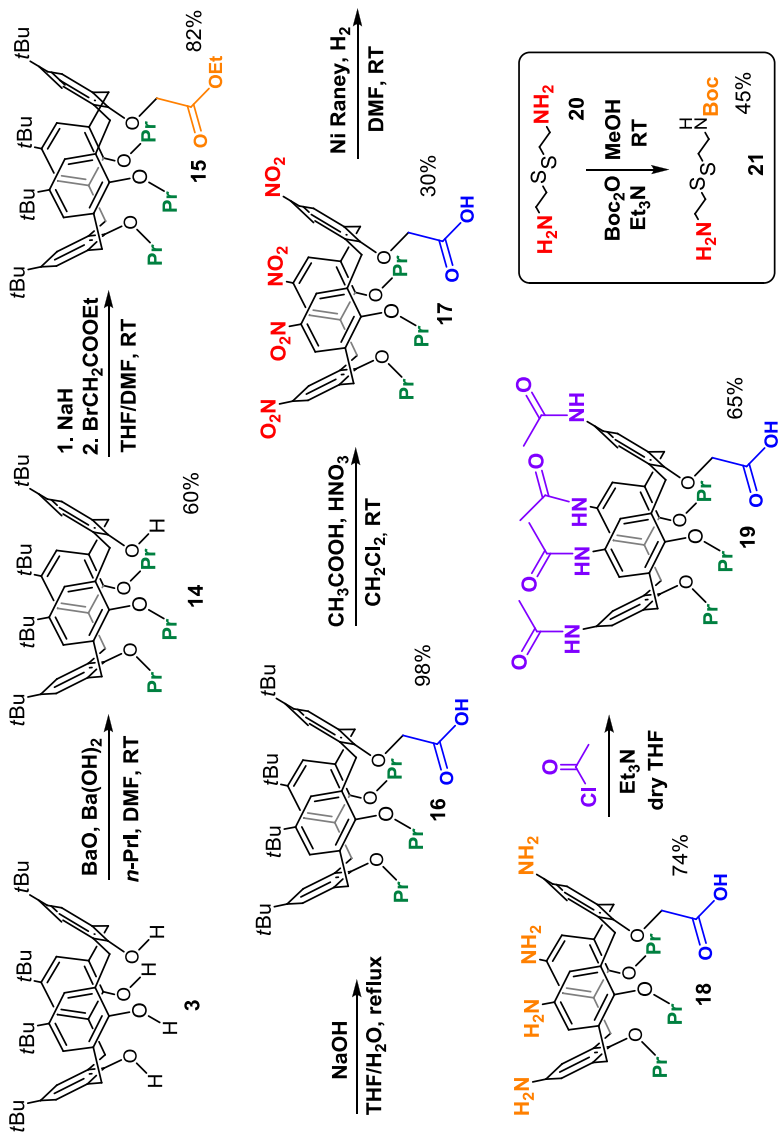
Scheme 3.1a Synthesis of *p*-acetamidocalix[4]arene **19**.
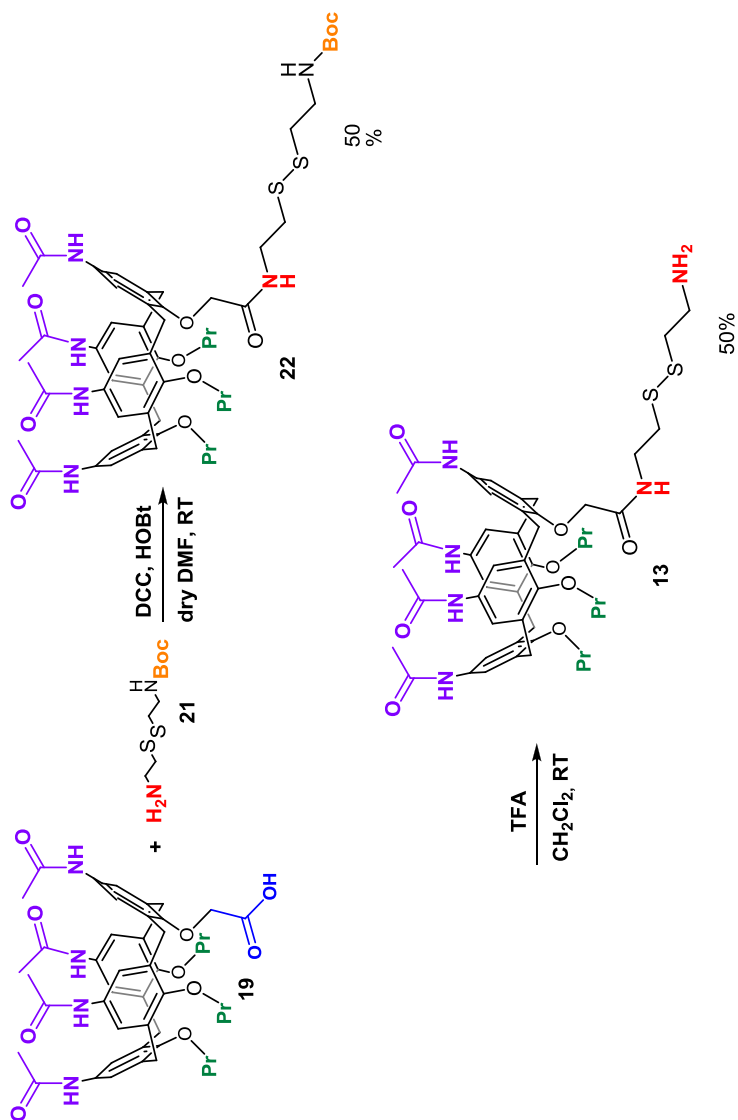
Scheme 3.1b Synthesis of *p*-acetamidocalix[4]arene **13**.
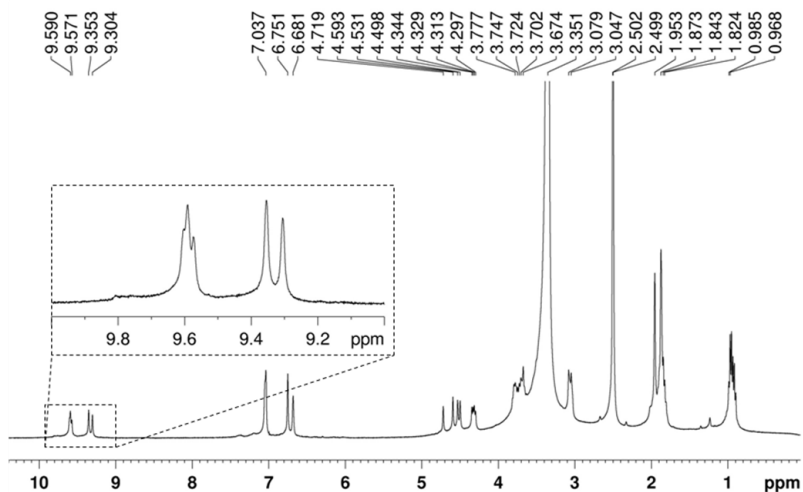
Figure 3.5 ^{1}H NMR spectrum of **19** (400 MHz, DMSO-d$_6$, 298 K)

Before the coupling reaction between **19** and the spacer arm, a mono-Boc protection of the diamino derivative **20** was necessary. This was performed following a quick and simple procedure in which the desired product **21** was isolated after two extractions.[72] At first the crude was washed with diethyl ether and 1M NaH$_2$PO$_4$ solution (pH = 4.2). Then the aqueous layer was basified to pH = 9.0 with 1M NaOH solution and washed with ethyl acetate. Finally the organic layer was concentrated affording the mono-Boc protected spacer arm **21**. Afterwards the derivative **19** was coupled with the spacer

---

[72] Niu, J.; Liu, Z.; Fu, L.; Shi, F.; Ma, H.; Ozaki, Y.; Zhang, X. *Langmuir* **2008**, *24*, 11988-11994.

arm **21** with N,N'-dicyclohexylcarbodiimide (DCC) and hydroxybenzotriazole (HOBt) in dry DMF, affording compound **22**. The treatment of **22** with trifluoroacetic acid (TFA) in dichloromethane, followed by a short column chromatography purification led to the isolation of the desired ligand *p*AC-**13**, which was characterized by ^{1}H and ^{13}C NMR spectroscopy and ESI(+) MS. The presence of a molecular ion peak at *m/z* 971.4 (M+H$^+$) in the ESI(+) mass spectrum confirmed the molecular formula. The ^{1}H-NMR of the final product **13** showed the signals of the spacer arm at δ = 2.86 (t, C*H$_2$*NH$_2$, *J* = 6.4 Hz, 2H), 3.02 (t, CH$_2$S, *J* = 6.6 Hz, 4H) ppm, and the singlet for OCH$_2$C(O) at δ = 4.78 ppm. The protons of the methylene bridges showed overlapped signals at δ = 3.13-3.24 and 4.40-4.49 ppm (**Figure 3.6**).
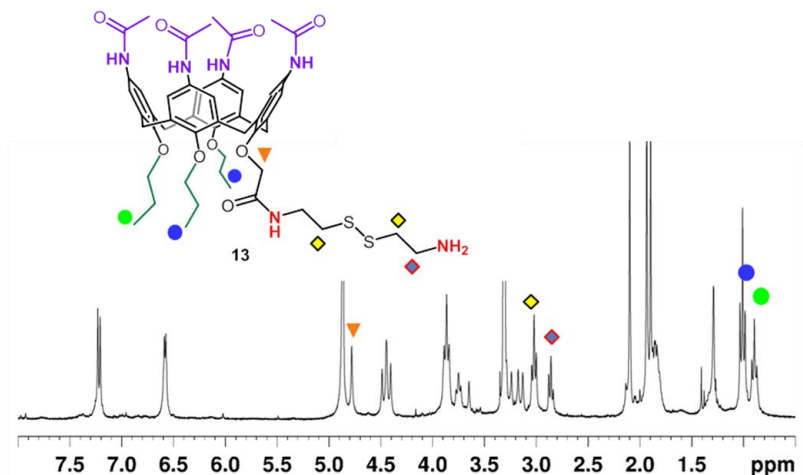

Figure 3.6 ^{1}H NMR spectrum of **13** (300 MHz, MeOD, 298K).

The treatment with trifluoroacetic acid is a well established procedure for the removal of Boc protective groups, almost quantitative. Surprisingly in this case compound **13** was obtained with only a 50% yield. Probably this low yield is ascribable to the degradation of the disulfide bond of the spacer arm.

3.2.2 Chemical proteomics experiment[73]

The chemical proteomics experiment (or "fishing" experiment) was performed by Prof. Casapullo and co-workers. Compound **13** was covalently linked to the agarose-gel activated with 1,1'-carbonyldiimidazole (CDI). Thus **13** was dissolved in acetonitrile containing 30% $NaHCO_3$ and 1.5% Et_3N and incubated with the CDI-agarose beads for 16h. The final concentration of **13** was 3μmol per milliliter of resin (assessed by reverse-phase HPLC analysis).

---

[73] In collaboration with Prof. Casapullo, Dipartimento di Farmacia, Università degli Studi di Salerno.
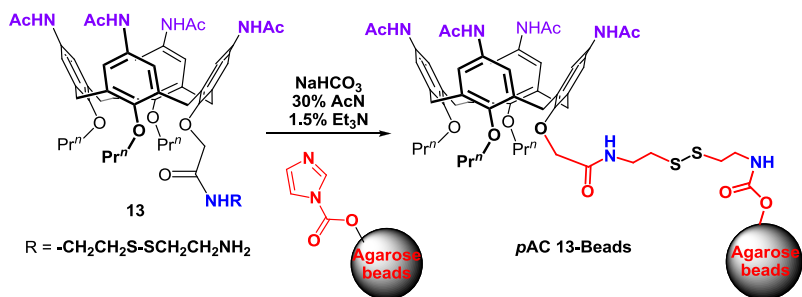
Figure 3.7 Immobilization of **13** on agarose beads.

Then samples of crude HeLa cells were incubated with the *p*AC **13**-modified beads. A calix-free matrix was used as a control experiment to discriminate between specific and aspecific interactions. The beads were washed three times with Phosphate-Buffered Saline (PBS) solution to remove aspecific bound proteins. The beads were then treated with dithiothretiol (DTT) to break the disulfide bridge of **13** and to release in solution the *p*AC-proteins complexes. The protein mixture was purified by SDS-PAGE, digested with trypsin and analyzed by mass spectrometry through nanoflow reversed-phase HPLC MS/MS. The ten most intense doubly and triply charged peptide ions were fragmented and the MS spectra were subjected to a Mascot database search. The results were compared with those of the free-matrix control experiment. Usually this kind of "fishing" experiment gives a huge number of potential partners, which is reduced by applying a filter of the Mascot scores and the Pep(sig) values.

The Mascot score is the probability that an observed match is not a random event, while the Pep is the Posterior Error Probability, defined as the probability of a random match being classed as significant. In this case only proteins with Mascot score > 30 and Pep(sig) > 1 were considered, in order to obtain results with high trustworthiness. In addition keratins were also excluded, as their presence is due to accidental operator contamination. To establish which proteins were the best potential partners for *p*AC **13**, the chemical proteomics experiment was performed three times, giving three sets of proteins (**Table 3.1**).

*p*AC-13-beads – Experiment #1

Accession	Score	Mass	Matches	Pep(sig)	Description
LDHA_HUMAN	156	36950	8	4	L-lactate dehydrogenase A chain
ACTA_HUMAN	47	42381	3	2	Actin, aortic smooth muscle
PDIA1_HUMAN	35	57480	9	3	Protein disulfide-isomerase

*p*AC-13-beads – Experiment #2

Accession	Score	Mass	Matches	Pep(sig)	Description
PDIA1_HUMAN	67	57480	6	4	Protein disulfide-isomerase
LDHA_HUMAN	66	36950	6	3	L-lactate dehydrogenase A chain
DECR_HUMAN	65	36330	6	2	2,4-dienoyl-CoA reductase, mitochondrial

*p*AC-13-beads – Experiment #3

Accession	Score	Mass	Matches	Pep(sig)	Description
PEBP1_HUMAN	185	21160	5	4	Phosphatidylethanolamine-binding protein 1
SERA_HUMAN	147	57368	8	3	D-3-phosphoglycerate dehydrogenase
PDIA1_HUMAN	139	57487	11	5	Protein disulfide-isomerase
DECR_HUMAN	68	36335	12	2	2,4-dienoyl-CoA reductase, mitochondrial
AK1C1_HUMAN	43	37229	4	2	Aldo-keto reductase family 1 member C1
PGAM1_HUMAN	31	28902	7	2	Phosphoglycerate mutase 1

Table 3.1 Proteins identified in each of the three different fishing experiments and not detected in the corresponding control experiments (Mascot score > 30, Pep(sig) value >1).

The intersection of these sets gave only a single protein as best partner (**Figure 3.8**).
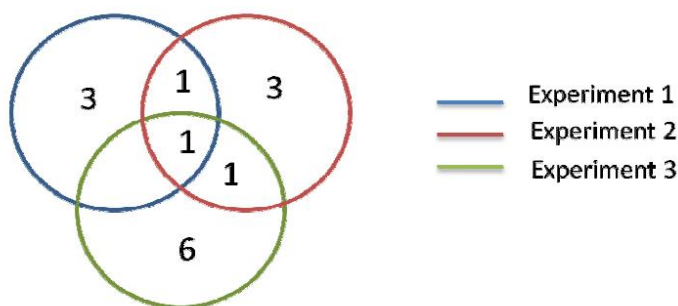
	Score	Mass	Matches	Pep(sig)	Description
Experiment 1	35	57480	9	3	Protein disulfide-isomerase
Experiment 2	67	57480	6	4	Protein disulfide-isomerase
Experiment 3	139	57487	11	5	Protein disulfide-isomerase

Figure 3.8 Venn diagram showing the intersection of the three sets of all the protein partners identified in the three different fishing experiments.

The protein identified was the Protein Disulfide Isomerase (PDI), a 57 kDa chaperone protein located in the endoplasmic reticulum.[74] PDI acts as a thiol oxidoreductase, it is able to catalyze the formation, breakage and rearrangement of disulfide bonds, and thus it is responsible for the regulation of oxidative protein folding as well as cell viability.[75] Several studies report that increased PDI levels were found in a

---

[74] (a) Goldberger, R. F.; Epstein, C. J.; Anfinsen, C. B. *J. Biol. Chem.* **1964**, *239*, 1406-1410; (b) Wilkinson, B.; Gilbert, H. F. *Biochim. Biophys. Acta Proteins Proteomics* **2004**, *1699*, 35-44.
[75] (a) Lovat, P. E.; Corazzari, M.; Armstrong, J. L. *Cancer Res.* **2008**, *68*, 5363-5369; (b) Frand, A. R.; Cuozzo, J. W.; Kaiser, C. A. *Trends Cell Biol.* **2000**, *10*, 203-210.

variety of human cancers, such as ovarian[76], prostate[77] and lung cancer.[78] PDI is considered a promising druggable target, as the inhibition of its activity leads to apoptosis in cancer.

The protein has five domains and in particular there are two cysteine residues in the **a** and **a'** domains which are essential for PDI activity.
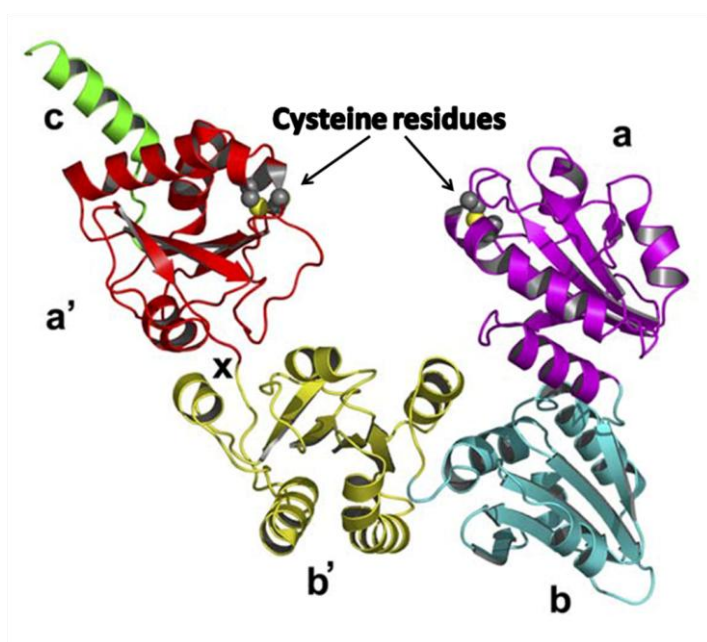

Figure 3.9 Representation of the PDI structure.

[76] Bonome, T.; Levinem D. A.; Shih, J.; Randonovich, M.; Pise-Masison, C. A.; Bogomolniy, F.; Ozbun, L.; Brady, J.; Barret, J. C.; Boyd, J.; Birrer, M. J. *Cancer Res.* **2008**, *68*, 5478-5486.
[77] Welsh, J. B.; Sapinoso, L. M.; Su, A. I.; Kern, S. G.; Wang-Rodriguez, J.; Moskaluk, C. A.; Frierson, H. F.; Hampton, G. M. *Cancer Res.* **2001**, *61*, 5974-5978.
[78] Beer, D. G. *et al. Nat. Med.* **2002**, *8*, 816-824.

The linker of derivative **13** has a disulfide bridge, hence it is possible to imagine that it may be responsible for the interaction with the protein. In order to verify whether the disulfide bridge of **13** may have a role in the interaction with PDI protein, a sulphur-free analog of **13** was synthesized. The new derivative **24** bears four propyl chains at the lower rim and four acetamido groups at the upper rim. It was obtained by acetylation of the corresponding tetramino calixarene **23**[79] (**Figure 3.10**).
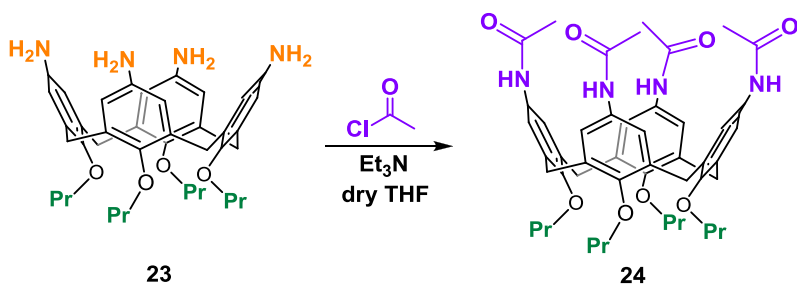
Figure 3.10 Synthesis of the tetracetamido calixarene **24**.

The interaction of **24** with PDI protein was studied through Surface Plasmon Resonance (SPR) methods by Prof. Casapullo and co-workers.[73]

[79] Jakobi, R. F.; Böhmer, V.; Gruettner, C.; Kraft, D.; Vogt, W. *New. J. Chem.* **1996**, *20*, 493-498.

Surface Plasmon Resonance is as a powerful optical detection technique for the investigation of biomolecular interactions in real time.[80] A light source passes through a prism, reflects on the back side of the sensor chip surface and arrives to the detector. At a certain incident angle, known as the resonance angle, light is absorbed by the electrons in the metal film on the sensor chip, causing them to resonate. These resonating electrons are also known as surface plasmons, which are sensitive to the surrounding environment. The result is an intensity loss in the reflected beam, which appears as a dark band on the detector and can be seen as a dip in the SPR reflection intensity curve (**Figure 3.11**). The shape and position of the SPR dip can then be used to convey information about the sensor surface. SPR is frequently used to study molecular binding interaction between free analyte molecules in solution and probe molecules which are immobilized on the sensor surface. As a molecular binding event takes place, the angular position of the dark band shifts (**Figure 3.11**).

---

[80] (a) Ritzefeld, M.; Sewald, N. *Journal of Amino Acids*, **2012**, 1-19; (b) Karlsson, R.; Katsamba, P. S.; Nordin, H.; Pol, E.; Myszka, D. G. *Anal. Biochem.* **2006**, *349*, 136–147.
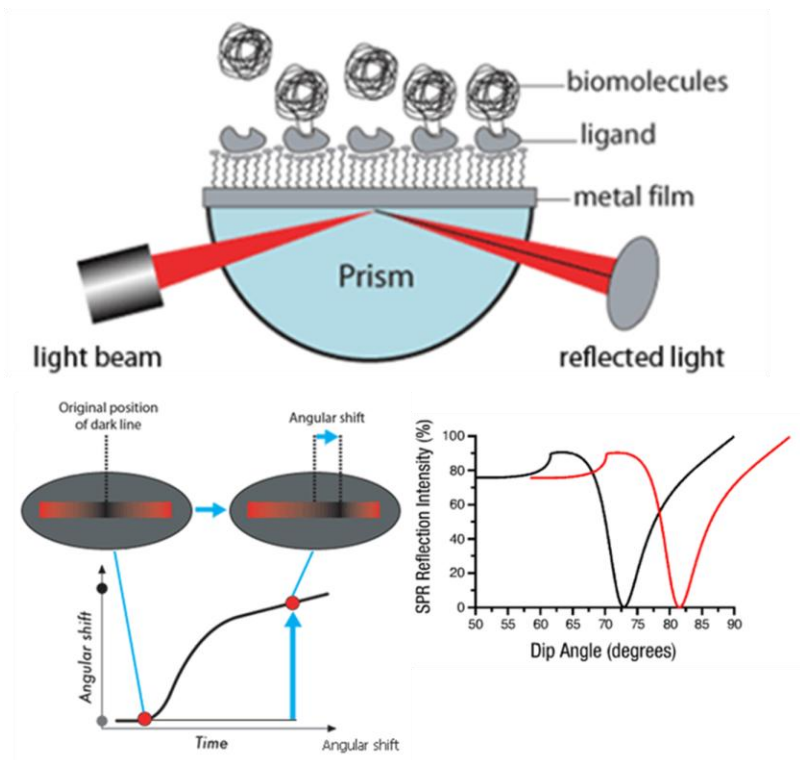
Figure 3.11 General principles of the SPR technique.

When an analyte with affinity to the immobilized ligand is introduced into the system, then binding events can be observed. Initially there are many binding sites available, resulting in a rapid increase in SPR response as the analyte binds to the ligand. While sample is continually injected into the system, analyte molecules continue to bind and the number of available binding sites decreases, corresponding to a decrease in the binding rate, until the system approaches

equilibrium and the number of molecules binding and unbinding becomes equal. When no more analyte is introduced into the system the molecules will continue to unbind, resulting in a decrease in SPR response (**Figure 3.12**). The association constant k_a can be extracted for the behavior of the binding response. Likewise the dissociation constant k_d can be extracted from the unbinding response. The ratio of these two rate constants affords the binding affinity (K_D) of the system.
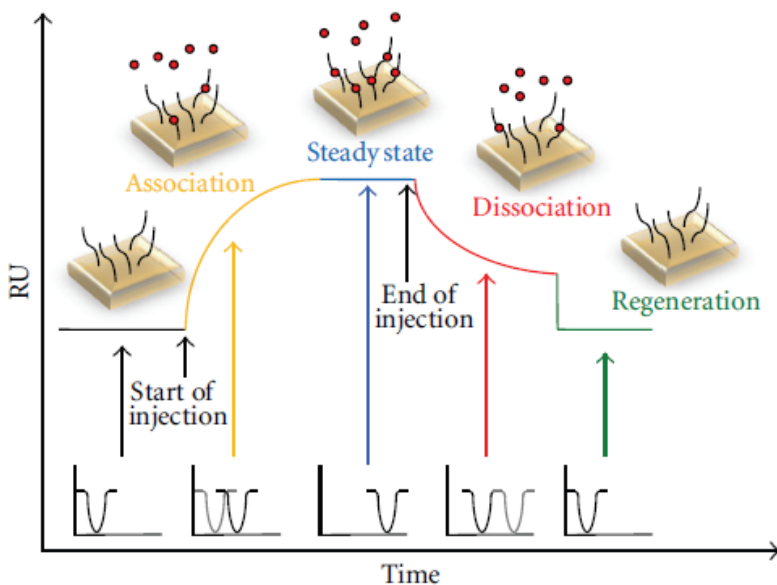

Figure 3.12

For our purposes PDI was immobilized on the surface of a CM5 chip, then solutions of **24** at three different concentrations (0.1-10 μM) were injected. The interaction experiments were carried out at a flow rate of 10 μl/min and the dissociation time was set at 600 seconds. Compound **24** was also injected over two different proteins, Peroxiredoxin 1 and Lamin B1, and over the unfunctionalized SPR chip, as a negative control.

The results showed a considerable affinity between the PDI and *p*AC **24**, with K_D = 11 μM, (**Figure 3.13**) while no binding was observed in the control experiments (**Figure 3.14-16**). These results confirmed the interactions between PDI and **24** and also allowed to rule out any participation of the disulfide bridge of **13**.
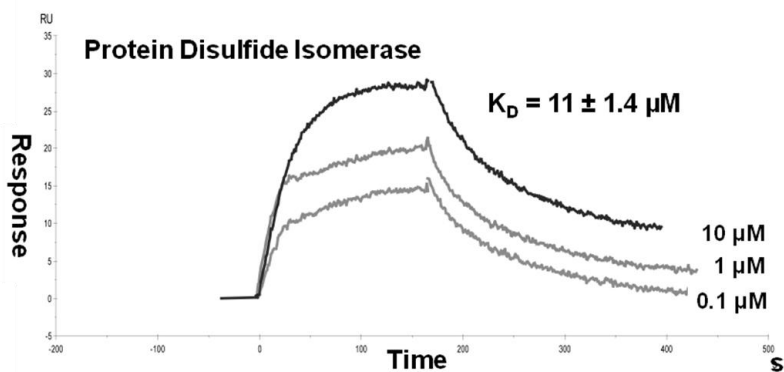

**Figure 3.13** Sensograms obtained after injections of *p*AC **24** on the immobilized PDI.
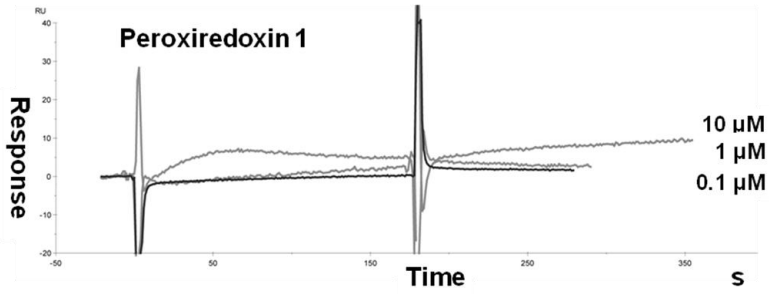
Figure 3.14 Sensorgrams obtained after injections of *p*AC **24** on the immobilized Peroxiredoxin 1.
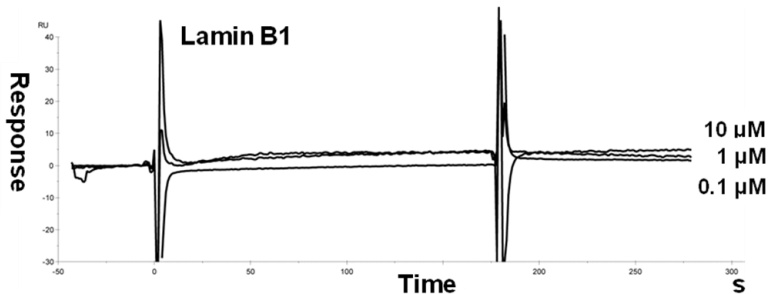

Figure 3.15 Sensorgrams obtained after injections of *p*AC **24** on the immobilized Lamin B1.
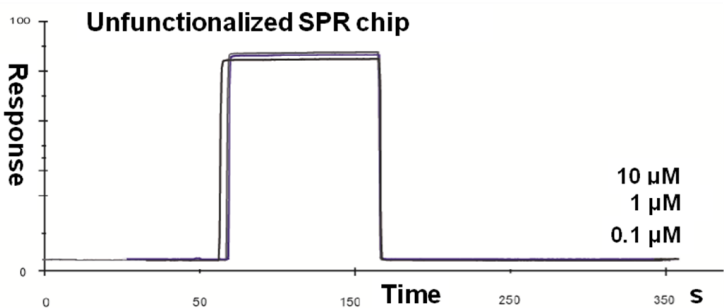

Figure 3.16 Sensorgrams obtained after injections of *p*AC **24** on the unfunctionalized SPR chip.

3.2.3 Molecular Docking

In order to gain more insight into the interaction of *p*AC **24** with PDI, a molecular docking study was performed. Protein Disulfide Isomerase presents four thioredoxin domains, **a**, **a'**, **b** and **b'**, arranged in the shape of a twisted "U" (**Figure 3.9**). The two active sites are located in the **a** and **a'** domains, while the **b'** domain contains a large hydrophobic pocket able to accommodate the substrates. The inside surface of the "U" is enriched in hydrophobic residues, facilitating interactions with misfolded proteins. Calixarene **24** is able to occupy the inside surface of the "U". The binding with the protein occurs in the hydrophobic pocket of the **b'** domain (**Figure 3.17**).
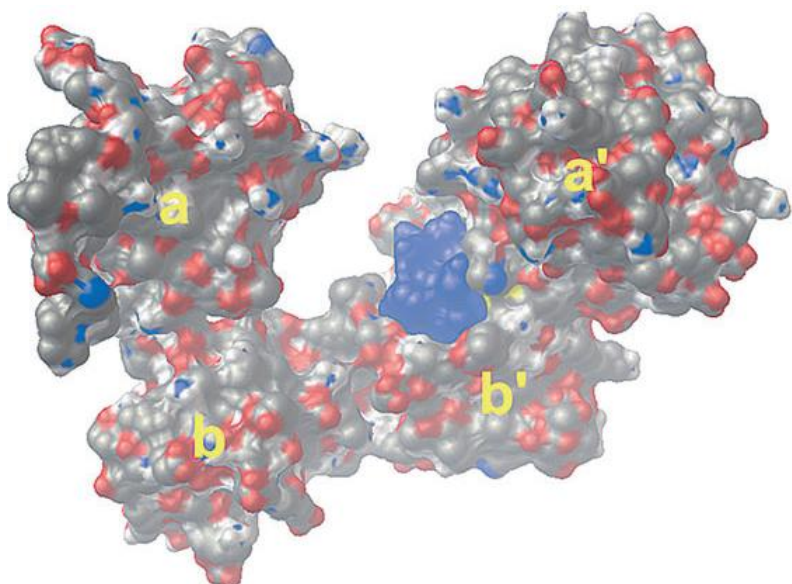
Figure 3.17 3D model of the binding mode of *p*AC **24** (depicted as a blue CKP representation) in the hydrophobic pocket in the **b'** domain of PDI.

In particular, **24** established two hydrogen bonds with Trp396 and His438, as well as π-stacking interactions between an aromatic ring of the calixarene core and Phe249 (**Figure 3.18a**). Moreover, the docking studies showed the establishment of van der Waals interactions between the hydrophobic walls of **24** and the apolar chains of isoleucine (Ile), phenylalanine (Phe) and leucine (Leu) amino acid residues in the protein binding site (**Figure 3.18b**).
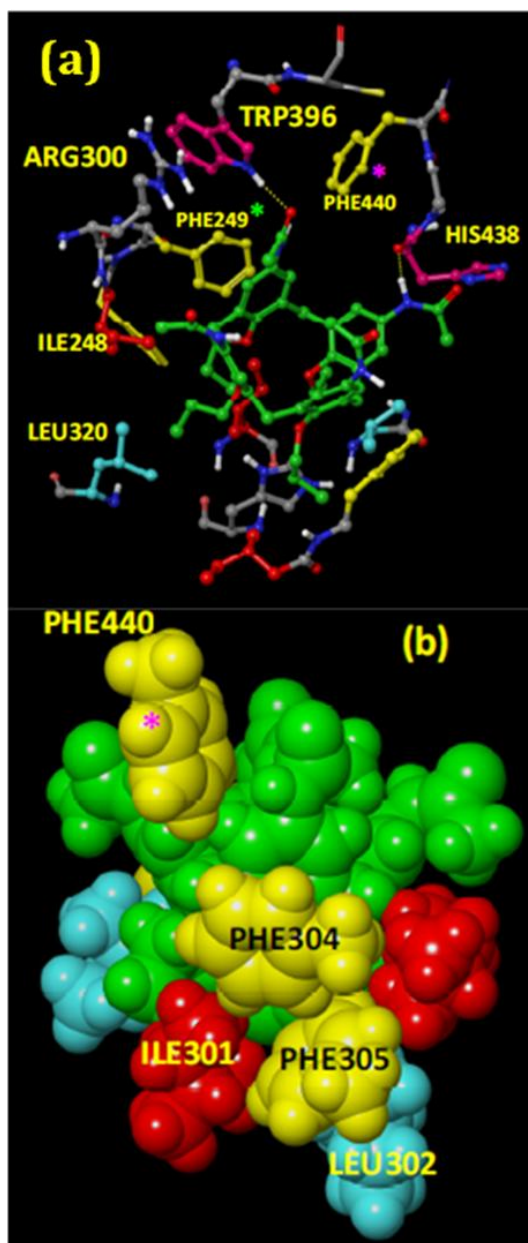
Figure 3.18 Interactions between **24** and PDI: (a) hydrogen bonds between amide groups of *p*AC **24** (in a green ball-and-

stick representation) and the TRP396 and HIS432 residues (in magenta) and π-stacking interactions with PHE249; (b) hydrophobic interactions of *p*AC **24** (in a green CPK model) with PHE, ILE and LEU amino acids.

The amino acid Trp396, located in the immediate proximity of the active site containing Cys397, plays an essential role in the redox-regulated conformational change between the reduced and oxidized forms of PDI.[81] This conformational change modulates the chaperone activity of PDI protein. It was reported that the mutation of Trp396 significantly impairs the redox-regulated conformational changes of PDI. Thus, the hydrogen-bond interaction between **24** and Trp396 could affect the catalytic activity of the enzyme by interfering with conformational change between reduced and oxidized PDI. In addition, the binding of the calixarene in the hydrophobic pocket of the protein could prevent the binding of other substrates.

Moreover the inhibition constant obtained by docking calculations is $K_i = 6.23$ μM, a value that is comparable to that obtained by SPR analysis ($K_D = 11$ μM).

[81] Wang, C.; Li, W.; Ren, J.; Fang, J.; Ke, H.; Gong, W.; Feng, W.; Wang, C. C. *Antiox. Redox Signaling* **2013**, *19*, 36-45

The role of the acetamido groups is crucial for the interaction with the protein. In fact, the molecular docking was also performed on the *p-tert*-butyl analogue of **24**, which has no possibility to establish hydrogen bonds. In this case the calixarene derivative showed a poor affinity for the PDI protein, with a $K_i = 8.23$ mM.

3.2.4   Biological activity studies[73,82]

Both the SPR analysis and Molecular Docking confirmed the ability of the *p*-tetracetamidocalix[4]arene **24** to bind the PDI protein. The next step was the investigation of the possible biological relevance of **24**. Considering that PDI is involved in the regulation of protein folding by promoting the rearrangement of disulfide bonds in substrate proteins, the potential ability of **24** to modulate the PDI activity was evaluated through an in vitro test based on the enzyme-catalyzed reduction of insulin, performed by Prof. Casapullo and co-workers.[73] In particular the test was based on the spectrophotometric measurement of the aggregation of reduced insulin chains. PDI reduces the insulin disulfide bonds in the presence of dithiothretiol (DTT) and the

---

aggregation of the reduced insulin chains can be measured at 620 nm.

PDI protein (0.8 µM) was exposed to different concentrations of *p*AC **24** (50 and 100 µM) at 37 °C for 30 min in a sodium phosphate buffer. Then a mixture of EDTA, DTT and insulin was added and the reaction was monitored every 5 minutes at 620 nm. The experiment was repeated in absence of **24** as a control and the specific PDI activities were estimated by subtracting the absorbance of the control buffer (**Figure 3.19**).
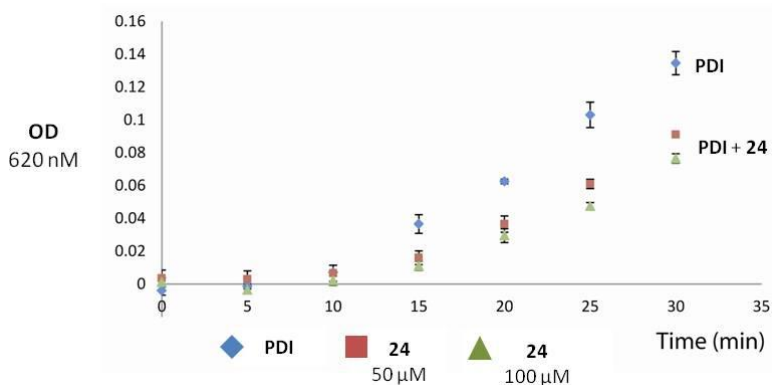

Figure 3.19 Effect of **24** on the PDI catalytic reduction of insulin

The plots in **Figure 3.19** clearly showed that the PDI activity was impaired in the presence of *p*AC **24** in a concentration-dependent fashion. Therefore the interaction between the calixarene and the PDI had a significant impact on the function of the protein.

Furthermore, thanks to a collaboration with Dr. Beatrice Macchi the in vitro ability of *p*AC **24** to inhibit the viability and metabolic activity of cancer cells was evaluated.[82] The derivative was tested against two different cell lines: CAL-27 (oral adenosquamous carcinoma cell line) and PC-3 (human prostate cancer cell line).

The cell lines were incubated for 24 h with dimethylsulfoxide solutions of compound **24** at different concentrations. The cell viability was evaluated by a trypan blue exclusion test and the metabolic activity through a MTS reduction assay. The cells were also incubated with a known chemotherapeutic drug, 7-ethyl-10-hydroxycamptothecin (SN38) and a commercial synthetic PDI inhibitor 16F16[83] as positive controls (**Figure 3.20**)
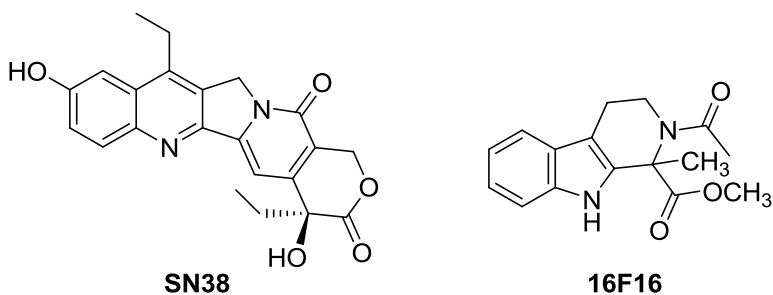

Figure 3.20 Chemical structures of **SN38** and **16F16**.

---

[83] Hoffstrom, B. G.; Kaplan, A.; Letso, R.; Schmid, R. S.; Turmel, G. J.; Lo, D. C.; Stockwell, B. R. *Nat. Chem. Biol.* **2010**, *6*, 900-906.

The results of the biological tests are expressed in **Table 3.2** as IC_{50} and CC_{50} values for the viability and metabolic assay respectively.

	Cell Lines	$IC_{50} \pm SD\ (\mu M)^a$	$CC_{50} \pm SD\ (\mu M)^b$
24	CAL-27	20.5±0.8	31±4
24	PC-3	24.5±0.9	283±10
SN38	CAL-27	3.0±0.9	3.2±0.3
SN38	PC-3	11.5±0.2	6.9±0.9
16F16	CAL-27	7.6±0.4	8.8±1.9
16F16	PC-3	25±0.6	14.7±1.6

[a]IC50 is the inhibitory concentration required to inhibit 50% of cell viability;
[b]CC50 is the metabolic activity cytotoxic inhibitory concentration 50%, evaluated in the CAL-27 and PC3 cell lines by MTS assay.

Table 3.2. Evaluation of the cytotoxicity of *p*AC **24** in comparison with SN38 and 16F16.

The information obtained from the biological assays were really interesting.[68] The calixarene derivative **24** was cytotoxic toward both the cell lines, with IC_{50} values of 20.5 and 24.5 μM for CAL-27 and PC-3 respectively, while the IC_{50} values of SN38 were slightly lower. Interestingly **24** showed the same ability of the commercial PDI inhibitor 16F16 to inhibit PC-3 cell proliferation. In fact their IC_{50} overlapped, thus suggesting a similar action mode.

Other interesting consideration can be made on the basis of the evaluation of the metabolic inhibitory effect. Particularly the CC_{50} values of **24** are higher than those for SN38 and 16F16. In the ideal situation IC_{50} concentrations lower than CC_{50} values are desirable, with CC_{50} values as high as possible. The ratio $SI = CC_{50}/IC_{50}$ is a value that gives information about the selectivity of a drug (SI = selectivity index). The higher the index the more selective the compound will be toward a pathogen.

The CC_{50} value of **24** for PC-3 cell line is 283 μM, which is 20 time higher than the commercial inhibitor 16F16. As a consequence the selectivity index for **24** is SI = 11.5, a really promising result, that indicates that *p*AC **24** has a good selectivity towards human prostate cancer cell lines.

3.2.5 Synthesis of an advanced intermediate for a new calixarene ligand

The interesting results achieved with derivative *p*AC **24** encouraged us to deepen the study of the biomolecular recognition abilities of novel calixarene derivatives through the chemical proteomics approach.

The derivative **24**, bearing four acetamido groups as hydrogen

bond donor/acceptor sites, was chosen as a basic compound for a preliminary investigation. Probably a more interesting behavior could be observed for a more complex derivative. Thus the next step in this PhD research project was the synthesis of a new calixarene derivative bearing different substituents at the exo rim and to evaluate its recognition properties. The designed compound **25** presents four L-hystidine moieties (**Figure 3.21**).
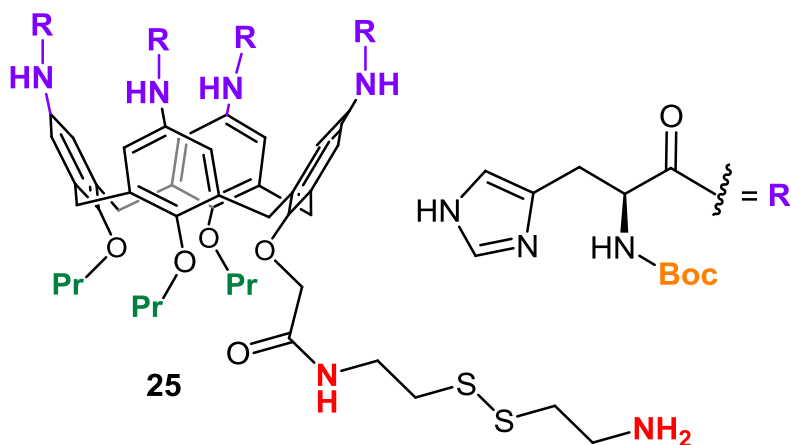

Figure 3.21 Structure of the *p*-tetrahistidinecalix[4]arene **25**

Differently by *p*AC **24**, the derivative **25** presents multiple hydrogen bond donor/acceptor sites and thus could establish multiple interactions with proteins. Indeed, as well as the amido groups directly bound at the *para* position on the calixarene aromatic rings, the designed compound **25** also

presents four amino groups of the amino acid portion, as well as two nitrogen atoms for each imidazole ring. The presence of all these possible binding sites could lead to the formation of new protein-calixarene complexes. The synthetic strategy for compound **25** is depicted in **Scheme 3.2a-b**.

In this case the synthetic approach was slightly different from the synthesis of *p*AC **13**. In fact compound **25** present Boc-protected amino groups to avoid competition reaction during the immobilization on the solid support.
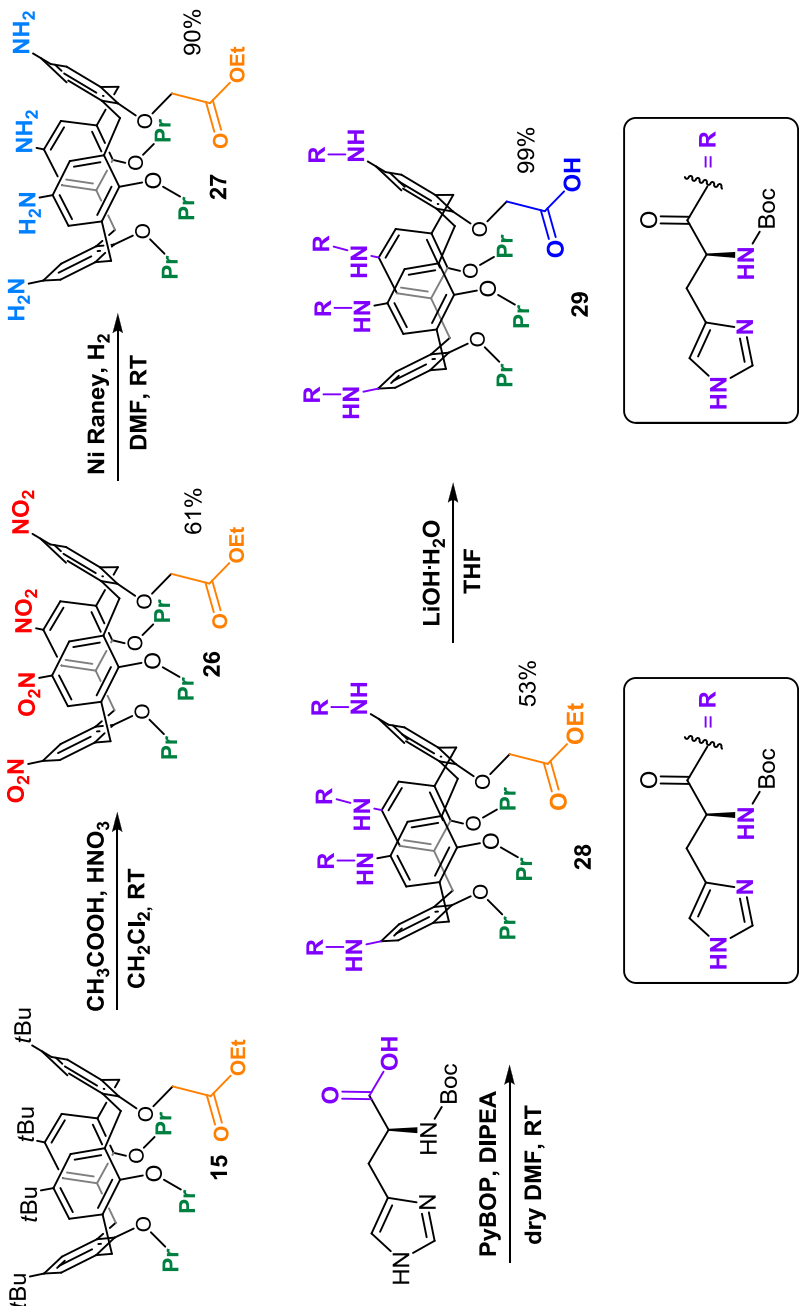
Scheme 3.2a Synthesis of **29**.
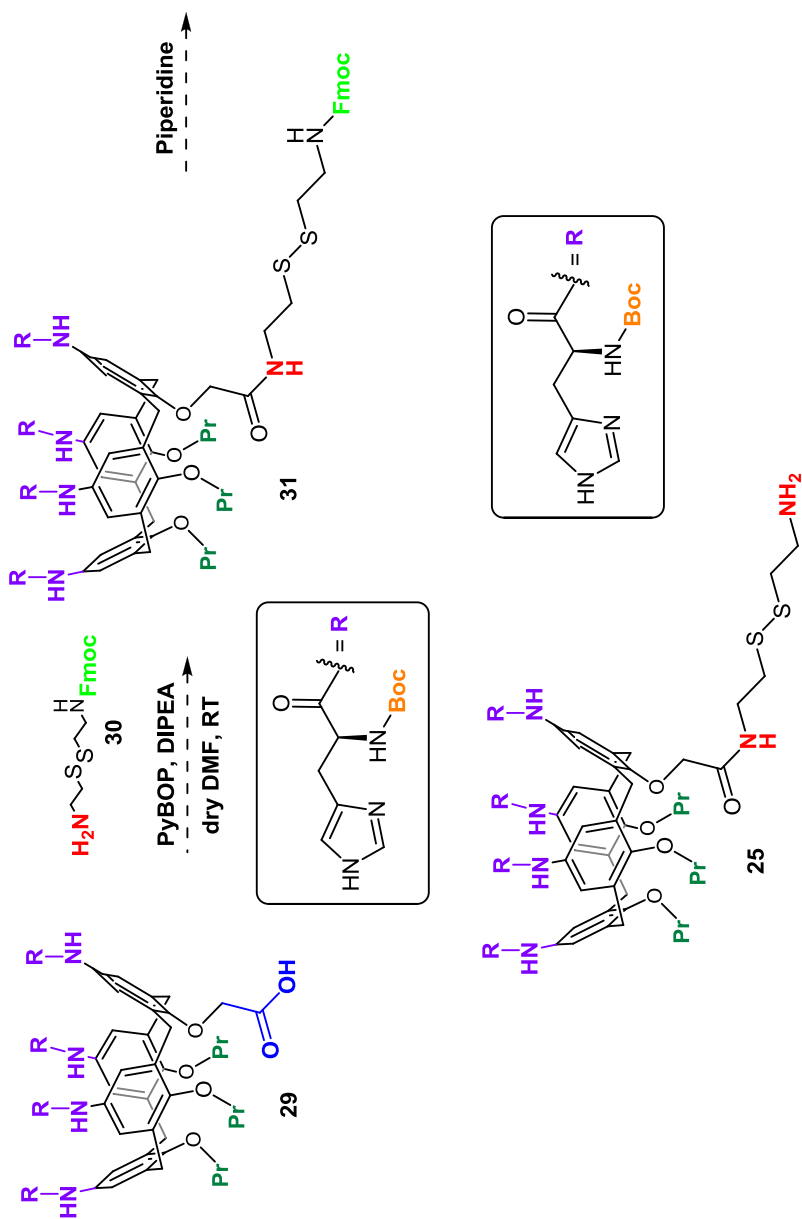
Scheme 3.2b Synthesis of **25**.

The tetranitro calix[4]arene **26**[70] was obtained by exhaustive nitration of the *p-tert*-butylated precursor **15**.[70] Then the nitro groups were reduced via Nickel Raney hydrogenation, affording the tetraminocalix[4]arene **27**.[70] The latter was used for the coupling with the desired amino acid, with (Benzotriazol-1-yloxy)tripyrrolidinophosphonium hexafluorophosphate (PyBOP) and N,N-diisopropylethilamine (DIPEA) as coupling reagents in dry DMF. A commercial N^α-Boc protected histidine was used for this purpose. In this case the carbonyl functionality at the calixarene endo rim was an ester group to avoid the formation of undesired side products during the coupling reaction. Therefore the ester group of **28** was hydrolyzed to carboxylic acid with lithium hydroxide in THF at room temperature, affording compound **29** in quantitative yields. The ^{1}H NMR spectrum of **29** showed the presence of the signals of the Boc groups at $\delta = 1.34$-1.39 ppm and the singlet of OCH_2COOH at $\delta = 4.73$ ppm. The aromatic protons showed signals at $\delta = 6.77$, 6.89 ppm and $\delta = 7.22$-7.30 ppm, overlapped with the protons of the imidazole rings. Finally at $\delta = 8.56$-8.63 were found the –NH signals of the imidazole units (**Figure 3.22**).
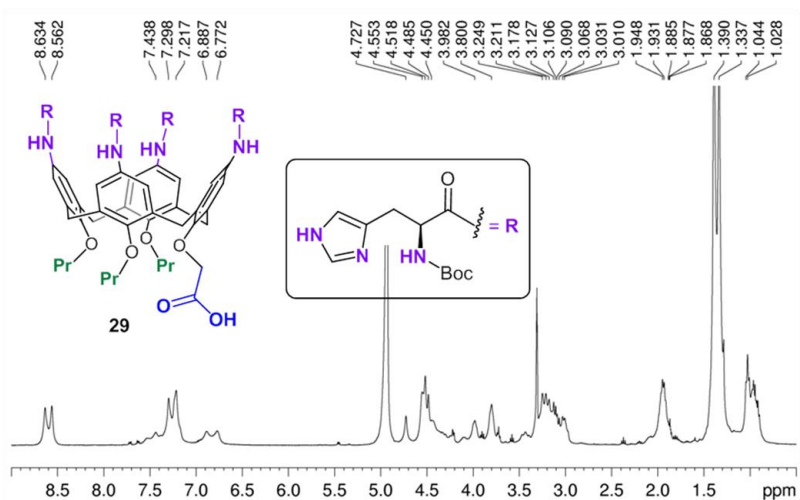
Figure 3.22 ^{1}H NMR spectrum of **29** (400 MHz, MeOD, 298K).

A Fmoc-protected spacer arm **30**, suitably synthetized, could be coupled to the carboxylic functionality of **29**, affording compound **31**. The removal of the Fmoc-protective group by treatment with piperidine in DMF cpuld lead to the isolation of the final product **25** (**Scheme 3.2b**). At last, the removal of Boc-groups could be performed after the immobilization on the solid support.

3.3 Conclusions

In this chapter a MS-based chemical proteomics approach was used to investigate the biomolecular recognition properties of calixarene derivatives bearing acetamido groups at the exo rim.[68] In particular this study revealed that *p*-acetamido calixarenes were able to bind the protein disulfide isomerase (PDI). The interaction between the derivative **24** and the PDI protein was deeply investigated through SPR analysis and molecular docking calculations.[68] Compund **24** was able to bind the protein inside the hydrophobic pocket in the **b**' domain, via the formation of hydrogen bonds through the acetamido groups, as well as van der Waals interactions through the calixarene scaffold and amino acid residues. Biological in vitro tests showed that *p*AC **24** was able to impair the PDI chaperone activity.[68] Besides it showed cytotoxic and cytostatic activity toward CAL-27 and PC-3 tumor cell lines.[68] On the basis of these results, a new derivative presenting histidine moieties at the exo rim was designed and the synthesis of an advanced intermediate is reported.

Chapter 4

4. Multivalent systems in glycosidase inhibition

Several systems in biology interact through multiple simultaneous molecular contacts. In the last few years this concept was adopted as new strategy for the design and development of drug candidates.

Multivalency is the ability of a molecule to bind another molecule via multiple simultaneous non-covalent interactions.[84] The valency represents the number of binding functionalities for a given compound. Multiple simultaneous interactions provide higher specificity and thermodynamic and kinetic stability compared to a single interaction. Therefore multivalent systems usually show affinity enhancement compared to the corresponding monovalent ligand. This behavior is known as "the multivalent effect".[85]

The multivalent effect is a consequence of several binding modes (**Figure 4.1**). The binding event between a ligand and its receptor is a reversible process, thus if the association/dissociation processes are fast enough the

---

[84] Mammen, M.; Choi, S. K.; Whitesides, G. M. *Angew. Chem. Int. Ed.* **1998**, *37*, 2754-2794.
[85] Lundquist, J. J.; Toone, E. J. *Chem. Rev.* **2002**, *102*, 555-578.

multivalent effect can be explained in terms of statistical rebinding events. In fact, the high local concentration of ligand should favor the rebinding of the substrate (**Figure 4.1a**). Other mechanisms such as favorable non-specific interactions (**Figure 4.1b-c**) and the presence of secondary binding interactions (subsite binding) can also be possible (**Figure 4.1d**).
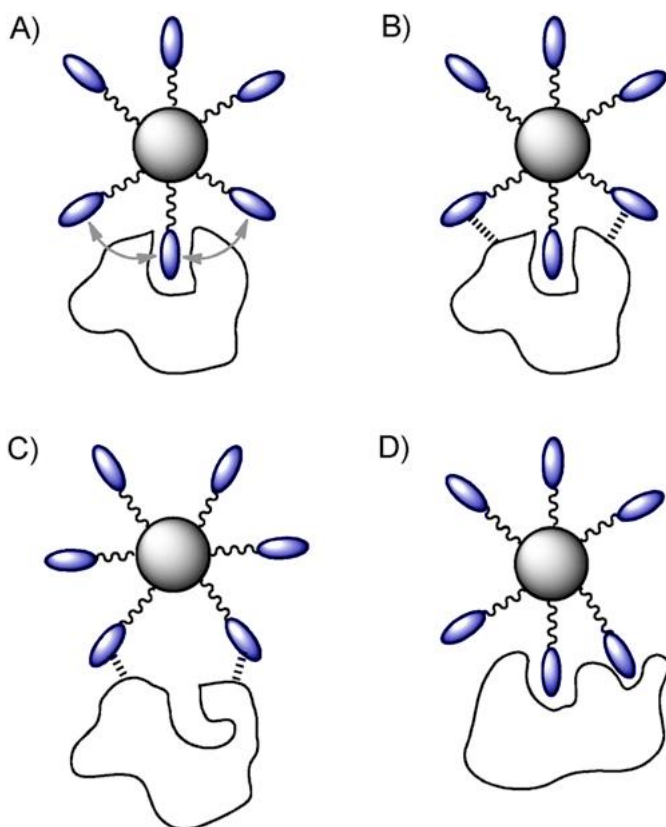

Figure 4.1 Possible binding modes in multivalent systems.

Recently glycosidase inhibitors have gained considerable clinical relevance.[86] The selective hydrolysis of glycosidic bonds in carbohydrates and glycoconjugates is extremely diffused in living organisms and is indeed involved in a wide range of key cellular processes in biological systems.[87] This process is found in a wide range of diseases such as diabetes, viral infection and tumor metastasis.[88] Very recently there have been enormous advancement in the research for glycosidase inhibitors thanks to the discovery of iminosugar-based multivalent clusters.[89] Applications of this inhibitors to glycosidases of therapeutic interest have led to very promising results in the field of rare genetic diseases such as cystic fibrosis[90] and Gaucher disease[91]. The major advances in the area of multivalent effect in glycosidase inhibition have been achieved with iminosugar clusters synthesized by Cu^I-catalyzed azide-alkyne cycloaddition (CuAAC),[92] in which

[86] Brás, N.; Cerqueria, N. M. F. S. A.; Ramos, M. J.; Fernandes, P. A. *Expert Opinion Ther. Patents* **2014**, *24*, 857-874.

[87] Davies, G. J.; Gloster, T. M.; Henrissat, B. *Curr. Opin. Struct. Biol.* **2005**, *15*, 637-645.

[88] (a) Lillelund, V. H.; Jensen, H. H.; Liang, X.; Bols, M. *Chem. Rev.* **2002**, *102*, 515–553; (b) Asano, N. *Glycobiology* **2003**, *13*, 93R –104R; (c) Gloster, T. M.; Davies, G. J. *Org. Biomol. Chem.* **2010**, *8*, 305 –320.

[89] Compain, P.; Bodlenner, A. *ChemBioChem* **2014**, *15*, 1239-1251.

[90] Compain, P.; Decroocq, C.; Joosten, A.; de Sousa, J.; Rodriguez-Lucena, D.; Butters, T. D.; Bertrand, J.; Clément, R.; Boinot, C.; Becq, F.; Norez, C. *ChemBioChem* **2013**, *14*, 2050-2058.

[91] Joosten, A.; Decroocq, C.; de Sousa, J.; Schneider, J.; Etamé, E.; Bodlenner, A.; Butters, T. D.; Compain, P. *ChemBioChem* **2014**, *15*, 309-319.

[92] Kolb, H. C.; Finn, M. G.; Sharpless, K. B. *Angew. Chem. Int. Ed.* **2001**, *40*, 2004-2021.

iminosugars with a terminal azido functionality are grafted onto a suitable scaffold bearing alkyne moieties.

4.1 Applications of multivalency in glycosidase inhibition

Since 1-deoxynojirimycin (DNJ) is a glycosidase inhibitor, it was chosen as ligand for the synthesis of several multivalent iminosugar clusters (**Figure 4.2**).
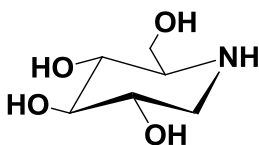

**1-deoxynojirimycin
DNJ**

Figure 4.2

One of the first studies on glycosidase inhibition through high valency clusters was based on a C_{60} platform. Multivalent fullerene-based adducts were prepared by CuAAC with twelve DNJ units (**Figure 4.3**).[93] For the first time strong affinity enhancements were observed, up to three orders of

---

[93] Compain, P.; Decroocq, C.; Iehl, J.; Holler, M.; Hazelard, D.; Mena Barragán, T.; Ortiz Mellet, C.; Nierengarten, J. F. *Angew. Chem. Int. Ed.* **2010**, *122*, 5889-5892.

magnitude with respect to a single DNJ unit. In particular, the best affinity enhancement was observed with the dodecavalent DNJ cluster with a C_6 linker, toward Jack bean α-mannosidase. A relative inhibition potency increase of almost 180-fold was observed, compared to the corresponding monovalent ligand.
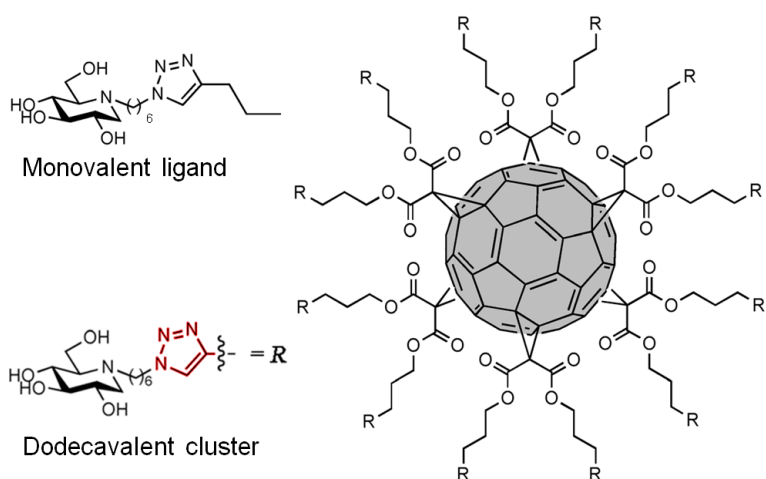
	Monovalent ligand	Dodecavalent cluster	rp	rp/n
α-mannosidase	322	0.15	2147	179

Glycosidase inhibitory activity (K_i [μM])
rp = relative inhibition potency;
rp/n = relative inhibition potency/number of iminosugar unit

**Figure 4.3** C_{60}-based iminosugar cluster and inhibition potency with α-mannosidase.

Even better results were achieved using β-cyclodextrins (βCD) as scaffolds.[94] In fact, as well as allowing the construction of high valency systems, the advantage of the β-cyclodextrin core relies in the different spatial orientation of the ligands. With appropriate functionalization methodologies, the iminosugar units can be grafted either on the primary or secondary face, or even on both of them.

The multivalent inhibitory effect was evaluated for a series of hepta- or 14-valent β-CD-based iminosugar clusters, with different ligands and alkyl spacer lengths (C_6 and C_9).

The nature of the scaffold is crucial for the modulation of the inhibitory activity and selectivity. In fact, while the C_{60} based iminosugar cluster showed multivalent effects for other glycosidases, like isomaltase and naringinase, the β-CD-based analogous, with similar valency and with same ligand (DNJ) and alkyl spacer length (C_6), manifested affinity enhancements toward α-mannosidase only.

The best affinity enhancements were observed for a 14-valent DNJ cluster, which showed inhibitory activity against Jack bean α-mannosidase in the nanomolar range (**Figure 4.4**).

---

[94] (a) Decroocq, C.; Rodriguez-Lucena, D.; Russo, V.; Mena Barragán, T.; Ortiz Mellet, C.; Compain, P. *Chem. Eur. J.* **2011**, *17*, 13825-13831; (b) Decroocq, C.; Joosten, A.; Sergent, R.; Mena Barragán, T.; Ortiz Mellet, C.; Compain, P. *ChemBioChem* **2013**, *14*, 2038-2049.
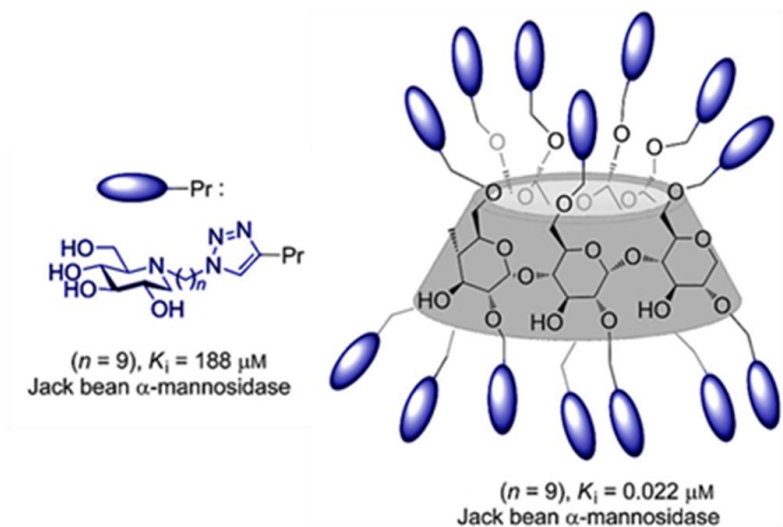
Monovalent ligand	14-valent cluster	rp	rp/n
188	0.022	8546	610

Glycosidase inhibitory activity (K_i [μM])
rp = relative inhibition potency;
rp/n = relative inhibition potency/number of iminosugar unit

Figure 4.4

The 14-valent DNJ cluster with a C_9 linker showed an enormous multivalent effect, with an affinity enhancement over the corresponding monovalent ligand of almost four orders of magnitude. The inhibition potency of each ligand was increased more than 600-fold (rp/n = 610).

Other studies were carried on different scaffolds with different spatial orientations, such as porphyrins.[95] Moreover

[95] Brissonnet, Y.; Ortiz Mellet, C.; Morandat, S.; Garcia-Moreno M. I.; Deniaud, D.; Matthews, S. E.; Vidal, S.; Sesták, S.; El Kirat, K.; Gouin, S. G. *J. Am. Chem. Soc.* **2013**, *135*, 18427-18435.

very recently first examples of cyclopeptoid-based iminosugar clusters were reported. The derivatives showed significant inhibitory multivalent effect for α-mannosidase.[96]

## 4.2 Calix[*n*]arenes as scaffolds for multivalent systems

Calix[*n*]arenes are particularly suitable as scaffolds for the synthesis of multivalent ligands, thanks to their variable number of reactive position for attaching the ligand functions and well defined different conformations.

The introduction of sugar moieties (D-glucose, N-acetyl-D-glucosamine, D-galactose etc.) at the exo rim of a calix[8]arene core for the synthesis of potential protein surface binders was reported.[97]

Tetravalent calix[4]arene iminosugar clusters were also reported and their binding affinity towards glycosidases was investigated (**Figure 4.5**).[95]

---

[96] Lepage, M. L.; Meli, A.; Bodlenner, A.; Tarnus, C.; De Riccardis, F.; Izzo, I.; Compain, P. *Beilstein J. Org. Chem.* **2014**, *10*, 1406-1412.
[97] Consoli, G.; Cunsolo, F.; Geraci, C.; Mecca, T.; Neri, P. *Tetrahedron Lett.* **2003**, *44*, 7467-7470.
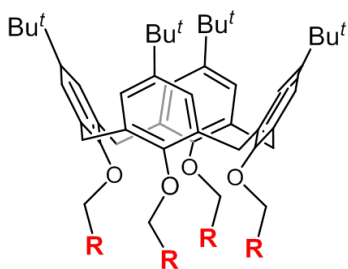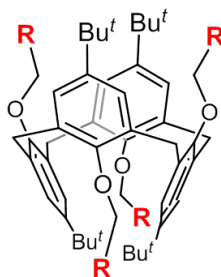
Conformation	K_i (μM)	rp	rp/n
cone	20	20	5
1,3- alternate	1.5	267	67
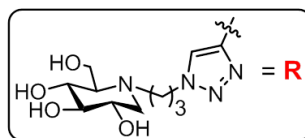
Inhibitory activity (K_i [μM]) against Jack bean α-mannosidase.
K_i monovalent ligand = 400 μM
rp = relative inhibition potency;
rp/n = relative inhibition potency/number of iminosugar unit

Figure 4.5 Tetravalent calix[4]arene clusters with different spatial orientation.

Although the identical valency, very different inhibition profiles were observed, thus indicating that the spatial distribution of the ligands is crucial for the inhibitory activity.

Applications of tetravalent and octavalent calixarene based clusters with sialic acid moieties were found in the inhibition of viral activities.[98] The clusters were obtained by copper-catalyzed cycloaddition of a propargyl thiosialoside with a

---

[98] Marra, A.; Moni, L.; Pazzi, D.; Corallini, A.; Bridi, D.; Dondoni, A. *Org. Biomol. Chem.* **2008**, *6*, 1396.1409.

calix[4]arene platform bearing azido groups (**Figure 4.6**).
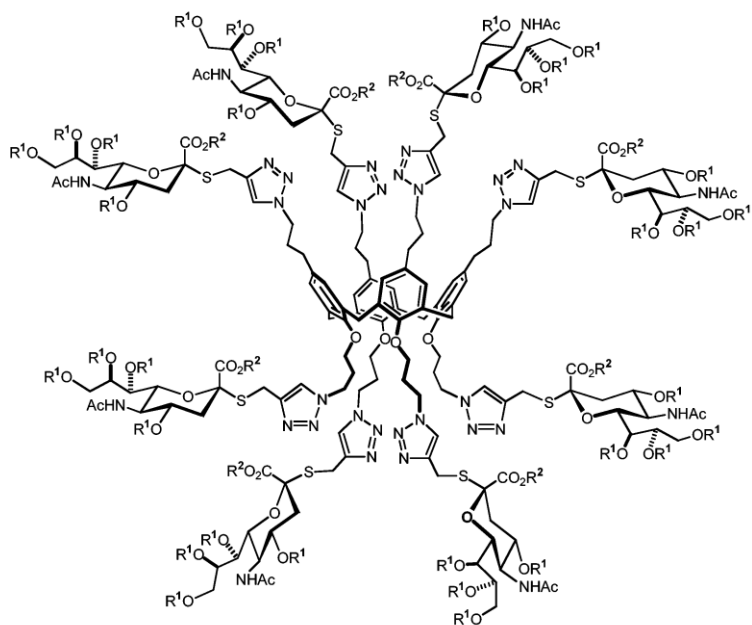
Figure 4.6 Representation of an octavalent sialoside calix[4]arene cluster.

The derivatives were able to inhibit the hemagglutination and the viral infectivity mediated both by BK and influenza A viruses at submillimolar concentrations.

4.3 Multivalent iminosugar calix[8]arene conjugates – Results and discussion

On the basis of the considerations reported above, the attention was focused on the synthesis of multivalent iminosugar-calix[8]arene conjugates **32-33** (**Figure 4.7**). These compounds have been obtained by Cu^I-catalysed azide-alkyne cycloaddition (CuAAC) between polyalkyne calix[8]arene scaffolds and azide-armed iminosugars. The calix[8]arene cores can ensure a high valency, up to eight sugar unit per compound (**32a-b**), which can be modulated by the presence of an intramolecular bridge (**33a-b**).
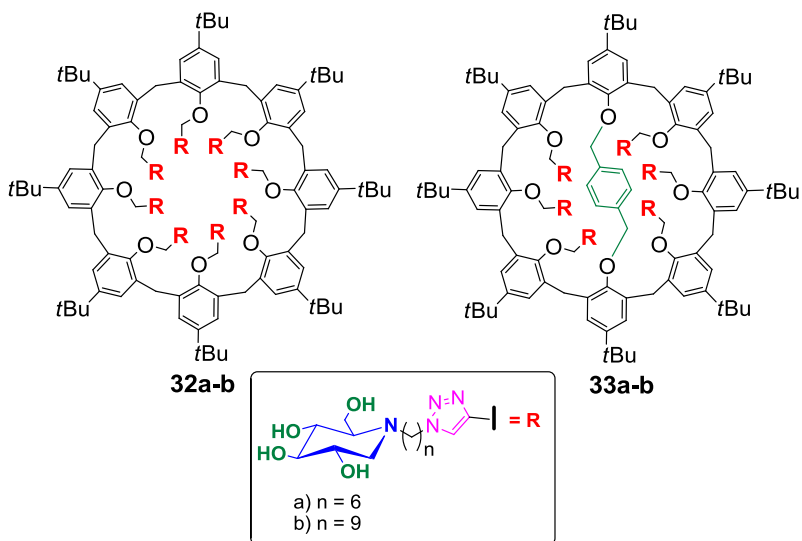

**Figure 4.7** Multivalent iminosugar-calix[8]arene conjugates **32-33**.

The intramolecular bridge was designed to evaluate whether a more rigid conformation is able to influence the potential inhibitory activity.

This project was developed in collaboration with Prof. Philippe Compain from the University of Strasbourg.

The glycosidase inhibition abilities of glycoconjugates **32-33** are herein reported.

4.3.1 Synthesis of the multivalent iminosugar-calix[8]arene conjugates

Calix[8]arenes conjugates **32**-**33** were obtained by Cu^I-catalyzed azide-alkyne cycloaddition (CuAAC) between calixarene scaffolds **36**-**37**, which present propargyl groups at the endo rim, and azide-armed DNJ units with different alkyl chains (C$_6$-C$_9$). The synthetic route is outlined in **Scheme 4.1a-b**.
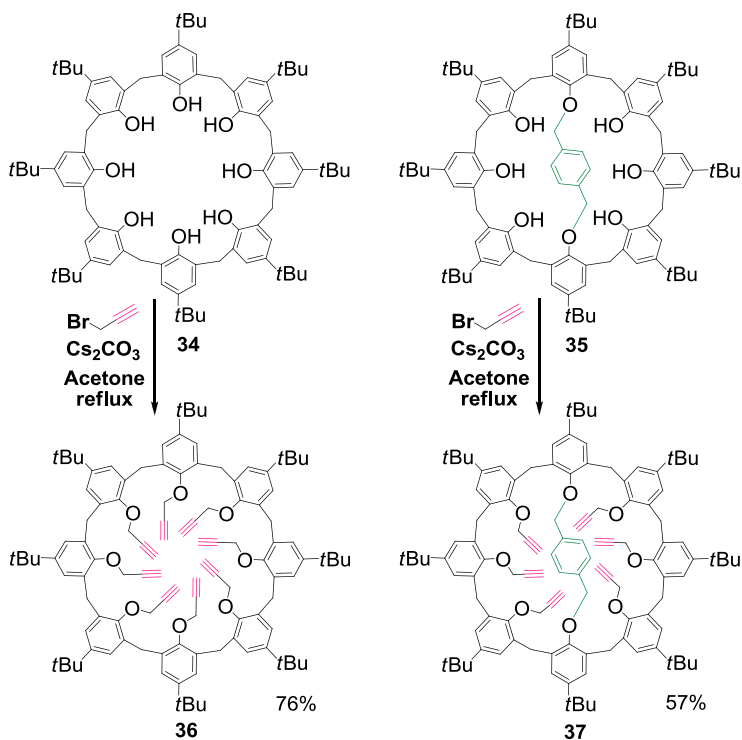
Scheme 4.1a

Polyalkyne calix[8]arenes **36**-**37** were synthesized by alkylation of the corresponding calix[8]arenes with propargyl bromide, using Cs_2CO_3 as a base and acetone as solvent. The bridged calix[8]arene **35** was obtained by a procedure which allows the selective alkylation at the 1,5-position.[99] This was

[99] (a) Consoli, G. M. L.; Cunsolo, F.; Geraci, C.; Neri, P. *Org. Lett.*, **2001**, *3*, 1605-1608; (b) Consoli, G. M. L.; Cunsolo, F.; Geraci, C.; Gavuzzo, E.; Neri, P. *Tetrahedron Letters*, **2002**, *43*, 1209-1211; (c) Gregoli, L.; Russo, L.; Stefio, I.; Gaeta, C.; Arnaud-Neu, F.; Hubscher-Bruder, V.; Khazaeli-Parsa, P.; Geraci, C.; Neri, P. *Tetrahedron Letters*, **2004**, *45*, 6277-6281.

possible thanks to the template effect of Cs^+. Indeed the calix[8]arene adopts a bend conformation in which the phenolic groups in positions 1 and 5 face each other and are suitable to be alkylated (**Figure 4.8**).
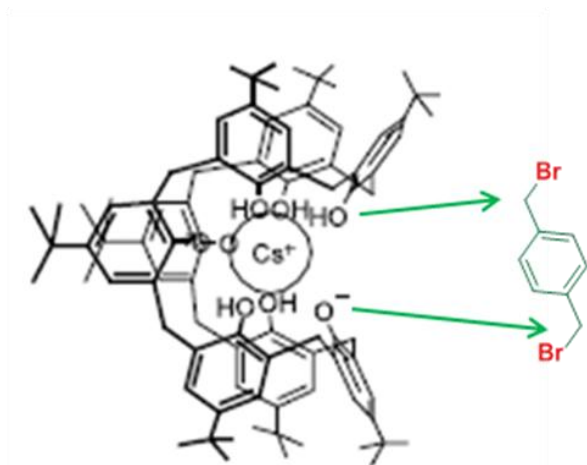

Figure 4.8

Afterwards a Cu^I-catalyzed azide-alkyne cycloaddition (CuAAC) was performed on both propargylated calix[8]arenes **36** and **37**. Two different azide-armed DNJ iminosugars were used (**Scheme 4.1b**), with different alkyl chains (C_6 and C_9) to evaluate the influence of the spacer length in the inhibitory activity. The cycloaddition reactions were performed by dissolving the calix[8]arene derivative in DMF in an ACE pressure tube. Then a solution of $Cu_2SO_4\cdot 5H_2O$ and sodium ascorbate in water was added and the reaction mixture was heated under microwave irradiation

104

at 800 W for 20-30 minutes. To remove the copper salts the crude products were treated with a solution of $CH_3CN/AcOEt/30w\%NH_4OH$ and filtrated on a small pad of silica. After flash column chromatography on silica gel products **38a**-**b** and **39a-b** were isolated.

Scheme 4.1b

106
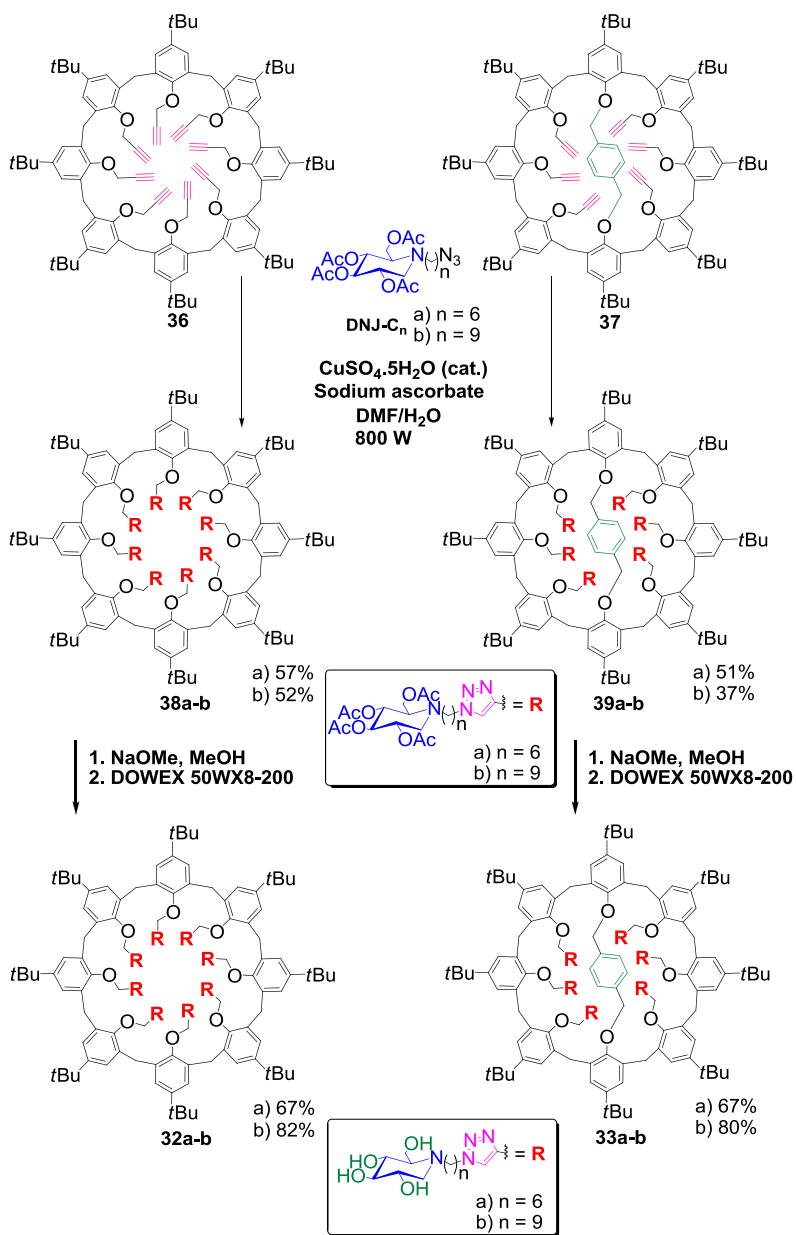
The ^{1}H and ^{13}C NMR spectra of derivative **38a** are reported as example. Due to the C_8 symmetry of **38a**, the ^{1}H NMR spectrum in CDCl$_3$ (**Figure 4.9**) showed one singlet at $\delta = 0.89$ ppm relative to *t*-Bu groups, one signal for the aromatic hydrogen atoms at $\delta = 6.80$ ppm and the hydrogen for the triazole rings, at $\delta = 7.78$ ppm.
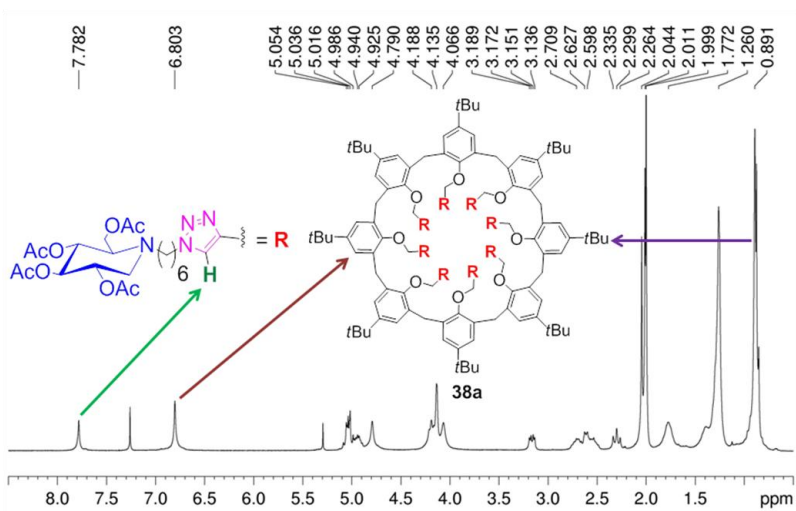

Figure 4.9 ^{1}H NMR spectrum of **38a** (300 MHz, CDCl$_3$, 298K).

Besides the ^{13}C NMR spectrum (**Figure 4.10**) showed the signal of the *tert*-butyl groups at 31.46 ppm and four signals for the carbonyl groups of the iminosugar units between 169 and 171 ppm. Similar NMR spectra were observed for derivative **38b**.
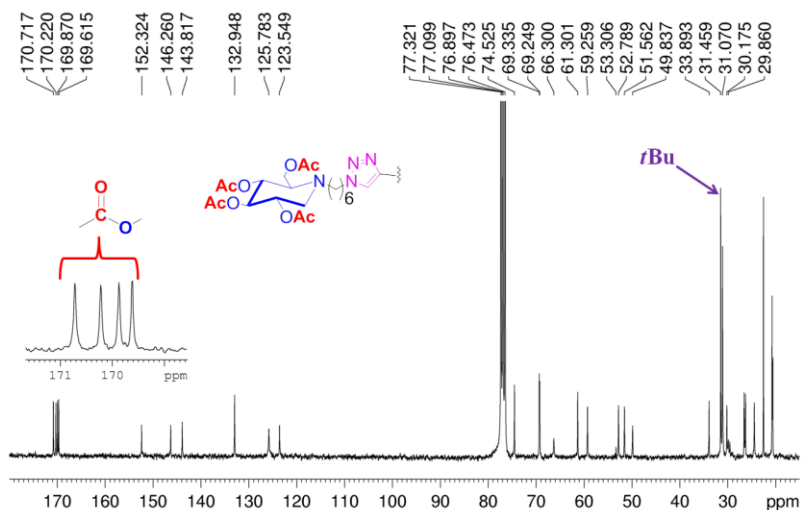
Figure 4.10 ^{13}C NMR spectrum of **38a** (75 MHz, CDCl$_3$, 298K).

Conversely the NMR spectra of **39a-b** were more complicated. In fact, due to the presence of the intramolecular bridge, the derivatives have a C_2 symmetry. The ^{1}H NMR spectrum of derivative **39a** (**Figure 4.11**) showed two sets of signals for the hydrogen on the C1-position of the iminosugar units at 3.10 and 3.18 ppm which integrate for four and two protons respectively. These two different types of proton showed correlation with the corresponding geminal partners at δ = 2.26-2.30 (overlapped). The singlet at δ = 3.32 ppm was attributed to the aliphatic protons of the intramolecular bridge, while the corresponding aromatic protons were found at δ = 5.82 ppm. The signals of the aromatic protons of the

108

calix[8]arene core were found at $\delta = 6.58, 6.61, 6.95, 6.98$ and 7.22-7.28 ppm (overlapped), while the hydrogen atoms on the triazole rings were found at $\delta = 7.22$-7.28 (overlapped with the aromatic signals) and 7.77 ppm.
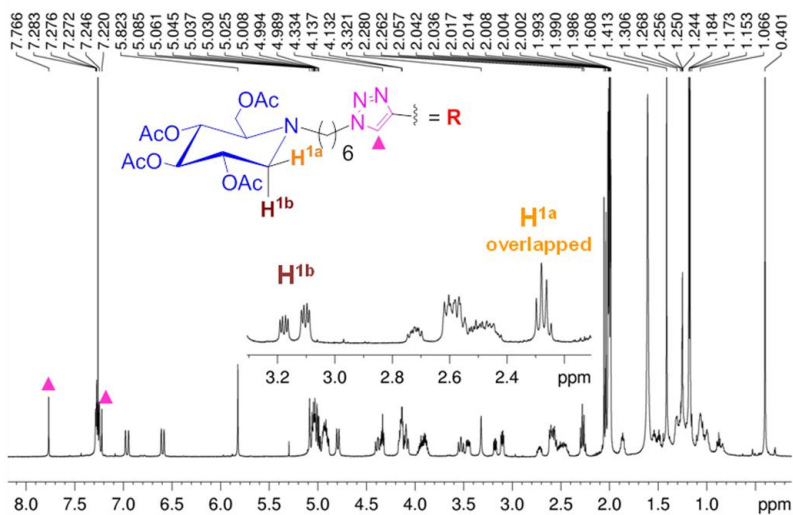

Figure 4.11 ^{1}H NMR spectrum of **39a** (600 MHz, CDCl$_3$, 298K).

In addition, the ^{13}C NMR spectrum of **39a** showed two signals related to the atoms in C1-position at $\delta = 53.06$ a 53.19 ppm, as well as several overlapped signals for the carbonyl of the acetyl groups between $\delta = 170$-172 ppm (**Figure 4.12**).
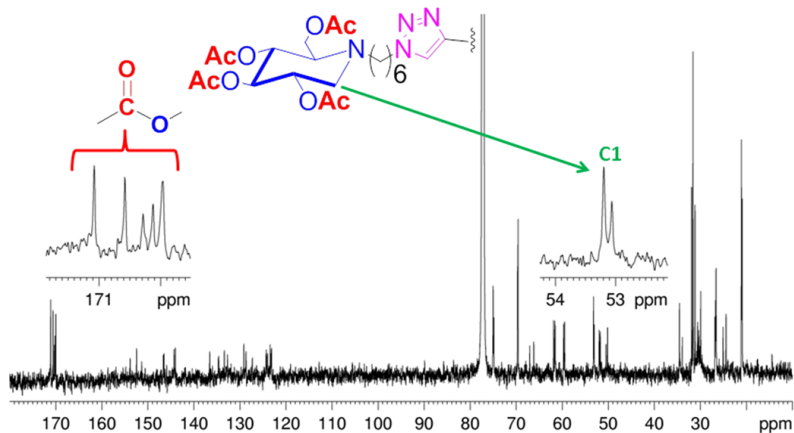
Figure 4.12 ^{13}C NMR spectrum of **39a** (150 MHz, CDCl$_3$, 298 K).

The last step of the syntheses was the removal of the acetyl groups of the iminosugar units. Each calixarene derivative was dissolved in dry methanol, then NaOMe was added and the reaction mixture was stirred at room temperature. Afterwards methanol and water were added until complete dissolution. Dowex 50WX8-200 ion-exchange resin was added until pH=6-7 was reached. Finally the solution was filtered and the solvent was removed under reduced pressure affording the desired final multivalent iminosugar calix[8]arenes **32a-b** and **33a-b** (**Figure 4.13**).
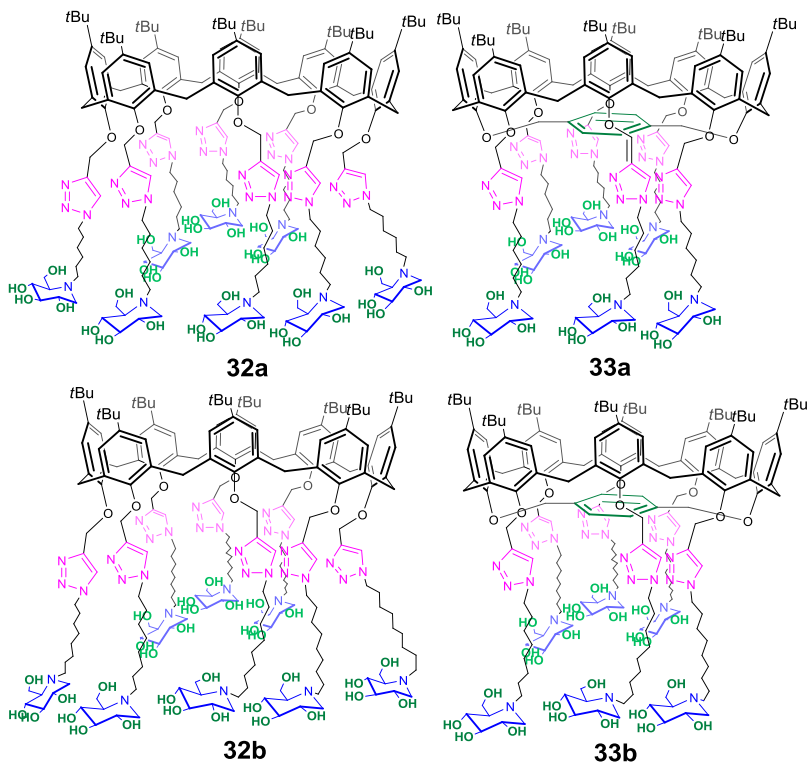
Figure 4.13 Multivalent iminosugar calix[8]arene conjugates.

4.3.2   Glycosidase inhibition studies[100]

Once the synthesis of **32a-b** and **33a-b** was completed, the inhibitory activity and the eventual multivalent effect were

---

evaluated. Preliminary inhibition studies were carried on Jack bean α-mannosidase by Prof. Compain and co-workers.[100] The inhibitory activities were determined by spectrophotochemically measuring the residual hydrolytic activities of the enzyme against *p*-nitrophenyl-α-D-mannopyranoside. A series of assay medium containing α-mannosidase in the presence or absence of various concentration of inhibitor were prepared and the release of *p*-nitrophenol was measured at 380 nm. The results were interesting and promising.

Compound	Valency	K_i (µM)	K_i mono (µM)	RP	RPN
32a	8	---	322	---	---
32b	8	0.32	188	588	73
33a	6	7.7	322	42	7
33b	6	0.38	188	495	82

RP = relative inhibition potency, K_i (monovalent ref)/K_i (glycocluster)
RPN = relative inhibition potency per iminosugar units = RP/n
n = number of iminosugar units

Table 4.1 Jack bean α-mannosidase inhibition studies.

The compounds displayed a multivalent effect comparable to cyclodextrin-based systems of similar valencies.[94] The bridged calix[8]arene core gave slightly better multivalent effects, especially with the iminosugars bearing longer alkyl

112

chains. In fact the most potent inhibitor was compound **33b**, which showed inhibition potency increase of 495-fold compared to the corresponding monovalent ligand and a 82-fold increase of activity per iminosugar unit. The evaluation of inhibitory activity against other glycosidases are currently under investigation.

4.3.3 Higher valency iminosugar clusters[100]

Recently a convergent strategy for the synthesis of high-valency iminosugar clusters was reported.[101] The strategy is based on two successive Cu^I-catalyzed azide-alkyne cycloadditions. With this approach azide-armed iminosugar dendrons can be grafted on the desired polyalkyne scaffold, thus tripling the initial valency. We decided to use this approach for the synthesis of higher valency iminosugar calix[8]arene conjugates, whose synthetic strategy is reported in **Scheme 4.2a-b**.

The DNJ iminosugar with longer alkyl chain (C9) was chosen for this purpose, as it gave the better affinity enhancements (See **Table 4.1**). A first Cu^I-catalyzed azide-alkyne cycloadditions was performed between DNJ-C_9 and the

---

[101] Joosten, A.; Schneider, J. P.; Lepage, M. L.; Tarnus, C.; Bodlenner, A.; Compain, P. *Eur. J. Org. Chem.* **2014**, 1866-1872.

trivalent scaffold **40** in order to obtain the trivalent iminosugar dendron **41**. The latter was then converted in the corresponding azide **42** by treatment with tetrabutylammonium iodide, NaN$_3$ in DMF (**Scheme 4.2a**).

Scheme 4.2a

Scheme 4.2b

115
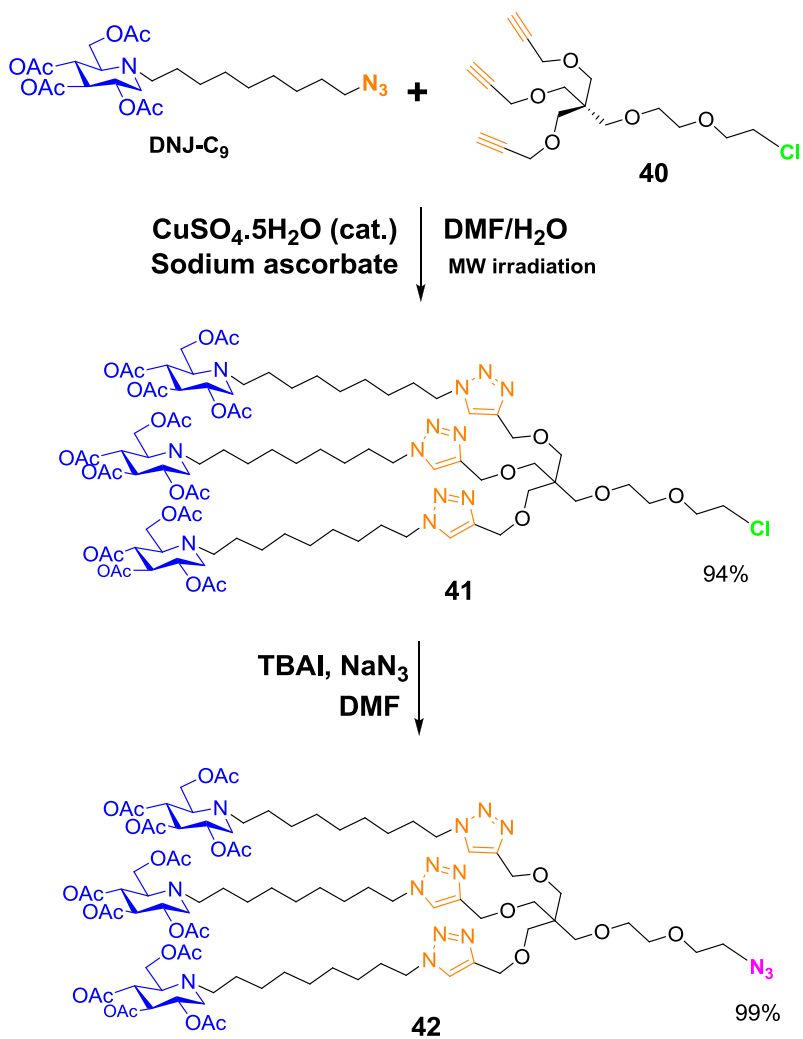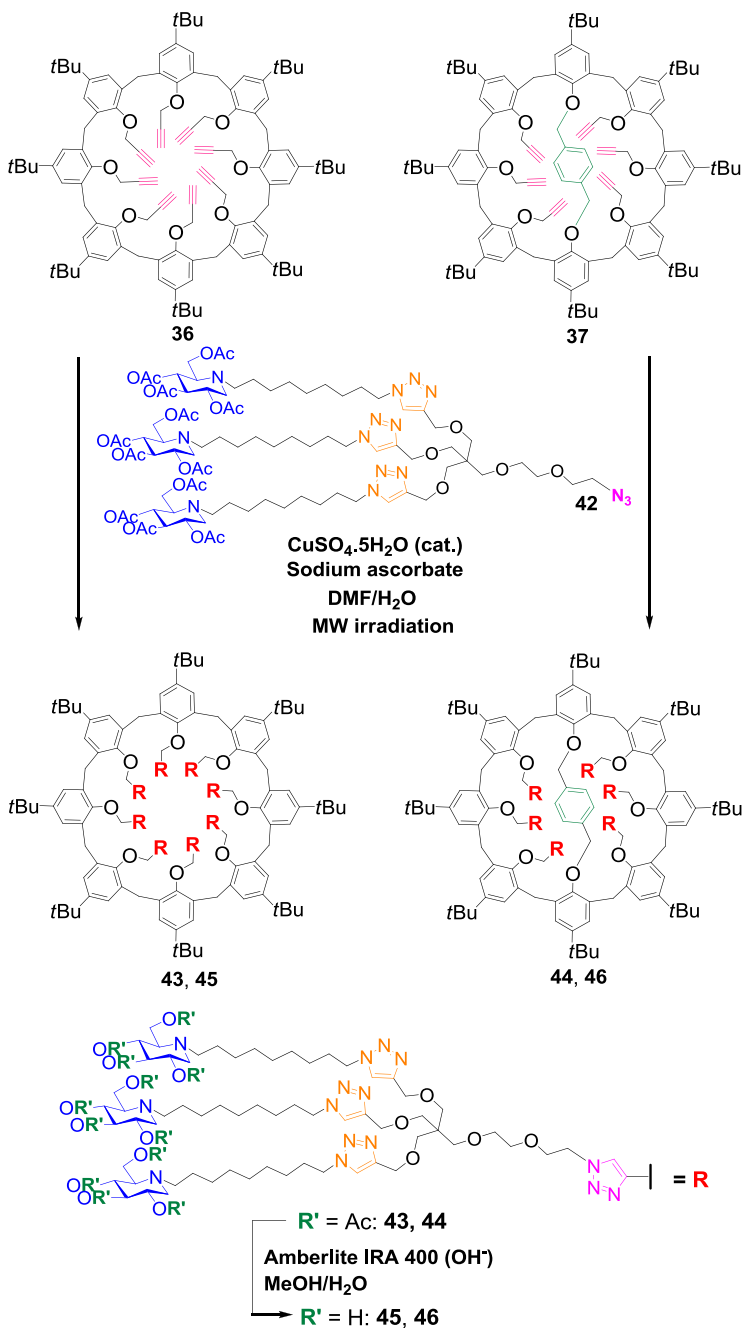
Afterwards the trivalent azide **42** was grafted on the two calix[8]arene scaffolds **36** and **37** with a second Cu^I-catalyzed azide-alkyne cycloadditions, affording compounds **43** and **44**. The final products **45**-**46** were obtained after the acetyl groups on the iminosugar units were removed by deprotection with MeOH/H$_2$O and ion exchange resin (**Scheme 4.2b**).

The characterization and the evaluation of the multivalent effect in glycosidase inhibition of the clusters described above is currently under investigation.

4.4 A new ligation strategy for the synthesis of glycoconjugates

During the three years of my PhD studies I had the opportunity to spend six months in Montpellier (FR) at the Institut des Biomolécules Max Mousseron (IBMM), in the Glycochemistry and Molecular Recognition (GMR) team, under the supervision of Professor Alberto Marra. During that period the attention was focused on the investigation of a new ligation strategy for the synthesis of glycoconjugates, with potential application in the field of multivalency.

Sulfonyl halides are very useful substrates in organic

synthesis. Quite important compounds are sulfonyl chlorides as they are key intermediates for the synthesis of sulfonamides, widely employed in medicinal chemistry for the development of new therapeutic agents.[102] Although aromatic sulfonyl chlorides are quite stable, many aliphatic and heteroaromatic sulfonyl chlorides encounter synthetic problems. For instance they are poor sulfonylating agents as they undergo dehydrochlorination under mild basic condition.[103] Moreover they are unstable and cannot be commercialized.

A good alternative are sulfonyl fluorides, as they are resistant to reduction and more stable in different conditions. Moreover recently sulfonyl fluorides have become very attractive reagents for click reactions.[104] Nothing has been so far reported about this class of compound bearing sophisticated substituents such as carbohydrate residues.

The aim of this research was to develop a synthetic approach for the realization of carbohydrate sulfonyl fluorides and their conversion into sulfonamides via aminolysis with aliphatic amines. This approach could then be applied to the synthesis of multivalent glycoconjugates (**Figure 4.14**).

---

[102] Haruki, H.; Pedersen, M. G.; Gorska, K. I.; Pojer, F.; Johnsson, K. *Science*, **2013**, *340*, 987–991.

[103] King, J. F. *Acc. Chem. Res*. **1975**, *8*, 10-17.

[104] Dong, J.; Krasnova, L.; Finn, M. G.; Sharpless, K. B. *Angew. Chem. Int. Ed.* **2014**, *53*, 9430 – 9448.
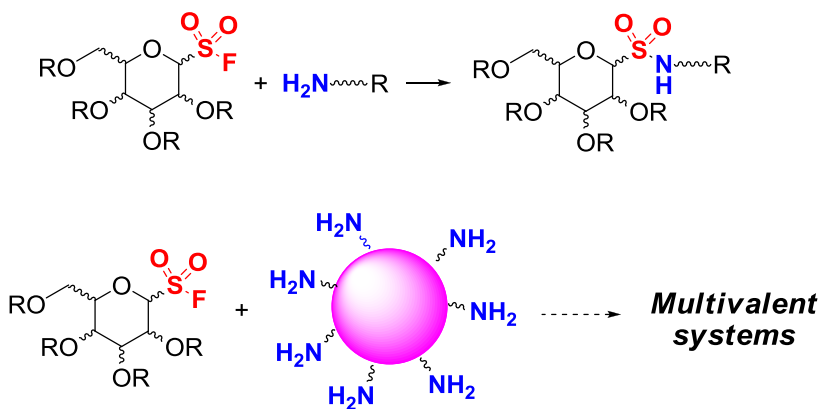
Figure 4.14

4.4.1 Results and discussion

At first much attention was dedicated to the preparation of anomeric sulfonyl fluorides. Galactosyl thiol **47** was used as a substrate, as it was easily accessible. Several attempts were made, attempting both the conversion of the corresponding sulfonyl chloride by halogen exchange reaction and the direct conversion of the thiol to sulfonyl fluoride (**Scheme 4.3**).
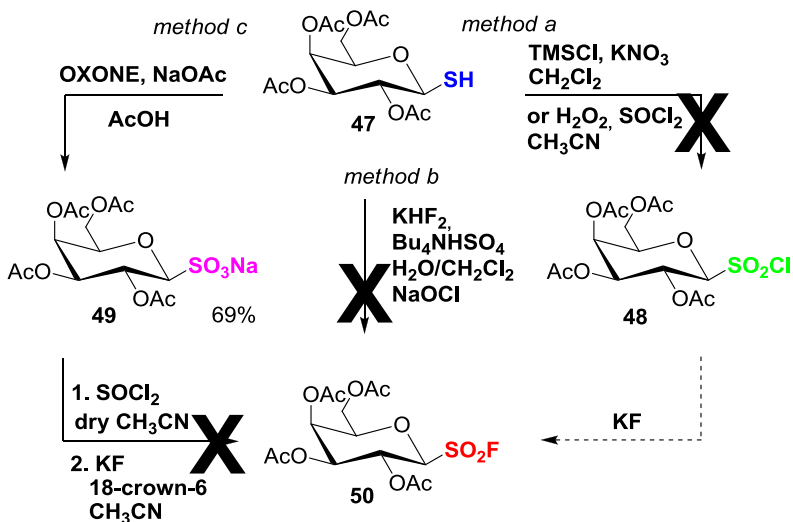
Scheme 4.3

Several conditions were used for the conversion of **47** in the sulfonyl chloride **48** (method a), however the reaction was unsuccessful and the thiol was transformed into the corresponding disulfide. The direct conversion of **47** in **50** (method b) led probably to the formation of the sulfonyl chloride as intermediate generated in situ. However instead of leading to the desired sulfonyl fluoride by halogen exchange, the substrate decomposed to give SO_2 and the corresponding anomeric glycosyl chloride. Also the attempt to generate the sulfonyl chloride from the sulfonate **49** and the transformation into the anomeric sulfonyl fluoride **50** by one-pot-chlorination-halogen exchange (method c) was unsuccessful.

119

After these discouraging results we decided to desist from continuing with this approach.

Afterwards the attention was focused on the introduction of an alkyl tether between the anomeric position and the sulfonyl group. For this purpose was used the known[105] C-glycoside thioacetate **53**, which could be obtained starting from simple reagents. The overall synthetic approach is depicted in **Scheme 4.4**.
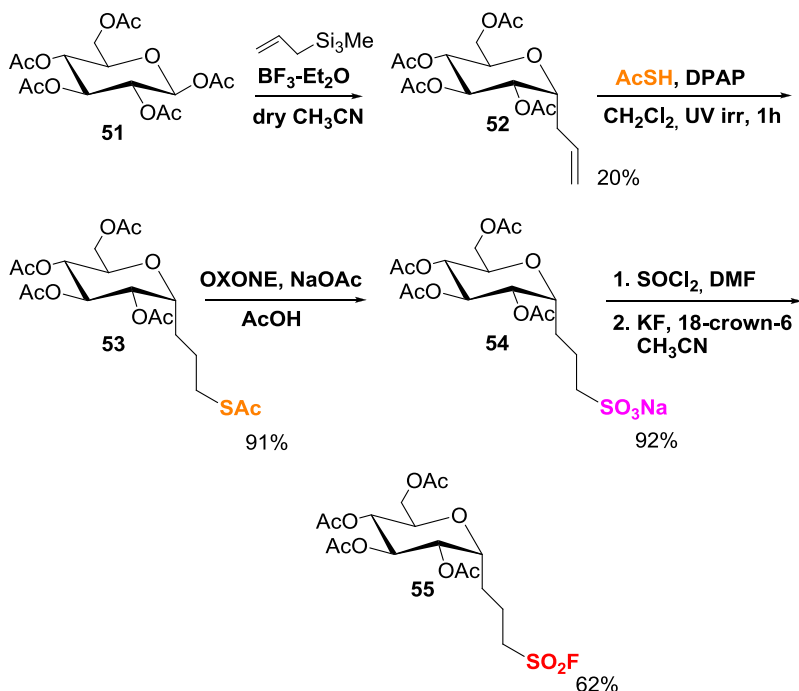
Scheme 4.4

[105] Lo Conte, M.; Staderini, S.; Chambery, A.; Berthet, N.; Dumy, P.; Renaudet, O.; Marra, A.; Dondoni, A. *Org. Biomol. Chem*. **2012**, *10*, 3269-3277.

The first step was a C-glycosylation reaction at the anomeric position of glucose pentacetate **51** with allyltrimethylsilane, which afforded compound **52**. Then a thiolene reaction between **52** and thioacetic acid was performed to obtain the thioacetate **53**. The latter was treated with Oxone to give the corresponding sulfonate salt **54** isolated by column chromatography in good yield. The sulfonate **54** was then transformed into the sulfonyl fluoride **55** via one-pot two-step chlorination reaction with $SOCl_2$ and triphenylphosphine and subsequent halogen exchange with potassium fluoride. The designed sulfonyl fluoride **55** was isolated by chromatography on a short column of silica gel. The product was very stable and it did not show any evidence of degradation even after several days in a sealed glass tube at room temperature.
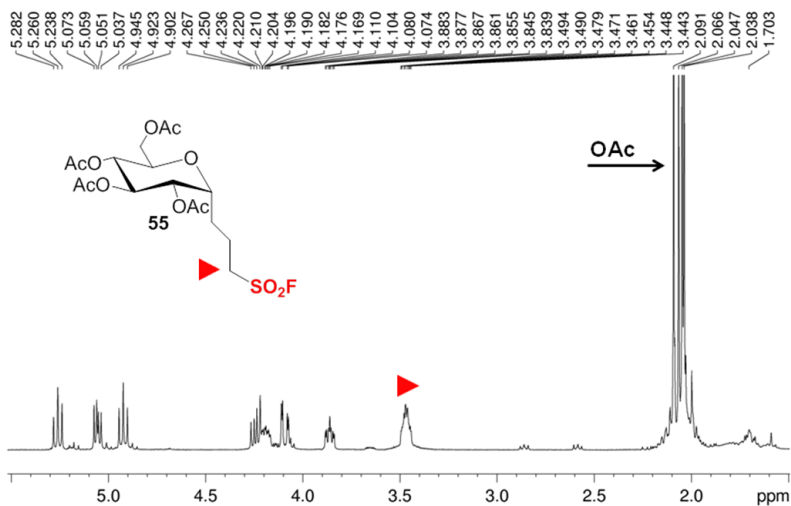
Figure 4.15 ^{1}H NMR spectrum of **55** (400 MHz, CDCl$_3$, 298K).

Subsequently the potential application of the sulfonyl fluoride in aminolysis reaction was explored. Using benzylamine as nucleophile, a series of reactions were performed in order to find the optimized conditions. All the parameters like the solvent, temperature and reaction time are listed in **Table 4.2**.
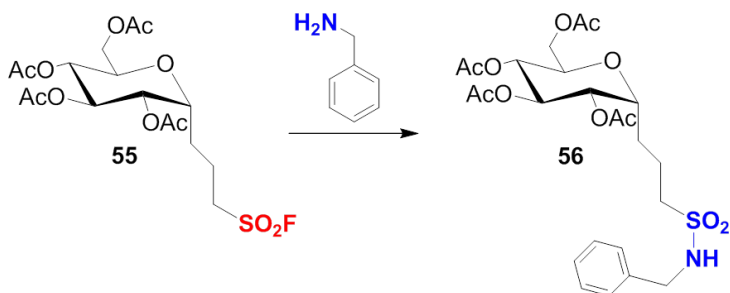
BnNH$_2$ (eq.)	Solvent	T (°C)	Time	yield[a]
2.5	CH$_2$Cl$_2$	r. t.	Overnight	---
10.0	CH$_3$CN	80	Overnight	34%
10.0	EtOH	80	3 h	69%
10.0	DMF	120	3 h	85%
10.0	DMF	r. t.	Overnight + 1 h at 80 °C	80%
10.0	DMF	80	3 h	90%
10.0	CH$_2$Cl$_2$	r. t.	24 h	17%
10.0	CH$_2$Cl$_2$/H$_2$O	r. t.	24 h	16%

[a]Isolated yield after silica gel column chromatography

Table 4.2

The results indicated that the reaction performed in DMF at 80 °C for 3 hours led to the isolation of sulfonamide **56** with the highest yield (90%).

Once the optimal conditions were found, the aminolysis reaction was extended to other aliphatic amines, to verify the applicability of the approach. The reaction with cyclohexyl amine and the more hindered dibutyl amine afforded the

desired sulfonamides, with 97% and 45% yield respectively (**Figure 4.16**). Unfortunately no reaction occurred with aromatic amines such as *p*-cyano and *p*-methoxy aniline, even with longer reaction times. However the sulfonyl fluoride was recovered unaltered.
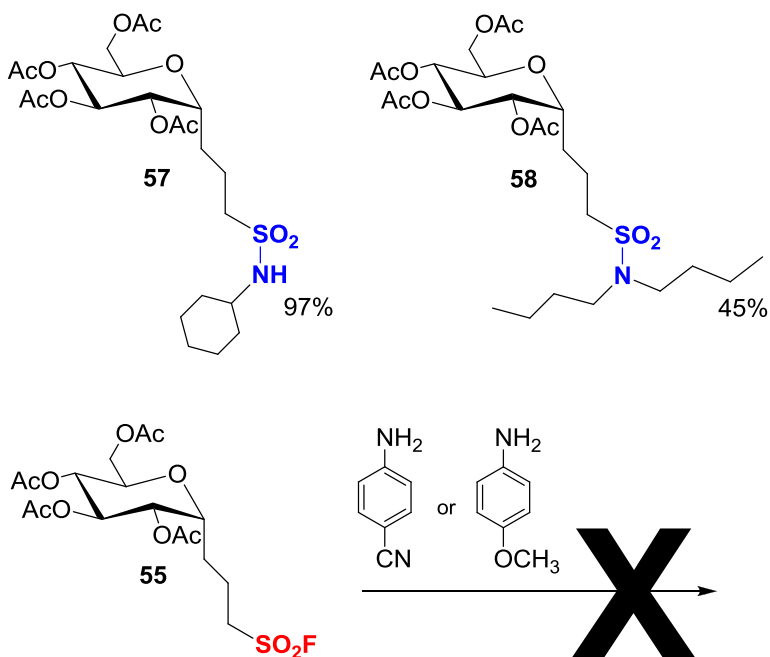

Figure 4.16

These are only preliminary studies, however the results obtained suggest the applicability of the sulfonyl fluorides for the synthesis of sulfamides by aminolysis reaction with aliphatic amines. This approach was applied to simple substrates but it can be extended to other carbohydrates.

4.5   Conclusions

The concept of multivalency and its application in the field of glycosidase inhibition was described in this chapter. This approach was applied to calix[8]arenes derivatives, for the synthesis of multivalent iminosugar-based clusters. Compounds **32a-b** and **33a-b** were obtained by Cu^{I}-catalyzed azide-alkyne cycloadditions between azide-armed iminosugars and calix[8]arenes bearing propargyl groups. The inhibitory activity of these compounds toward α-mannosidase was evaluated.[100] The compounds showed a good multivalent effect.

Higher valency iminosugar clusters **45-46** were also synthesized and the evaluation of the multivalent effect in glycosidase inhibition is currently under investigation.[100]

Moreover, the investigation on a new ligation strategy for the synthesis of glycoconjugates was reported. The study was performed at the Institut des Biomolecules Max Mousseron in Montpellier (FR), thanks to a collaboration with Professor Alberto Marra. The preliminary results are promising and encouraging.

Chapter 5

5.   Experimental section

All chemicals were reagent grade and were used without further purification. Anhydrous solvents were purchased from Aldrich. When necessary compounds were dried in vacuo over $CaCl_2$. Reaction temperatures were measured externally. Reactions were monitored by TLC on Merck silica gel plates (0.25 mm) and visualized by UV light, or by sprying with H_2SO_4-$Ce(SO_4)_2$ or phosphomolybdic acid. Melting points were determined with a Kofler apparatus. Elemental analyses were performed with a Perkin–Elmer elemental analyzer.

ESI(+)-MS measurements were performed on a Waters QTof Premiere mass spectrometer equipped with electrospray ion source, using a mixture of H_2O/CH_3CN (1:1) and 5% HCOOH as solvent. Flash chromatography was performed on Merck silica gel (60, 40-63 μm).

1D NMR spectra were recorded on a Bruker Avance-600 spectrometer [600 (^{1}H) and 150 MHz (^{13}C)], Bruker Avance-400 spectrometer [400 (^{1}H) and 100 MHz (^{13}C)], Bruker Avance-300 spectrometer [300 (^{1}H) and 75 MHz (^{13}C)] and Bruker Avance-250 spectrometer [250 (^{1}H) and 63 MHz (^{13}C)]; chemical shifts are reported relative to the residual solvent peak.

5.1 Calixarene based DNA intercalators

General comments: The circular dichroism spectra were recorded with a JASCO J-815 spectropolarimeter equipped with a 150 W xenon lamp. The ellipticity was obtained by calibrating the instruments with a 0.06% (w/v) aqueous solution of ammonium d-10-camphorsulfonate and with a 0.08% (w/v) aqueous solution of tris(ethylenediamine)cobalt(III) chloride complex $\{(-)-\Delta-[Co(en)_3]-Cl_3\}_2 \cdot NaCl \cdot 6H_2O$. The measurements were performed at a constant temperature of 25 °C in quartz cells and were corrected for the contribution from the cell and solvent. The temperature was controlled by a Jasco PTC-423S/15 Peltier-type temperature control system cooled with an external water circulator. The spectra were corrected to take into account the dilution effect after each addition. The HPLC system consisted of a Jasco PU-2089 Plus pump and a Jasco MD-2010 Plus multiwavelength detector. The HPLC column was a Waters Spherisorb® 10 μm CN 10_250 mm semipreparative column.

Compounds **1**,[45] **2**[42c] and **9**[44] were synthesized according to literature procedures. Poly(dA)–poly(dT) sodium salt was purchased from Sigma–Aldrich. Water was purified through a Millipore Milli-Q system. All CD experiments were

conducted in 10–2 m phosphate buffer at pH = 7.4 containing 0.1 m NaCl. The pH of the solution was measured with a glass electrode. The concentrations of polynucleotides in base pairs were determined by absorption spectroscopy by using the molar extinction coefficient 12000 $m^{-1}cm^{-1}$ at 260 nm.

Synthesis of 10a–12a: Compound **1** (0.105 g, 0.147 mmol) and (±)-**2a** (0.233 g, 0.735 mmol) were dissolved in dry CH_2Cl_2 (15 mL), and then dry Et_3N (0.101 mL, 0.735 mmol) was added. The reaction mixture was stirred at room temperature for 48 h. Then, the mixture was washed twice with H_2O, the organic phase was dried with Na_2SO_4, and the solvent was removed under reduced pressure. The products were isolated by silica gel flash column chromatography (CH_2Cl_2/Et_2O, 96:4). Compounds (±)-**11a** and **12a** were purified by HPLC (mobile phase: hexane/isopropyl alcohol, 80:20, v/v; flow rate 1.6 mL/min).
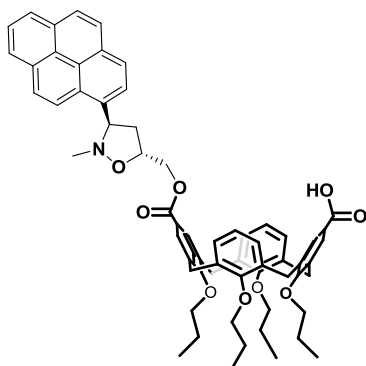
(±)-**10a**

Compound (±)-10a: 22 mg, 15% yield. ESI(+) MS: *m/z* = 981.7 [M + H]+, 1003.1 [M + Na]+. M.p. _200 °C (dec.). ^{1}H NMR (400 MHz, CDCl$_3$, 298 K): δ = 0.97–1.01 (overlapped, OCH$_2$CH$_2$C*H*$_3$, 12H), 1.87–1.96 (overlapped, OCH$_2$C*H*$_2$CH$_3$, 8H), 2.66 and 2.83 (br. AB, CH$_2$isox, 2H), 2.78 (br. s, CH$_3$N, 3H), 3.18–3.26 (overlapped, ArCH$_2$Ar, 4H), 3.80–3.85 (overlapped, OC*H*$_2$CH$_2$CH$_3$, 4H), 3.90–3.96 (overlapped, OC*H*$_2$CH$_2$CH$_3$, 4H), 4.41–4.48 (overlapped, Ar-C*H*$_2$Ar, 4H), 4.45 and 4.56 (AB, C(O)OCH$_2$isox, 2H), 4.70 (br. s, OCHisox, 1H), 4.80 (br. s, NCHisox, 1H), 6.44–6.62 (overlapped, ArH, 6H), 7.39 (br. s, ArH, 2H), 7.50 (br. s, ArH, 2H), 7.99–8.47 (overlapped, ArHpyrene, 9H) ppm. ^{13}C NMR (100 MHz, CDCl$_3$, 298K): δ = 10.30, 10.35, 23.24, 23.33, 29.72, 30.96, 41.77, 44.02, 65.40, 69.30, 75.30, 76.90, 77.24, 122.42, 122.57, 122.81, 123.44, 124.61, 124.81, 124.95, 125.09, 125.38, 126.03, 127.47, 127.89, 128.38, 128.45, 128.53, 128.81, 129.94, 130.23, 130.43, 130.56,

130

130.64, 130.73, 131.37, 134.20, 134.35, 135.47, 135.60, 156.20, 161.25, 161.54, 166.46, 169.68 ppm. $C_{63}H_{65}NO_9$ (980.2): calcd. C 77.20, H 6.68; found C 77.28, H 6.59.

(±)-**11a**
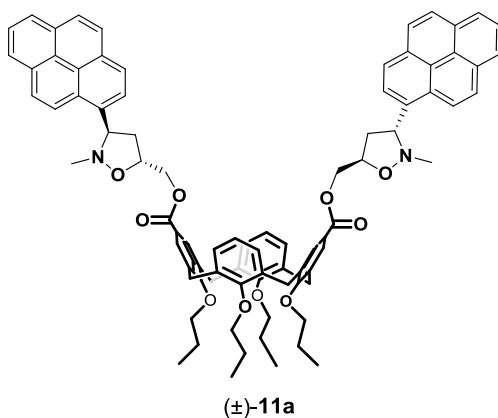
Compound (±)-11a: 19 mg, 10% yield. ESI(+) MS: m/z = 1280.4 [M + H]+. M.p. _180 °C (dec.). ^{1}H NMR (400 MHz, CDCl$_3$, 298 K): δ = 0.96 (t, J = 7.4 Hz, OCH$_2$CH$_2$CH_3, 6H), 1.01 (t, J = 7.3 Hz, OCH$_2$CH$_2$CH_3, 6H), 1.83–1.99 (overlapped, OCH$_2$CH_2CH$_3$, 8H), 2.68 and 2.87 (br. AB, CH$_2$ isox, 4H), 2.80 (br. s, CH$_3$N, 6H), 3.20 and 4.44 (AX, J = 13.2 Hz, ArCH_2Ar, 4H), 3.25 and 4.46 (AX, J = 13.2 Hz, ArCH_2Ar, 4H), 3.75 (t, J = 6.8 Hz, OCH_2CH$_2$CH$_3$, 4H), 4.02 (t, J = 7.6 Hz, OCH_2CH$_2$CH$_3$, 4H), 4.58 and 4.50 (AB, C(O)OCH$_2$isox, 4H), 4.76 (br. s, OCHisox 2H + NCHisox 2H), 6.22 (br. s, ArH, 4H), 6.37 (br. s, ArH, 2H), 7.65 (br. s,

ArH, 2H), 7.67 (br. s, ArH, 2H), 7.98–8.49 (overlapped, ArHpyrene, 18H) ppm. ^{13}C NMR (100 MHz, CDCl$_3$, 298K): δ = 10.15, 10.53, 23.28, 23.35, 30.95, 41.96, 44.14, 65.34, 69.24, 75.10, 76.7, 76.9, 122.36, 122.63, 123.30, 124.46, 124.82, 124.97, 125.06, 125.37, 126.03, 127.41, 127.48, 127.86, 128.14, 130.26, 130.39, 130.65, 130.70, 131.39, 133.57, 136.23, 155.76, 161.82, 166.47 ppm. C$_{84}$H$_{82}$N$_2$O$_{10}$ (1279.6): calcd. C 78.85, H 6.46; found C 78.95, H 6.36.
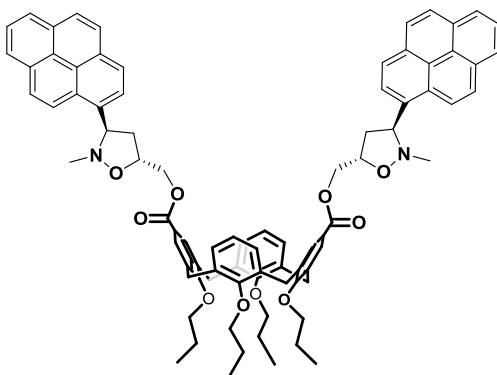
**12a**

Compound 12a: 15 mg, 8% yield. ESI(+) MS: m/z = 1280.4 [M + H]+. M.p. _170 °C (dec.). ^{1}H NMR (400 MHz, C$_6$D$_6$, 298 K): δ = 0.84–0.91 (overlapped, OCH$_2$CH$_2$CH_3, 12H), 1.73–1.86 (overlapped, OCH$_2$CH_2CH$_3$, 8H), 2.44 and 2.72 (br. AB, CH$_2$ isox, 4H), 2.73 (br. s, CH$_3$N, 6H), 3.07 and 4.39 (AX, J = 13.2 Hz, ArCH_2Ar, 4H), 3.14 and 4.45 (AX, J =

13.6 Hz, ArCH_2Ar, 4H), 3.65 (t, J = 7.2 Hz, OCH_2CH$_2$CH$_3$, 2H), 3.70 (t, J = 7.6 Hz, OCH_2CH$_2$CH$_3$, 2H), 3.86 (t, J = 7.2 Hz, OCH_2CH$_2$CH$_3$, 4H), 4.54–4.69 (overlapped, C(O)OCH$_2$isox, OCH, NCH, 8H), 6.25 (t, J = 7.4 Hz, ArH, 2H), 6.41 (d, J = 7.4 Hz, ArH, 2H), 6.64 (d, J = 6.9 Hz, ArH, 2H), 7.76–8.00 (overlapped, ArHpyrene, 22H) ppm. ^{1}H NMR (400 MHz, CDCl$_3$, 298 K): δ = 0.96 (t, J = 7.4 Hz, OCH$_2$CH$_2$CH_3, 6H), 1.01–1.06 (overlapped, OCH$_2$CH$_2$CH_3, 6H), 1.85–1.99 (overlapped, OCH$_2$CH_2CH$_3$, 8H), 2.66 and 2.85 (br. AB, CH$_2$isox, 4H), 2.79 (br. s, CH$_3$N, 6H), 3.23 (d, J = 13.6 Hz, ArCH$_2$Ar, 2H), 3.27 (d, J = 13.8 Hz, ArCH$_2$Ar, 2H), 3.72–3.78 (overlapped, OCH_2CH$_2$CH$_3$, 4H), 4.04 (t, J = 7.2 Hz, OCH_2CH$_2$CH$_3$, 4H), 4.44–4.52 (overlapped, ArCH_2Ar, 4H), 4.57 and 4.50 (AB, C(O)OCH$_2$ isox, 4H), 4.76 (br. s, OCH, 2H and NCH, 2H), 6.20–6.38 (overlapped, ArH, 6H), 7.70 (br. s, ArH, 4H), 7.98–4.49 (overlapped, ArHpyrene, 18H) ppm. 13C NMR (63 MHz, CDCl$_3$, 298K): δ = 10.12, 10.57. 23.27, 23.37, 30.99, 41.77, 44.04, 65.28, 69.22, 75.12, 76.82, 77.23, 122.40, 122.60, 123.29, 124.51, 124.81, 124.96, 125.07, 125.37, 126.02, 127.47, 127.85, 128.11, 128.83, 130.31, 130.41, 130.63, 130.70, 131.37, 133.47, 136.33, 155.86, 155.90, 162.12, 166.70 ppm. $C_{84}H_{82}N_2O_{10}$ (1279.6): calcd. C 78.85, H 6.46; found C 78.93, H 6.38.

Synthesis of Compounds 10b and 11b: Compound **1** (0.210 g, 0.29 mmol) and (±)-**2b** (0.206 g, 0.65 mmol) were dissolved in dry pyridine (5 mL). The reaction mixture was stirred at room temperature for 24 h, and then the solvent was removed under reduced pressure. The pure products were isolated by flash column chromatography with silica gel (CH$_2$Cl$_2$/Et$_2$O, 98:2).

(±)-**10b**
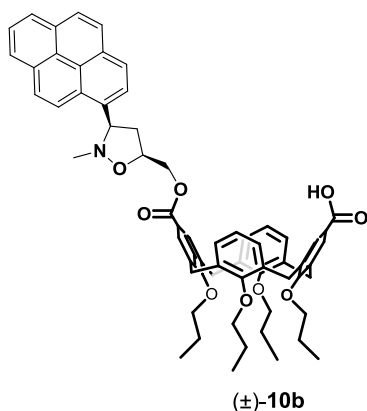
Compound (±)-10b: 28 mg, 10% yield. ESI(+) MS: *m/z* = 981.0 [M + H]+. M.p. _200 °C (dec.). ^{1}H NMR (250 MHz, CDCl3, 298 K): δ = 0.94–1.05 (overlapped, OCH$_2$CH$_2$C*H*$_3$, 12H), 1.86–1.94 (overlapped, OCH$_2$C*H*$_2$CH$_3$, 8H), 2.28–2.41 (br. m, CH$_2$isox, 1H), 2.73 (s, CH$_3$N, 3H), 3.08–3.23 (overlapped, ArC*H*$_2$Ar, 4H and CH$_2$ isox, 2H), 3.82–3.89 (overlapped, OC*H*$_2$CH$_2$CH$_3$, 8H), 4.23–4.53 (overlapped, ArC*H*$_2$Ar, 4H and C(O)OCH$_2$isox, 2H), 4.66–4.72 (overlapped, OCH, 1H and NCH, 1H), 6.60–6.74 (overlapped,

134

ArH, 6H), 7.20 (s, ArH, 2H), 7.36 (s, ArH, 2H), 7.99–8.38 (overlapped, ArHpyrene, 9H) ppm. ^{13}C NMR (63 MHz, CDCl$_3$, 298 K): δ = 10.24, 10.36, 10.39, 22.71, 23.18, 23.32, 29.71, 30.32, 30.90, 41.06, 43.43, 65.95, 69.22, 76.72, 77.22, 122.18, 122.43, 122.92, 123.64, 123.95, 124.17, 124.82, 124.94, 125.08, 125.41, 125.45, 126.03, 127.40, 127.90, 128.60, 128.71, 128.83, 129.85, 130.04, 130.18, 130.27, 130.61, 130.65, 131.37, 132.53, 134.59, 134.96, 135.09, 135.31, 156.45, 156.64, 160.82, 161.03, 166.69 ppm. C$_{63}$H$_{65}$NO$_9$ (980.2): calcd. C 77.20, H 6.68; found C 77.29, H 6.59.

(±)-**11b**
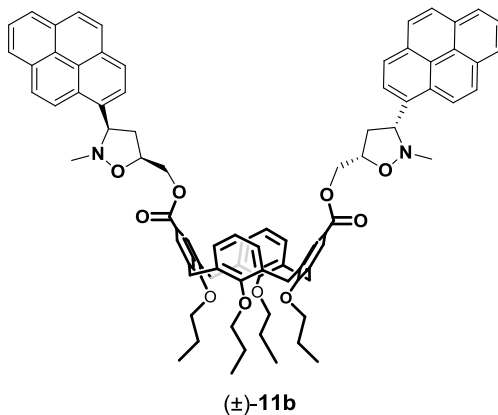
Compound (±)-11b: 41 mg, 11% yield. ESI(+) MS: m/z = 1280.4 [M + H]+. M.p. _170 °C (dec.). ^{1}H NMR (400 MHz, CDCl$_3$, 298 K): δ = 0.91 (t, J = 7.4 Hz, OCH$_2$CH$_2$CH_3, 6H), 1.07 (t, J = 7.3 Hz, OCH$_2$CH$_2$CH_3, 6H), 1.84–1.97

(overlapped, OCH$_2$CH$_2$CH$_3$, 8H), 2.31 and 3.20 (br. AX, CH$_2$ isox, 4H), 2.79 (br. s, CH$_3$N, 6H), 3.16–3.22 (overlapped, ArCH$_2$Ar, 4H), 3.69 (t, J = 6.3 Hz, OCH$_2$CH$_2$CH$_3$, 4H), 4.04 (t, J = 7.6 Hz, OCH$_2$CH$_2$CH$_3$, 4H), 4.39–4.44 (overlapped, ArCH$_2$Ar, 4H), 4.42 and 4.62 (AB, C(O)OCH$_2$isox, 4H), 4.72 (br. s, NCHisox, 2H), 4.79 (br. s, OCHisox, 2H), 6.13–6.21 (overlapped, ArH, 6H), 7.73 (br. s, ArH, 4H), 7.99–8.42 (overlapped, ArHpyrene, 18H) ppm. ^{13}C NMR (150 MHz, CDCl$_3$, 298K): δ = 9.98, 10.72, 23.17, 23.46, 30.86, 42.21, 43.73, 66.46, 69.12, 74.84, 122.33, 122.40, 123.32, 124.20, 124.85, 124.95, 125.08, 125.36, 125.49, 126.01, 127.32, 127.49, 127.85, 128.68, 130.52, 130.60, 130.65, 131.38, 132.88, 132.93, 133.17, 136.64, 155.32, 162.24, 166.78 ppm. C$_{84}$H$_{82}$N$_2$O$_{10}$ (1279.6): calcd. C 78.85, H 6.46; found C 78.95, H 6.36.

Cell Viability Assays: FTC133, 8305C, and U87MG cell lines were seeded in 96-well plates. The cells were grown in an appropriate medium supplemented with 10% fetal bovine serum and incubated at 37 °C, 5% CO$_2$ conditions, for 24 h before the cytotoxicity assessments. The cells were exposed to increased concentrations of the compounds. After 24 h of incubation, the cell survival was determined by MTT assay

according to the literature procedure.[106] In brief, MTT solution [50 μL, 5 mg/mL in phosphate-buffered saline (PBS), Sigma] was added to each well and incubated for 2 h. The medium was subsequently removed from the wells, and the resulting formazan crystals were dissolved in DMSO (100 μL). The culture plates were rocked gently for 30 min to dissolve the crystals before the optical density was measured at 570 nm with an enzymelinked immunosorbent assay (ELISA) microplate reader. In all ex periments, four replicate wells were measured for each drug concentration.

Circular Dichroism: The CD spectra were recorded with samples in a standard quartz cell of 1 cm path length in the 235–400 nm range. For each spectrum, five runs were averaged with a 5 min equilibration interval before each scan. All spectra were recorded at fixed poly(dA)–poly(dT) concentration (19.7 μm in base pair) in the absence or in the presence of different concentrations of **10b** (4.3 mM solution in DMSO) from 0 to ca. 32 μm.

---

[106] Pope, A. J.; Bruce, C.; Kysela, B.; Hannon, M. J. *Dalton Trans.* **2010**, *39*, 2772-2774.

Molecular Modeling

Preparation of Ligands: The 3D structures of the ligands were generated with the Winmostar (4.101) software,[107] and all geometries were fully optimized with the same software with the semiempirical AM1[108] Hamiltonian implemented in MOPAC2012 (14.04W).[109] Compounds **10** were optimized as carboxylates (charge = −1).

Molecular Dynamics Simulations: The molecular dynamics simulations of the DNA–ligand complexes were performed with the YASARA structure package (13.9.8).[52] A periodic simulation cell with boundaries extending 10 Å from the surface of the complex was employed. The box was filled with water, and a density of 0.997 g/mL with explicit solvent was utilized. The pKa utility of YASARA was used to assign pKa values at pH = 7.2,[110] the cell was neutralized with 22 Na+ ions (23 for **10**), and NaCl was added to reach 0.9% concentration by mass; under these conditions, ligands **10** were deprotonated at the carboxylic acid function. Water molecules were deleted to readjust the solvent density to 0.997 g/mL. The Amber03 force field was used with long-

[107] Senda, N. *Idemitsu Giho* **2006**, *49*, 106-111.

[108] Dewar, M. J. S.; Zoebish, E. G.; Healy, E. F.; Stewart, J. J. P. *J. Am. Chem. Soc.* **1985**, *107*, 3902-3909.

[109] Stewart, J. J. P. *MOPAC*, Stewart Computational Chemistry, Colorado Springs, **2012**.

[110] Krieger, E.; Nielsen, J. E.; Spronk, C. A. E. M.; Vriend, G. *J. Mol. Graphics Modell.* **2006**, *25*, 481-486.

range electrostatic potentials calculated with the particle mesh Ewald (PME) method with a cutoff of 7.86 Å.[111] The ligand force-field parameters were generated with the AutoSMILES utility,[112] which employs semiempirical AM1 geometry optimization and assignment of charges, followed by assignment of the AM1BCC atom and bond types with refinement by using the restrained electrostatic potential (RESP) charges, and finally the assignments of general AMBER force field atom types. A short MD simulation was run for the solvent only. The entire system was then energy-minimized through a steepest-descent minimization to remove conformational stress, followed by a simulated annealing minimization until convergence (< 0.01 kcal/mol Å). The MD simulation was then initiated; the *NVT* ensemble at 298 K was used, and the time steps for intramolecular and intermolecular forces were integrated every 1.25 and 2.5 fs, respectively. The MD simulation was stopped after 5 ns and, on the last frame, a second cycle of energy minimization, identical to the first, was applied.

Docking Protocol: The DNA–ligand complexes, as obtained after coarse minimization or MD simulation and energy

[111] Duan, Y.; Wu, C.; Chowdhury, S.; Lee, M. C.; Xiong, G. M.; Zhang, W.; Yang, R.; Cieplak, P.; Luo, R.; Lee, T.; Caldwell, J.; Wang, J. M.; Kollman, P. *J. Comput. Chem.* **2003**, *24*, 199-2012.

[112] Jakalian, A.; Jack, D. B.; Bayly, C. I. *J. Comput. Chem.* **2002**, *23*, 1623-1641.

minimization, were prepared with Vega ZZ[113] (3.0.3.18) with Gasteiger charges assigned to the proteins and AM1BCC ones assigned to the ligands. The graphical user interface AutoDockTools (1.5.7 rc1)[114] was used to establish the Autogrid points and to visualize the docked ligand–nucleic acid structures. Docking was performed with the AutoDock (4.2.5.1) software.[55] To define all binding sites and to have structural inputs, a grid-based procedure was used.[115] Here, the output was saved as a PDBQT file. The grid box was set and the output was saved as a gpf file. The ligand-centered maps were generated by the program AutoGrid (4.2.5.1) with a spacing of 0.375 Å and dimensions that encompass all atoms extending 10 Å from the surface of the ligand (for blind docking, DNA-centered maps were generated with a spacing of 0.375 Å and dimensions that encompass all atoms extending 10 Å from the surface of DNA). All of the parameters were inserted at their default settings. In the docking tab, the macromolecule and ligand were selected, and the GA parameters were set as ga_runs = 100, ga_pop_size = 150, ga_num_evals = 2500000 for coarse docking and 20000000 for fine docking, ga_num_generations = 27000, ga_elitism = 1, ga_mutation_rate = 0.02, ga_crossover_rate = 0.8, ga_crossover_mode = two points, ga_cauchy_alpha = 0.0,

[113] Pedretti, A.; Villa, L.; Vistoli, G. *J. Comput.-Aided Mol. Des.* **2004**, *18*, 167-173.
[114] Sanner, M. F. *J. Mol. Graphics Modell.* **1999**, *17*, 57-61.
[115] Goodford, P. J. *J. Med. Chem.* **1985**, *28*, 849-857.

ga_cauchy_beta = 1.0, number of generations for picking worst individual = 10, output was selected as LGA, and the file was saved as a dpf file.

## 5.2 Biomolecular recognition abilities of calixarenes through the chemoproteomic approach

General comments: Derivatives **18**[71], **21**[72], and **23**[79] were synthesized according to literature procedures. **SN38** (7-ethyl-10-hydroxycamptothecin) and the known PDI inhibitor **16F16** were purchased from Sigma-Aldrich. Molecular modeling studies were performed with the MacroModel-9.0/Maestro-4.1[116] program.

[116] Mohamadi, F.; Richards, N. G.; Guida, W. C.; Liskamp, R.; Lipton, M.; Caufield, C.; Chang, G.; Hemdrickson, T.; Still, W. C. *J. Comput. Chem.* **1990**, *11*, 440-467.
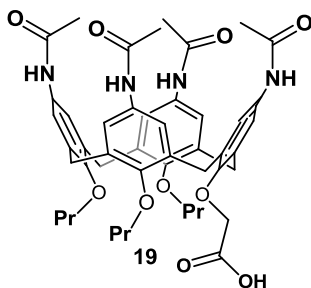
Derivative 19. A cold solution of acetyl chloride (1.76 mmol, 0.125 mL) in dry THF (11 mL) was slowly added to a solution of tetraminocalix[4]arene derivative **18** (0.27 mmol, 0.18 g) and dry Et$_3$N (1.47 mmol, 0.20 mL) in dry THF (65 mL) at 0 °C. The reaction mixture was allowed to warm at room temperature and stirred overnight. The solvent was then removed under reduced pressure. The crude product was dissolved in AcOEt, washed with a saturate solution of NaHCO$_3$ (2 x 50 mL), with 1 M HCl (2 x 50 mL) and brine, dried over Na$_2$SO$_4$ and filtered. The solvent was removed by rotary evaporator. The product was purified by silica gel chromatography (AcOEt:MeOH, 7:3) (0.075 g; 33% yield); ESI(+)MS: m/z = 859.5 (M+Na+); ^{1}H NMR (600 MHz, DMSO-d6, 298 K): δ 0.89-0.98 (overlapped, CH$_2$CH$_2$CH_3, 9H), 1.82-1.87 (overlapped, CH$_2$CH_2CH$_3$, 6H), 1.95 (s, C(O)CH$_3$, 12H), 3.06 (d, ArCH_2Ar, J = 12.8 Hz, 4H), 3.67-3.81(overlapped, CH_2CH$_2$CH$_3$, 6H), 4.29-4.71 (overlapped, OCH_2C(O) + ArCH$_2$Ar, 6H), 6.68 (s, ArH, 2H), 6.75 (s, ArH, 2H), 7.04 (br s, ArH, 4H), 9.30 (s, NH, 1H), 9.35 (s, NH, 1H),

9.58 (br t, NH, 2H); ^{13}C NMR (150 MHz, DMSO-d6, 298 K):

δ 10.5, 11.1, 23.6, 23.7, 24.7, 24.4, 31.9, 32.4, 71.8, 78.2,

78.3, 121.7, 121.9, 121.9, 133.6, 133.9, 134.3, 135.3, 135.5,

136.6, 136.9, 153.9, 154.1, 154.8, 171.0, 171.2, 172.1. Anal.

Calcd for $C_{47}H_{56}N_4O_{10}$: C, 67.45; H, 6.74. Found: C, 67.54;

H, 6.64.
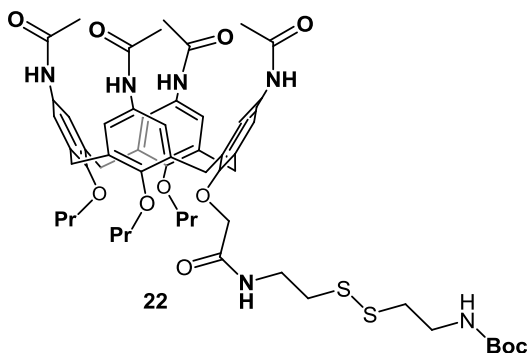
Derivative 22. A sample of **19** (0.09 mmol, 0.075 g) was

dissolved in dry DMF (4.5 mL) and then HOBt (0.40 mmol,

0.053 g) and DCC (0.40 mmol, 0.082 g) were added. The

reaction mixture was stirred at room temperature for 1h. A

solution of compound **21** (0.40 mmol, 0.100 g) in dry DMF

(3.0 mL) was added to the reaction mixture, which was then

stirred for 5 days. CH_2Cl_2 was added and the solution was

washed sequentially with 1 M NaH_2PO_4 (3 x 15 mL), a

saturate solution of $NaHCO_3$ (2 x 15 mL), and water (2 x 15

mL). The organic phase was dried over Na_2SO_4 and filtered. The solvent was removed under reduced pressure and the product was purified by flash column chromatography on silica gel (AcOEt:MeOH, 85:15) (0.024 g, 22% yield); ESI(+)MS: m/z = 1071.2 (M+H+); ^{1}H NMR (600 MHz, CD_3OD, 298 K): δ 0.91 (t, $CH_2CH_2CH_3$, J = 7.5 Hz, 3H), 1.02 (t, $CH_2CH_2CH_3$, J = 7.3 Hz, 6H), 1.44 (s, Boc, 9H), 1.85-2.11 (overlapped, $CH_2CH_2CH_3$ 6H + C(O)CH_3, 12H), 2.84 (t, CH_2N, J = 6.6 Hz, 4H), 3.02 (t, CH_2S, J = 6.6 Hz, 4H), 3.14-3.25 (overlapped, ArCH_2Ar, 4H), 3.76 (t, $CH_2CH_2CH_3$, J = 5.9 Hz, 2H), 3.88 (t, $CH_2CH_2CH_3$, J = 7.3 Hz, 4H), 4.42-4.50 (overlapped, ArCH$_2$Ar, 4H), 4.79 (s, OCH_2C(O), 2H), 6.60 (s, ArH, 4H), 7.21 (s, ArH, 2H), 7.24 (s, ArH, 2H); ^{13}C NMR (150 MHz, CD_3OD, 298 K): δ 10.5, 10.8, 23.8, 24.1, 28.8, 30.8, 32.5, 32.79, 38.4, 39.4, 40.7, 75.1, 77.7, 78.9, 80.2, 121.4, 121.8, 121.9, 122.4, 134.1, 134.4, 134.7, 135.3, 135.8, 137.4, 152.8, 154.4, 155.1, 158.3, 171.0, 171.3, 173.2. Anal. Calcd for $C_{56}H_{74}N_6O_{11}S_2$: C, 62.78; H, 6.96. Found: C, 62.87; H, 6.87.
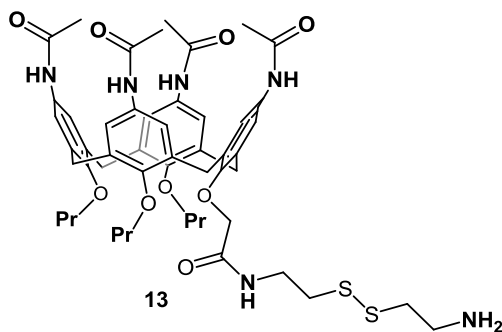
pAc Derivative 13. A solution of **22** (0.022 mmol, 0.024 g) in CH$_2$Cl$_2$ (2 mL) was cooled at 0 °C. TFA (2 mL) was added and the reaction mixture was allowed to warm at room temperature and stirred for 5 h under nitrogen. CH$_2$Cl$_2$ was added and then the mixture was washed twice with a saturate solution of NaHCO$_3$ and water. The aqueous phases were washed with AcOEt twice, the organic phases were dried over Na$_2$SO$_4$ and the solvent was removed under reduced pressure. The pure product **13** was purified by flash column chromatography on silica gel (AcOEt:MeOH, 48:52 and one drop of Et$_3$N) (10.0 mg, 47% yield); ESI(+)MS: m/z = 971.4 (M+H+), 993.48 (M+Na+); ^{1}H NMR (300 MHz, CD$_3$OD, 298 K): δ 0.89 (t, CH$_2$CH$_2$C*H*$_3$, J = 7.3 Hz, 3H), 1.01 (t, CH$_2$CH$_2$C*H*$_3$, J = 7.3 Hz, 6H), 1.81-1.93 (overlapped, CH$_2$C*H*$_2$CH$_3$ 6H + C(O)C*H*$_3$, 9H), 2.09 (s, C(O)C*H*$_3$, 3H), 2.86 (t, CH$_2$N, J = 6.4 Hz, 4H), 3.02 (t, CH$_2$S, J = 6.6 Hz, 4H), 3.13-3.24 (overlapped, ArC*H*$_2$Ar, 4H), 3.75(t, OC*H*$_2$CH$_2$CH$_3$, J = 6.7 Hz, 2H), 3.86 (t, OC*H*$_2$CH$_2$CH$_3$, J = 7.2 Hz, 4H), 4.45 (overlapped, ArCH$_2$Ar, 4H), 4.78 (s,

145

OC*H₂*C(O), 2H), 6.57-6.59 (overlapped, ArH, 4H), 7.21 (s, ArH, 2H), 7.23 (s, ArH, 2H); ^{13}C NMR (63 MHz, CD$_3$OD, 298 K): δ 8.90, 9.26, 22.2, 22.5, 22.6, 28.8, 28.9, 29.2, 30.8, 31.2, 31.5, 36.7, 38.9, 39.1, 39.2, 73.6, 76.1, 77.4, 119.8, 120.3, 120.4, 120.8, 132.6, 132.8, 133.7, 134.2, 135.9, 151.2, 152.8, 153.6, 169.4, 169.7, 171.7. Anal. Calcd for C$_{51}$H$_{66}$N$_6$O$_9$S$_2$: C, 63.07; H, 6.85. Found: C, 63.15; H, 6.76.

Immobilization of *p*AC 13 on CDI-agarose beads: *p*AC **1a** (3 μmol) (Scheme S1) was dissolved in ACN containing 40% NaHCO3 and 1.5% TEA and reacted with 300 μL of CDI-Agarose beads for 16 h under rotary shacking at room temperature. Immobilization yield (30%) was assessed by injecting small aliquots of the reaction mixture in HPLC at t = 0 and after 16 h of reaction (**Figure 5.1**). The chromatographic analysis was performed by using an Agilent 1100 series chromatograph equipped with Phenomenex Jupiter C18, 5μm, 150x2.00 mm column at the flow rate of 0.200 ml/min and evaluating the reduction of *p*AC **13** peak areas. After 16 h of reaction the supernatant was discarded and functionalized matrix was stored at 4 °C in acetone until usage. A control matrix was prepared by adding 1.5 μmol of TIOS, solubilized in the same reaction buffer, to 150 μl of

CDI-Agarose. Linker immobilization was established by analysing a small aliquot of beads with Kaiser test. Briefly, after extensive washings with ethanol, 20 μl of ninidrin (6% in ethanol), 20 μl of phenol (80% in ethanol), and 20 μl of KCN were added to the matrix. The development of a violet colour, indicating the presence of primary amines onto the beads surface, was detected after 5 min at 50 °C.
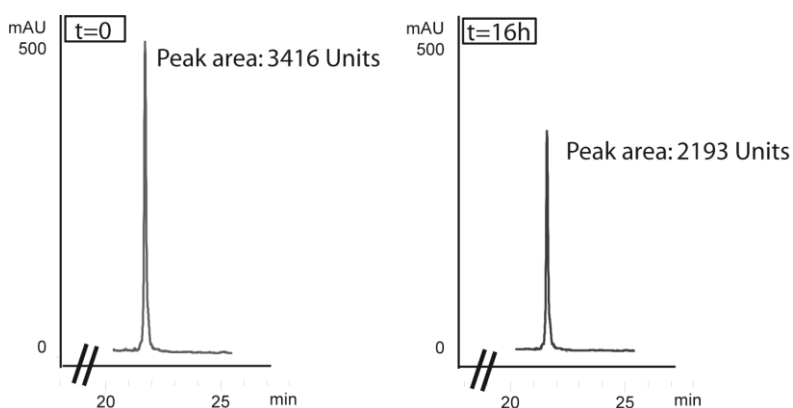
**Figure 5.1** Left panel shows the peak of free *p*AC **13** in 50 μL of reaction buffer at t = 0. The right panel shows the peak of free *p*AC **13** in 50 μL of reaction buffer after 16 h incubation. The reduction of the peak area demonstrates that *p*AC **13** has been anchored onto the CDI-Agarose beads.
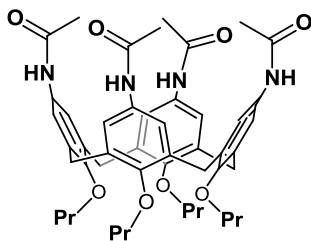
24

Synthesis of pAc derivative 24: A cold solution of acetyl chloride (5.22 mmol, 0.37 mL) in dry THF (32 mL) was added to a solution of tetraminocalix[4]arene derivative **23** (0.79 mmol, 0.52 g) and dry Et$_3$N (4.34 mmol, 0.60 mL) in dry THF (195 ml) at 0 °C. The reaction mixture was allowed to warm at room temperature and stirred overnight. The solvent was then removed under reduced pressure. The crude product was dissolved in AcOEt, washed with a saturate solution of NaHCO$_3$ (2 × 50 mL), with 1 M HCl (2 ×50 mL) and brine, dried over Na$_2$SO$_4$ and filtered. The solvent was removed by rotary evaporator to give a yellow solid. The product **24** was purified by silica gel chromatography (CH$_2$Cl$_2$:MeOH, 95:5 *v/v*) (0.28 g; 43% yield). ESI(+)MS: m/z = 821.8 (M+H+), 844.5 (M+Na+), 860.3 (M+K+); ^{1}H NMR (300 MHz, DMSO-*d*6, 298 K): δ 0.95 (t, CH$_2$CH$_2$C*H$_3$*, *J* = 7.2 Hz, 12H), 1.83-1.91 (overlapped, CH$_2$C*H$_2$*CH$_3$ 8H + C(O)C*H$_3$*, 12H), 3.04 (d, ArC*H$_2$*Ar, *J* = 12.9 Hz, 4H), 3.75 (t, C*H$_2$*CH$_2$CH$_3$, *J* = 7.2 Hz, 8H), 4.31 (d, ArC*H$_2$*Ar, *J* = 12.9 Hz, 4H), 6.86 (s, Ar*H*, 8H), 9.45 (s, C(O)N*H*, 4H); ^{13}C NMR (63 MHz, DMSO-*d*6, 298 K): δ 10.5, 22.9, 24.0, 31.0, 76.7,

119.8, 133.4, 134.4, 152.2, 167.8. Anal. Calcd for $C_{48}H_{60}N_4O_8$: C, 70.22; H, 7.37. Found: C, 70.31; H, 7.29.

Biomolecular fishing for partners: HeLa cells were grown in Dulbecco's modified Eagle medium (DMEM) supplemented with fetal bovine serum (10% (v/v)), penicillin (100 UmL-1), streptomycin (100 mgmL-1), glutamine (4 mM), HEPES (10 mM), and sodium pyruvate (10 mM) at 37 °C in a 5% CO_2 atmosphere (all reagents were from Sigma–Aldrich). The cells were collected by centrifugation (10000 rpm, 3 min) and washed three times with phosphate saline buffer (PBS; sodium phosphate (50 mM), NaCl (150 mM), pH 7.5). Pellets were re-suspended in ice-cooled PBS containing Igepal (0.1%) and a protease inhibitor cocktail and lysed by dounce homogenation. Lysates were clarified by centrifugation at 10000g for 10 min at 4 °C and the protein concentration was determined using Bradford assay and adjusted to 1 mg/ml. *p*AC-**13-**beads (50 μL) and the same amount of the control-matrix were separately incubated with 1 mg of HeLa total protein extract under continuous shaking (1 h, 4 °C). Beads were then collected and washed three times with PBS (pH 7.4). Proteins strictly bound to solid matrices were isolated by breaking the disulphide bond contained into the TIOS linker with DTT 40 mM. The suspension was

maintained at 37 °C for 15 minutes to favor disulphide bridge cleavage. SDS-PAGE loading buffer (60 mM Tris/HCl pH 6.8, 2% SDS, 0.001% bromophenol blue, 10% glycerol, 2% 2-mercaptoethanol) was added to each sample and, after 5 min at 95 °C, prior SDS-PAGE separation and Coomassie G-250 (Bio-Rad, Hercules, CA) staining. In the attempt to evaluate the electrophoretic profile of the putative *p*AC-**13** partners, we run a 10% SDS PAGE. We coloured the SDS-PAGE both by Comassie G-250 and by silver staining depending on the loading quantity. Since the run comparison between the calixbeads and the control (beads only) in the two SDS-PAGE profiles was not informative for our purpose, we decided to avoid the SDS-PAGE separation to reduce the protein loss due to the partition procedure, multiple *in situ* protein digestion, and peptide extraction. Then, in the following experiments, SDS PAGE was only used to purify proteins eluted prior digestion. More in details, proteins eluted from the beads were loaded onto SDS-PAGE but the separation was stopped after 10 minutes. Gels were stained with Coomassie G-250 (Bio-Rad, Hercules, CA), and the full short run, containing all proteins eluted from the beads, was cut out, washed with ultrapure water and CAN, and subjected to *in situ* protein digestion as described by Shevchenko.[117]

---

[117] Shevchenko, A.; Tomas, H.; Havlis, J.; Olsen, J. V.; Mann, M. *Nat. Protoc.* **2006**, *6*, 2856-2860.

Briefly, each slice was reduced with 1,4-dithiothreitol (DTT, 10 mM) and alkylated with iodoacetamide (50 mM), then washed and rehydrated in trypsin solution (12 ngmL^{-1}) on ice for 1 h. After the addition of ammonium bicarbonate (30 μL, 10 mM, pH 7.5), protein digestion was allowed to proceed overnight at 37 °C. Supernatants were collected and peptides were further extracted from gel slices using 100% acetonitrile. Finally, second supernatants were collected and combined with first ones. Peptide samples were dried and dissolved in formic acid (FA, 10%) before MS analysis. Peptide mixtures (5 μL) were injected into a nano-ACQUITY UPLC system (Waters) and separated on a 1.7 mm BEH C18 column (Waters) at a flow rate of 400 nLmin^{-1}. Peptide elution was achieved with a linear gradient [solution A: H_2O (95 %), CH_3CN (5 %), FA (0.1%); solution B: CH_3CN (95 %), H_2O (5 %), FA (0.1 %); 15–50% B over 55 min]. Peptide samples re-suspended in formic acid (FA, 10%) and analysed with an ACQUITY UPLC system (Waters) coupled to a LTQOrbitrap XL (ThermoScientific). The ten most intense doubly and triply charged peptide ions were chosen for fragmentation. Mascot generic files (mgf) for database search were generated by the software MassMatrix MS data file conversion. Database searches were carried out on the Mascot server (http://www.matrixscience.com). The SwissProt database (release 2012_03, 21 March 2012, 535248 sequence entries,

189901164 amino acids abstracted from 208076 references) was employed. Searches were performed allowing two missed cleavages; carbamidomethyl (C) as fixed modification and oxidation (M) and phosphorylation (ST) as variable modifications; peptide tolerance 25 ppm; MS/MS tolerance 0.8 Da.

The entire fishing/control procedure was repeated 3 times (Experiments #1-3). In this way, three sets of potential protein partners for pAC **13** were obtained after excluding those of control experiments. The "pep(sig)" value represents the number of peptides found for the identified protein, while the protein Mascot score is the probability that the observed match is not a random event. A filter has been applied to select the proteins identified with high trustworthiness, reported in bold black, setting the value of pep(sig) >1 and protein Mascot score > 30. In gray are reported keratins (their presence is due to accidental operator contamination) and all the proteins identified with solely 1 pep(sig) and Mascot score ≤ 30. The three sets of data were then intersected to exclude all not-common candidates. In this way, a single common protein was found, that was considered as the best potential specific partner of pAC **13**, the protein disulfide isomerase (PDI), as illustrated by the corresponding Venn diagram (**Figure 5.2**).
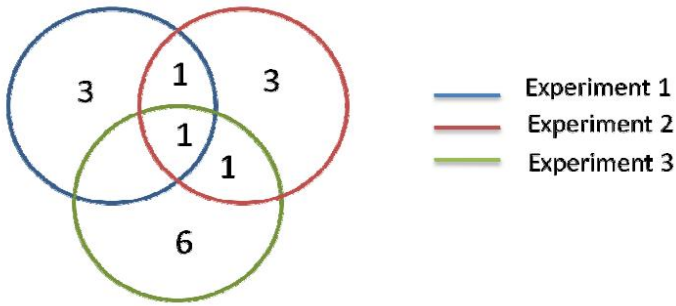
	Score	Mass	Matches	Pep(sig)	Description
Experiment 1	35	57480	9	3	Protein disulfide-isomerase
Experiment 2	67	57480	6	4	Protein disulfide-isomerase
Experiment 3	139	57487	11	5	Protein disulfide-isomerase

Figure 5.2 Venn diagram showing the intersection of the three sets of all the protein partners identified in the three different experiments.

Surface Plasmon Resonance: Protein disulphide isomerase (PDI, Enzo Life Sciences) and Peroxiredoxin 1 and Lamin b1 (Origene), as negative controls, were immobilized onto CM5 sensor chip using standard amine coupling procedures. HBSP, which consisted of 10 mM HEPES pH 7.4, 150 mM NaCl, 0.005% v/v surfactant P20, was used as running buffer. The carboxymethyl dextran surface was activated as already described and proteins were diluted to a final concentration of 30 ng/μl in 10 mM sodium acetate, pH 4.5 and injected separately onto the flow cells. After protein injections a DRU of ~10000 was recorded. The activated carboxymethyl

dextran surface was finally blocked with a 7-min injection of 1.0 M ethanolamine-HCl, pH 8.5, at 5 μl/min. *p*AC **24** solutions (0.1-10 μM), were prepared in running buffer containing 1% of DMSO and injected at least three times. Since the dissociation back to baseline was achieved within a reasonable time frame, no regeneration was required. The interaction experiments were carried out at a flow rate of 10 μl/min. The dissociation time was set at 600 seconds. Rate constants for associations (ka) dissociations (kd) and the dissociation constants (KD) were obtained by globally fitting data from injections of all concentrations, using the BIA evaluation software, using the simple 1:1 Langmuir binding model (**Figures 5.3-5.5**).
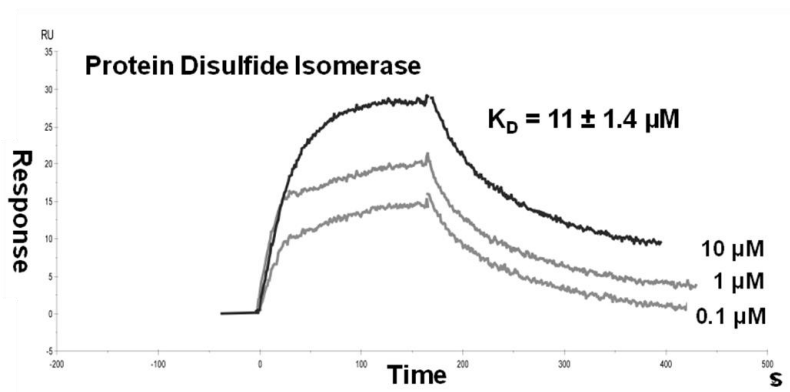
Figure 5.3 Sensograms obtained after injections of *p*AC **24** on the immobilized PDI.
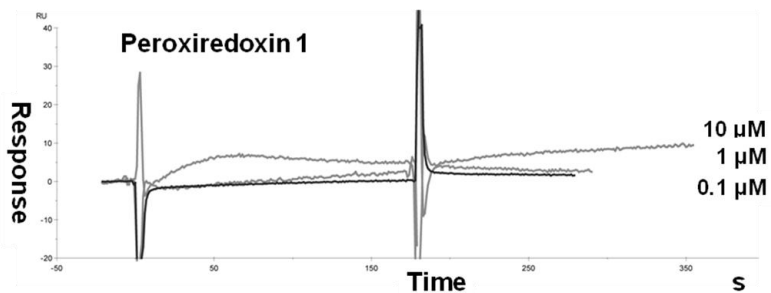
Figure 5.4 Sensorgrams obtained after injections of *p*AC **24**
(three different concentrations, 0.1–10 μM)
on the immobilized Peroxiredoxin 1.
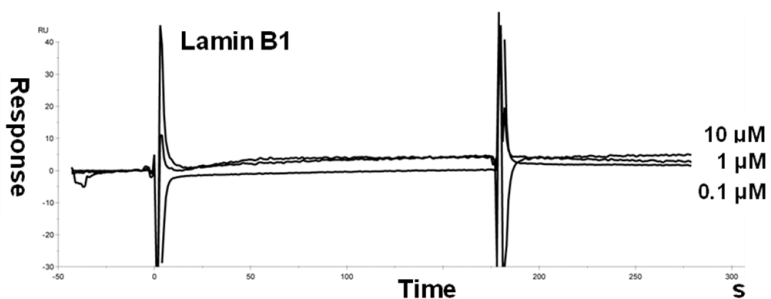
Figure 5.5 Sensorgrams obtained after injections of *p*AC **24**
(three different concentrations, 0.1–10 μM)
on the immobilized Lamin B1.
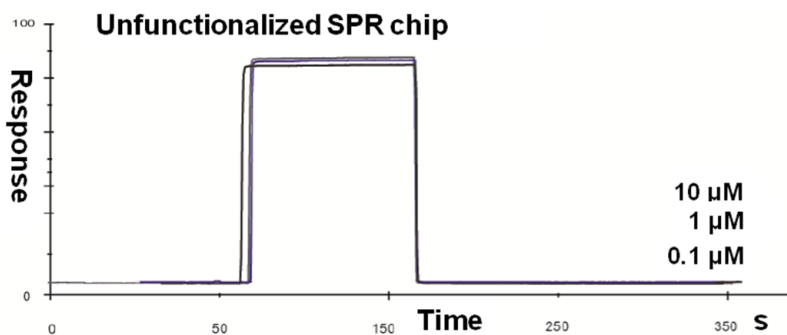
Figure 5.6. Sensorgrams obtained after injections of *p*AC **24**
(three different concentrations, 0.1–10 µM) on
the unfunctionalized SPR chip.

Measurement of PDI activity: PDI activity was assayed by measuring the PDI catalysed reduction of insulin in the presence of DTT at 620 nm. Recombinant PDI protein (0.8 µM) was incubated with *p*AC **24** (50 and 100 µM) at 37 °C for 30 min in sodium phosphate buffer (100 mM sodium phosphate). Later on, samples of the free and the recombinant PDI protein previously treated with *p*AC **24**, were added to a mixture containing EDTA (2 mM), DTT (0.75 mM), and insulin (0.1 mM, Sigma). The reaction was allowed to proceed at room temperature and measured every 5 minutes at 620 nm in a 96-well plate. Specific PDI activities, with and without the tested compound, were estimated by subtracting

the absorbance of control buffer at each time point (**Figure 5.7**).
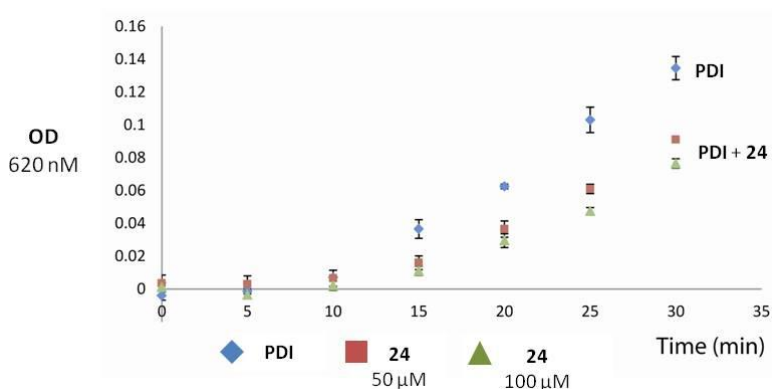
Figure 5.7 Effect of **24** on the PDI catalytic reduction of insulin.

Biological assays:

Cell Lines

The cell lines CAL-27 (oral adenosquamous carcinoma cell line) and PC-3 (human prostate cancer cell line) were grown in RPMI (Life Technologies, Paisley, UK) supplemented with 10% heat-inactivated fetal bovine serum (FBS; Life Technologies), 2mM glutamine (Hyclone, Cramlington, UK), 50 U/ml penicillin and 50 U/ml streptomycin (Hyclone), hereafter defined as CM. They were grown in adhesion culture, respectively, at a density of 3x105 cells per ml and splitted twice a week.

157

MTS Assay

PBMC was evaluated by MTS assay. Inhibition of cell metabolic activity was detected through formazan product formation, using a commercial colorimetric kit (MTS [3,4-(5-dimethylthiazol-2-yl)-5-(3-carboxymethoxyphenyl)-2-(4-sulfophenyl)-2H-tetrazolium salt]) (Cell Titer 96 Aqueous One Solution; Promega). This colorimetric standard assay measures the activity of the enzymes that reduce MTS to formazan. The assay was performed by seeding $5x10^3$ CAL-27 or PC-3 cells in 100 μl of CM per well in 96 wells plate in triplicate in absence or in the presence of 0.35, 0.75, 1.5, 3.0, 6.0, and 12 μM of *p*AC **24**, **SN38** (7-ethyl-10-hydroxy-camptothecin) and the known PDI inhibitor **16F16**,[83] as positive controls, for 24 hours. Twenty microliters of 'Cell Titer 96 Aqueous One Solution' reagent was added directly to culture wells at the end of the culture period and samples were incubated for 1 h. Successively the absorbance was read at 490.

Cytotoxic Assay

The effect of *p*AC **24, SN38**, and **16F16** on cytotoxicity of CAL-27 and PC-3 cell lines was assessed by evaluating dead and living cells, respectively, using the trypan blue dye exclusion test. After 24 hours of culture both CAL-27 and PC-

3 cell lines were seeded in duplicate at 3x105 per well in the absence or in the presence of 0.35, 0.75, 1.5, 3.0, 6.0, and 12 μM of *p*AC **24**, **SN38**, and the known PDI inhibitor **16F16** as positive controls. After the incubation time, cells were stained with a colorant selective for dead cells, Trypan blue 0.1%, diluted in Phosphate buffered saline. The viable cells were counted and expressed as millions of viable cells per milliliter.

	Cell Lines	$IC_{50} \pm SD$ $(\mu M)^a$	$CC_{50} \pm SD$ $(\mu M)^b$
24	CAL-27	20.5±0.8	31±4
24	PC-3	24.5±0.9	283±10
SN38	CAL-27	3.0±0.9	3.2±0.3
SN38	PC-3	11.5±0.2	6.9±0.9
16F16	CAL-27	7.6±0.4	8.8±1.9
16F16	PC-3	25±0.6	14.7±1.6

[a]IC50 is the inhibitory concentration required to inhibit 50% of cell viability;
[b]CC50 is the metabolic activity cytotoxic inhibitory concentration 50%, evaluated in the CAL-27 and PC3 cell lines by MTS assay

Table 5.1. Evaluation of the cytotoxicity of *p*AC **24** in comparison with SN38 and 16F16.

Statistical Analysis

Cumulative results from three or two determinations were used to calculate the initial compound concentration effective in inhibiting by 50% metabolic assay (CC_{50}) or in inhibiting by 50% cell viability (IC_{50})±SD. The values were calculated according to the best-fit curve, y value versus log x, where y is the value of the examined function and x is the drug concentration.

Docking studies: Docking calculations were performed with the AutoDock 4.2 program.[55] The experimental structure of PDI in its reduced state[118] was used for the calculations. 3D structures of the ligands were created and energy minimized with MacroModel-9.0/Maestro-4.14 program. For all the docked structures, all bonds at the upper rim were treated as active torsional bonds. Grid boxes of 80 Å, covering the four **a**, **b**, **b'**, and **a'** domains, were used for the docking calculations (grid spacing = 0.375 Å). In particular, regarding the **a** and **a'** domains, the boxes were centered at the sulfur atoms of the catalytic residues C53 and C397 residues. In order to achieve a representative conformational space during the docking calculations, from three to ten calculations were

[118] Wang, C.; Li, W.; Ren, J.; Fang, J.; Ke, H.; Gong, W.; Feng, W.; Wang, C. C. Antioxid. Redox Signal **2013**, *19*, 36-45.

performed. The Lamarckian genetic algorithm was applied for sampling and default docking parameters were used with the following exceptions: ga-pop-size, 500; ga-num-evals, 10000000; ga-num-generations 500000, and ga-run, 250.

Docking studies were performed on *p*AC **24** derivative and *p*AC-**13**-bead model (**Figure 5.8**) to verify the accessibility of the matrix-bound calixarene (*p*AC-**13**-beads) into the enzyme active site without disrupting the PDI complex, as required by the pulldown experiments. Tetrapropxy-*p*-tert-butylcalix[4]arene (**TBC**, **Figure 5.8**), devoid of the critical acetamido groups, was also studied as a comparative calixarene derivative and as a negative control case. The calculated inhibition constants (*Ki*) for these three derivatives are reported in **Table 5.2**.
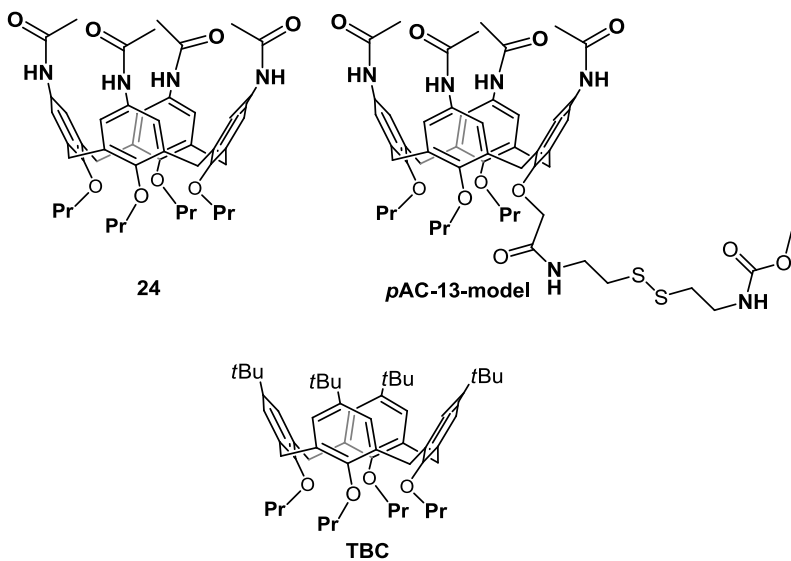
Figure 5.8

	K_i
24	6.23 μM
pAC-13-bead model	15.69 μM
TBC	8.23 mM

Table 5.2. Calculated inhibition constants (K_i) of calix[4]arene derivatives in **Figure 5.8**.

28
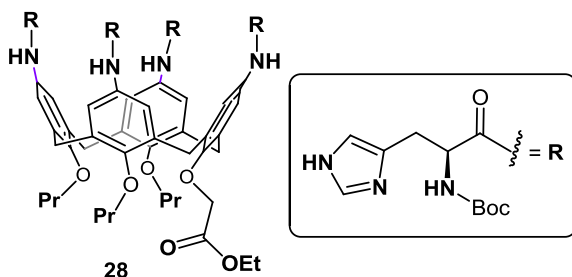
Synthesis of derivative 28: Compound **27** (50.0 mg, 0.07 mmol) was dissolved in dry DMF (8.75 ml), then PyBOP (872.0 mg, 1.68 mmol), DIPEA (0.50 ml, 2.92 mmol) and N^{α}-Boc-Histidine (428.0 mg, 1.68 mmol) were added. The reaction mixture was stirred at room temperature for 72h then H_2O (30ml) was added and the white precipitate was filtered. The product was purified by flash column chromatography (CH_2Cl_2:MeOH, 9:1).

Compound 28: 53% yield; ESI(+) MS: m/z = 1646.8 ($M+H^+$), 1668.9 ($M+Na^+$), 834.7 ($M+Na^{2+}$), 823.7 ($M+H^{2+}$); $[\alpha]_D^{25}$ = + 1.76 (c = 1, MeOH); ^{1}H NMR (400 MHz, MeOD, 298 K) δ 0.98 (t, $OCH_2CH_2CH_3$, J = 7.4 Hz, 3H), 1.05 (t, $OCH_2CH_2CH_3$, J = 7.4 Hz, 6H), 1.28 (t, OCH_2CH_3, J = 7.2 Hz, 3H), 1.36-1.39 (overlapped, Boc, 36H), 1.93 (q, $OCH_2CH_2CH_3$, J = 7.4 Hz, 4H), 1.96-2.03 (m, $OCH_2CH_2CH_3$, 2H), 2.91-3.02 (overlapped, $CH_2^{histidine}$, 6H), 3.11-3.18 (overlapped, $CH_2^{histidine}$ + $ArCH_2Ar$, 6H + 4H), 3.72-3.82 (overlapped, $OCH_2CH_2CH_3$, 4H), 3.90 (t, $OCH_2CH_2CH_3$, J = 7.8 Hz, 2H), 4.19 (q, OCH_2CH_3, J = 7.1 Hz, 2H), 4.32-4.36 (m, $CH^{histidine}$, 2H), 4.41-4.47 (overlapped, $CH^{histidine}$ +

163

ArCH$_2$Ar, 2H + 2H), 4.68 (d, ArCH$_2$Ar, J = 12.9 Hz, 2H), 4.84 (s, OCH$_2$C(O)OCH$_2$CH$_3$, 2H), 6.55 (s, ArH, 2H), 6.76 (s, ArH, 2H), 6.94 (br s, CH$^{\text{imidazole}}$, 4H), 7.00 (s, ArH, 2H), 7.03 (br s, NCH$^{\text{imidazole}}$, 4H), 7.14 (s, ArH, 2H), 7.96 (s, NH$^{\text{imidazole}}$, 4H), 8.02 (s, NH$^{\text{imidazole}}$, 4H); ^{13}C NMR (100 MHz, MeOD, 298 K) δ 10.51, 11.00, 14.59, 24.36, 28.70, 30.47, 32.00, 32.54, 56.16, 56.35, 61.61, 71.85, 78.24, 78.44, 80.93, 118.24, 122.73, 132.86, 133.46, 135.36, 135.80, 136.70, 136.79, 136.94, 137.03, 154.27, 154.43, 155.17, 157.58, 171.60, 171.75.
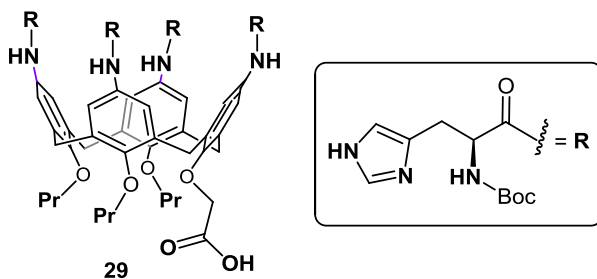
Synthesis of derivative 29: Compound **28** (31.2 mg, 0.019 mmol) was suspended in dry THF (4.5 ml). A solution of LiOH·H$_2$O (3.2 mg, 0.076 mmol) in H$_2$O (0.9 ml) was added and the reaction mixture was stirred at room temperature for 6 h. The solvent was removed under reduce pressure, then H$_2$O (5 ml) and a few drops of 1M HCl solution were added until pH = 4-5 was reached. The product was thus concentrated and MeOH was added. The precipitate was removed by filtration

and the filtrate was concentrated affording compound **29**. (99% yield); ESI(+) MS: m/z = 828.3 (M+HK^{2+}), 809.4 (M+H^{2+}); $[\alpha]_D^{25}$ = + 1.10 (c = 1, MeOH); ^{1}H NMR (400 MHz, MeOD, 298 K) δ 0.92-0.96 (overlapped, OCH$_2$CH$_2$C*H$_3$*, 6H), 1.03 (t, OCH$_2$CH$_2$C*H$_3$*, J = 6.6 Hz, 3H), 1.34-1.39 (overlapped, Boc, 36H), 1.87-1.98 (overlapped, OCH$_2$C*H$_2$*CH$_3$, 6 H), 3.01-3.25 (overlapped, CH$_2$^{histidine} + ArCH$_2$Ar, 8H + 4H), 3.78-3.82 (m, OC*H$_2$*CH$_2$CH$_3$, 4H), 3.96-4.00 (m, OC*H$_2$*CH$_2$CH$_3$, 2H), 4.48-4.55 (overlapped, ArCH$_2$Ar + CH^{histidine}, 4H + 4H), 4.73 (s, OC*H$_2$*COOH), 6.77 (s, ArH, 2H), 6.89 (s, ArH, 2H), 7.22-7.30 (overlapped, ArH + CH^{imidazole} + NCH^{imidazole}, 2H + 4H + 4H), 7.44 (s, ArH, 2H); 8.56-8.63 (overlapped, NH^{imidazole}, 4H); ^{13}C NMR (100 MHz, MeOD, 298 K) δ 9.97, 10.34, 10.86, 23.59, 24.01, 24.23, 28.86, 29.40, 30.72, 31.59, 31.93, 32.33, 55.63, 55.79, 78.71, 79.01, 80.37, 80.96, 118.65, 122.69, 131.53, 131.67, 133.39, 135.15, 136.61, 137.05, 137.17, 149.22, 153.46, 157.42, 170.90, 171.17, 171.37.

$$H_2N \diagdown S_S \diagdown \overset{H}{N} Fmoc$$
30
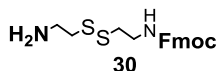
Synthesis of derivative 30: Compound **21** (409 mg, 1.62 mmol) were dissolved in CH$_2$Cl$_2$ (16.2 ml), then DIPEA (0.55

ml, 3.24 mmol) and FmocCl (628 mg, 2.43 mmol) were added. The reaction mixture was stirred at room temperature for 1 h. Then water (10 ml) was added and the organic phase was collected, dried over Na_2SO_4 and concentrated. The crude product was dissolved in trifluoroacetic acid (16 ml) and the solution was stirred at room temperature for 45 min. Afterwards TFA was removed under reduced pressure, the crude was dissolved in CH_2Cl_2 and washed with $NaHCO_3$ sat. sol. and brine. The organic phase was dried over Na_2SO_4 and the solvent was removed under reduced pressure. The pure product was isolated after silica gel chromatography (CH_2Cl_2:MeOH, 9:1) although the formation of a insoluble precipitate.

(7% yield); ESI(+) MS: m/z = 354.5; ^{1}H NMR (250 MHz, CDCl$_3$, 298 K): δ 2.66 (t, CH_2NH$_2$, J = 6.2 Hz, 2H), 2.78 (t, CH_2N, J = 5.9 Hz, 2H), 2.90-2.97 (overlapped, CH$_2$S, 4H), 3.08 (d, CH$_2$^{Fmoc}, J = 6.5 Hz, 2H), 4.06 (t, CH^{Fmoc}, J = 6.5 Hz), 7.25-7.41 (overlapped, ArH, 4H), 7.59 (t, ArH, J = 6.7 Hz, 2H), 7.76 (t, ArH, J = 7.1 Hz, 2H); ^{13}C NMR (63 MHz, CDCl$_3$, 298 K): δ 38.94, 40.61, 42.52, 48.04, 48.28, 52.83, 120.16, 124.74, 127.15, 127.49, 141.34, 145.88, 181.85.

5.3 Multivalent iminosugar calix[8]arene conjugates

Synthesis of derivatives 36-37: To a suspension of the desired calix[8]arene (1,0 g) in acetone (100 ml) Cs_2CO_3 (1.25 eq. per OH) was added. The reaction mixture was stirred at reflux for 2 hours. Then the system was cooled to room temperature and propargyl bromide (2.5 eq. per OH) was added. The reaction mixture was then stirred at reflux for 20 hours, then it was cooled to room temperature and the solvent was removed under reduced pressure. HCl 1N (150 ml) was added to the flask and the mixture was stirred for 15 mins. Then CH_2Cl_2 was added and the product was partitioned. The organic phases were collected, dried over Na_2SO_4 and the solvent was removed under reduced pressure. The crude product was dissolved in a small amount of CH_2Cl_2 and then MeOH was added. The precipitated was filtered, affording the pure product as a white solid.
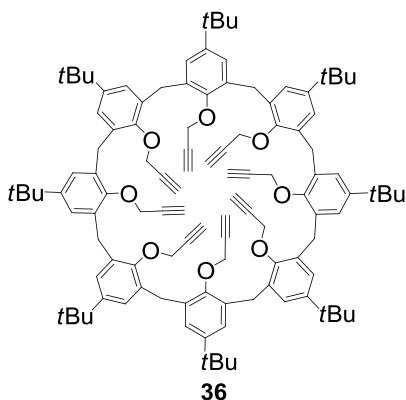
36

Compound 36: (76% yield); ESI(+) MS: *m/z* = 1603.1 (M+H⁺), 1624.9 (M+Na⁺); ¹H NMR (400 MHz, CDCl₃, 298K): δ 1.11 (s, *t*Bu, 72H), 2.30 (br t, H^propargyl, 8H), 4.10 (s, ArC*H₂*Ar, 16H), 4.21 (d, OC*H₂*C, 2.1 Hz, 16H), 6.95 (s, Ar*H*, 16H); ¹³C NMR (100 MHz, CDCl₃, 298K): δ 31.19, 31.55, 34.42, 60.87, 75.42, 79.70, 126.29, 133.39, 146.86, 153.06.


37

Compound 37: (57% yield); ESI(+) MS: *m/z* = 1628.7 (M+H⁺), 1647.9 (M+Na⁺), 1667.9 (M+K⁺); ¹H NMR (600 MHz, CDCl₃, 298K): δ 0.55 (s, *t*Bu, 18H), 1.17 (s, *t*Bu, 36H),

36

Compound 36: (76% yield); ESI(+) MS: m/z = 1603.1 (M+H$^+$), 1624.9 (M+Na$^+$); ^{1}H NMR (400 MHz, CDCl$_3$, 298K): δ 1.11 (s, *t*Bu, 72H), 2.30 (br t, H^{propargyl}, 8H), 4.10 (s, ArCH_2Ar, 16H), 4.21 (d, OCH_2C, 2.1 Hz, 16H), 6.95 (s, ArH, 16H); ^{13}C NMR (100 MHz, CDCl$_3$, 298K): δ 31.19, 31.55, 34.42, 60.87, 75.42, 79.70, 126.29, 133.39, 146.86, 153.06.

37
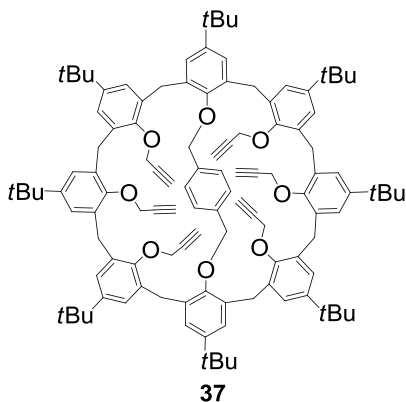
Compound 37: (57% yield); ESI(+) MS: m/z = 1628.7 (M+H$^+$), 1647.9 (M+Na$^+$), 1667.9 (M+K$^+$); ^{1}H NMR (600 MHz, CDCl$_3$, 298K): δ 0.55 (s, *t*Bu, 18H), 1.17 (s, *t*Bu, 36H),

1.38 (s, *t*Bu, 18H), 2.46 (br t, $H^{propargyl}$, 4H), 2.56 (br t, $H^{propargyl}$, 2H), 3.56 (s, OCH_2^{xylene}, 4H), 4.10 (s, $ArCH_2Ar$, 8H), 4.21 (s, $ArCH_2Ar$, 8H), 4.57 (s, $OCH_2^{propargyl}$, 8H), 4.74 (s, $OCH_2^{propargyl}$, 4H), 5.95 (s, Ar*H*, 4H), 6.70 (s, Ar*H*, 4H), 6.91 (s, Ar*H*, 4H), 7.24 (br d, Ar*H*, J = 2.2 Hz, 4H), 7.27 (s, Ar*H*, 4H); ^{13}C NMR (150 MHz, $CDCl_3$, 298K): δ 30.97, 31.09, 31.58, 31.83, 34.04, 34.51, 60.59, 61.45, 75.16, 75.63, 80.04, 80.40, 124.58, 124.75, 126.31, 127.20, 128.29, 129.03, 132.41, 133.10, 133.65, 134.94, 136.43, 146.25, 146.42, 146.53, 151.48, 152.59, 154.43.

General procedure for the cycloaddition reactions: Compound **36**/**37** (10-15 mg) and **DNJC₆/DNJC₉** (1.2 eq/alkyne) were dissolved in DMF (0.8-1.0 ml) in an ACE pressure tube. Then a yellow solution of $Cu_2SO_4 \cdot 5H_2O$ (0.1 eq/alkyne) and sodium ascorbate (0.2 eq/alkyne) in water (0.2-0.25 ml) was added. The reaction mixture was heated under microwave irradiation for 20-30 min, in a common microwave oven (800 W). The mixture was concentrated, diluted in a 9:1:1 (v/v/v) solution of CH_3CN/AcOEt/30w%NH_4OH and filtrated with the same eluent (30 ml) on a small pad of SiO_2. The filtrate was

concentrated and then purified by flash chromatography on silica gel.

38a
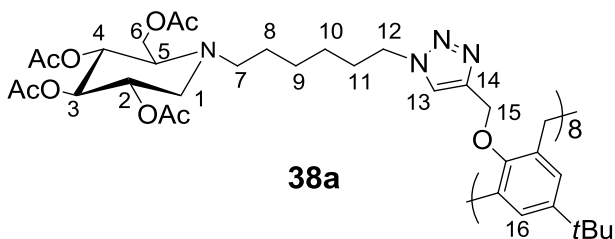
Compound 38a: (AcOEt-AcOEt:MeOH 98:2, 51% yield); ESI(+) MS: m/z = 5250.74; $[\alpha]_D^{28.3}$ = +3.59 (c = 1, CHCl$_3$); ^{1}H NMR (300 MHz, CDCl$_3$, 298K): δ 0.89 (s, tBu, 72H), 1.25 (br, H9+H10, 32H), 1.39 (br, H8, 16H), 1.77 (br, H11, 16H), 2.00-2.04 (m, Ac, 96H), 2.30 (t, H1^a, J = 10.6 Hz, 8H), 2.53 (m, H7^a, 8H), 2.61 (m, H5, 8H), 2.70 (m, H7^b, 8H), 3.16 (dd, H1^b, J = 11.6 Hz, J = 4.9 Hz, 8H), 4.06 (s, H15, 16H), 4.14 (br, H6, 16H), 4.18 (overlapped, H12, 16H), 4.79 (s, H14, 16H), 4.92 (m, H2, 8H), 5.03 (overlapped, H3+H4, 16H), 6.80 (s, H16, 16H), 7.79 (s, H13, 8H); ^{13}C NMR (75 MHz, CDCl$_3$, 298K): δ 20.90, 20.96, 21.07, 24.79, 26.64, 26.91, 30.17, 30.51, 31.41, 34.23, 50.19, 51.90, 53.13, 59.61, 61.65, 66.63, 69.59, 69.68, 74.86, 123.90, 126.12, 133.29, 144.15, 146.59, 152.66, 169.94, 170.19, 170.54, 171.04.

38b
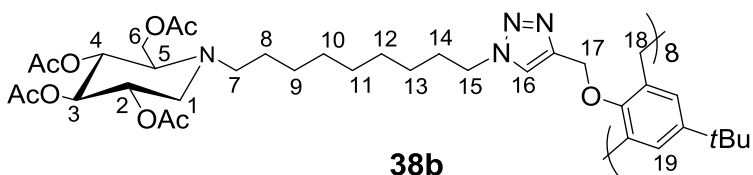
Compound 38b: (AcOEt:Petroleum Ether, 8:2, 52% yield); ESI(+) MS: m/z = 5587.11; $[\alpha]_D^{27}$ = +5.21 (c = 1, CHCl$_3$); ^{1}H NMR (600 MHz, CDCl$_3$, 298K): δ 0.90 (s, tBu, 72H), 1.24 (overlapped, H9-H13, 80H), 1.39 (br, H8, 16H), 1.76 (br, H14, 16H), 2.00-2.06 (overlapped, Ac, 96H), 2.32 (t, H1^a, J = 10.9 Hz, 8H), 2.55 (m, H7^a, 8H), 2.62 (br d, H5, J = 9.2 Hz, 8H), 2.70 (m, H7^b, 8H), 3.17 (dd, H1^b, J = 11.4 Hz, J = 5.1 Hz, 8H), 4.06 (s, H18, 16H), 4.14 (br, H6, 16H), 4.18 (br, H15, 16H), 4.79 (s, H17, 16H), 4.95 (m, H2, 8H), 5.0-5.07 (overlapped, H3+H4, 16H), 6.80 (s, H19, 16H), 7.78 (s, H16, 8H); ^{13}C NMR (150 MHz, CDCl$_3$, 298 K): 20.90, 20.97, 21.07, 21.09, 24.84, 26.78, 27.48, 29.28, 29.74, 29.92, 30.57, 31.43, 34.25, 50.31, 52.07, 53.18, 59.69, 61.60, 66.65, 69.66, 69.74, 74.93, 123.86, 126.12, 133.30, 144.22, 146.57, 152.71, 169.96, 170.22, 170.58, 171.11.
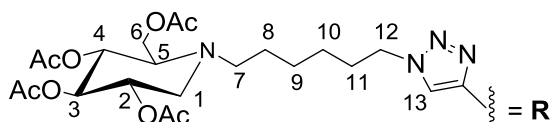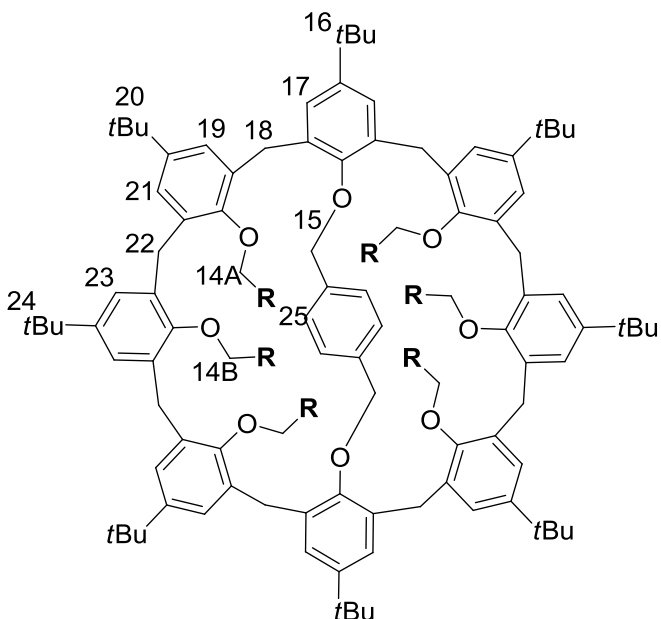
39a

Compound 39a: (AcOEt/Petroleum Ether 9:1 - AcOEt, 51% yield); ESI(+) MS: m/z = 4364.31; $[\alpha]_D^{30.3}$ = +3.99 (c = 1, CHCl$_3$); ^{1}H NMR (600 MHz, CDCl$_3$, 298K): δ 0.40 (s, tBu16, 18H), 0.95-1.54 (overlapped, H8-H10 + H12A, 44H), 1.17 (s, tBu20, 36H), 1.41 (s, tBu24, 18H), 1.86 (t, H11, J = 7.2 Hz, 12H), 1.98-2.06 (overlapped, 72H), 2.25-2.30 (overlapped, H1A^a+H1B^a, 6H), 2.42-2.62 (overlapped, H7A^a + H7B^a + H5A + H5B + H7B^b, 14H), 2.69-2.74 (m, H7A^b, 4H), 3.10 (dd, H1A^b, J = 11.5 Hz, J = 5.22 Hz, 4H), 3.18 (dd, H1B^b, J =

11.5 Hz, *J* = 5.2 Hz, 2H), 3.32 (s, H15, 4H), 3.44-3.48 (overlapped, ArC*H₂*Ar, 4H), 3.53 (t, ArC*H₂*Ar, *J* = 14.4 Hz, 4H), 3.86-3.97 (overlapped, H12A, 8H), 4.07-4.17 (overlapped, H6A + H6B, 12H), 4.33 (t, H12B, *J* = 7.8 Hz, 4H), 4.36-4.40 (overlapped, ArC*H₂*Ar, 4H), 4.79 (d, ArC*H₂*Ar, *J* = 13.2 Hz, 4H), 4.89-4.96 (overlapped, H3A + H3B, 6H), 4.97-5.08 (overlapped, H2A + H2B + H4A + H4B, 12H), 5.82 (s, H17, 4H), 6.58 (s, ArH, 2H), 6.61 (s, ArH, 2H), 6.95 (s, ArH, 2H), 6.98 (s, ArH, 2H), 7.22-7.28 (overlapped, ArH + H13B, 6H), 7.77 (s, H13A, 4H); ^{13}C NMR (150 MHz, CDCl₃, 298 K): δ 20.90, 20.97, 21.07, 24.41, 25.04, 26.58, 26.70, 26.82, 29.92, 30.31, 30.39, 30.57, 31.14, 31.58, 31.88, 33.92, 34.51, 34.54, 50.12, 50.45, 51.73, 51.92, 51.97, 53.06, 53.19, 59.46, 59.69, 61.53, 61.60, 61.86, 66.18, 67.03, 69.60, 69.69, 74.85, 75.00, 123.12, 123.26, 123.42, 124.04, 124.28, 127.31, 128.71, 129.17, 132.72, 133.40, 134.63, 134.74, 136.56, 144.05, 144.34, 146.49, 146.66, 152.42, 153.81, 169.96, 170.12, 170.28, 170.58, 171.08.
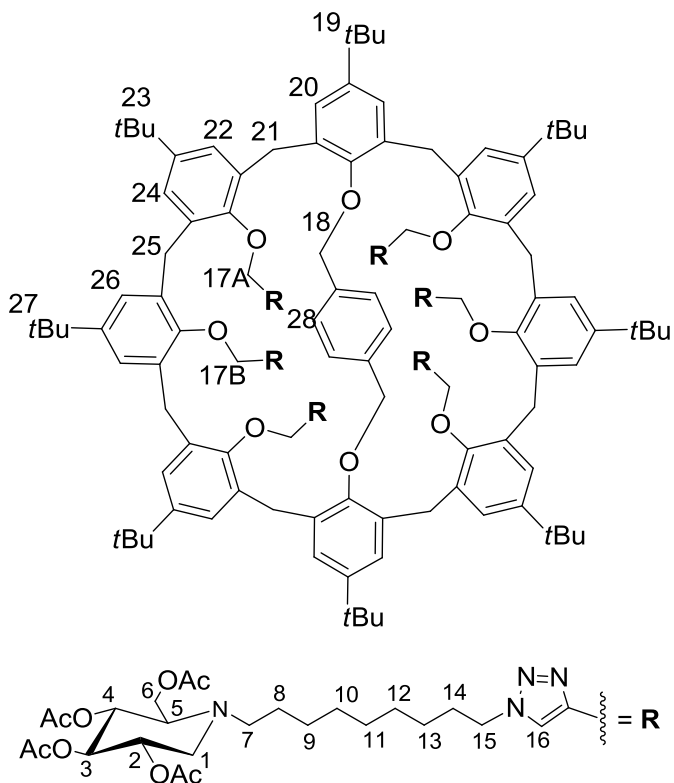
Compound 39b: (AcOEt/Petroleum Ether 72:28 − AcOEt, 37% yield); ESI(+) MS: m/z = 4616.59; $[\alpha]_D^{31.6}$ = +7.43 (c = 1, CHCl$_3$); ^{1}H NMR (600 MHz, CDCl$_3$, 298K): δ 0.41 (s, tBuH19, 18H), 1.05-1.30 (overlapped, H9-H13, 60H), 1.18 (s, tBuH23, 36H), 1.39 (s, tBuH27, 18H), 1.54 (br, H14A, 8H), 1.86 (br, H14B, 4H), 2.00-2.02 (overlapped, CH_3C(O), 72H), 2.29-2.34 (overlapped, H1A[a] + H1B[a], 6H), 2.52-2.57 (overlapped, H7A[a] + H7B[a], 6H), 2.61-2.64 (overlapped, H5A+H5B, 6H), 2.66-2.74 (overlapped, H7A[b] + H7B[b], 6H), 3.14-3.20 (overlapped, H1A[b] + H1B[b], 6H), 3.34 (s, H18, 4H),

3.43 (d, ArCH_2Ar, J = 14.4 Hz, 4H), 3.51 (d, ArCH_2Ar, J = 16.8 Hz, 4H), 3.89-3.99 (m, H15A, 8H), 4.10-4.17 (overlapped, H6A + H6B, 12H), 4.33 (t, H15B, J = 7.3 Hz, 4H), 4.39 (d, ArCH_2Ar, J = 16.6 Hz, 4H), 4.78 (d, ArCH_2Ar, J = 14.2 Hz, 4H), 4.92-4.97 (overlapped, H2A + H2B, 6H), 5.00-5.08 (overlapped, H3A + H3B + H4A + H4B + H17A + H17B, 24H), 5.84 (s, ArH, 4H), 6.60 (s, ArH, 4H), 6.96 (s, ArH, 4H), 7.24 (s, ArH, 4H), 7,26 (overlapped, ArH + H16A, 8H), 7.78 (s, H16B, 2H); ^{13}C NMR (150 MHz, CDCl$_3$, 298 K): δ 20.90, 20.96, 21.06, 21.08, 21.27, 22.91, 24.65, 24.92, 26.70, 26.72, 27.39, 27.51, 29.07, 29.18, 29.61, 29.67, 29.92, 30.09, 30.42, 30.61, 30.76, 31.15, 31.59, 31.86, 32.14, 33.93, 34.51, 50.31, 50.60, 51.99, 52.16, 53.16, 53.21, 59.66, 59.73, 60.61, 61.53, 61.68, 66.24, 67.14, 69.66, 69.75, 74.93, 74.99, 123.14,123.38, 124.05, 124.31, 127.34, 128.64, 129.21, 131.92, 132.80, 133.39, 134.74, 136.66, 144.19, 144.40, 145.88, 146.43, 146.51, 151.28, 152.43, 153.88, 169.96, 170.17, 170.24, 170.58, 171.10, 171.37.

General procedure for deacetylation reactions: The acetylated compound (10-15 mg) was dissolved in dry methanol (0.3-0.5 ml) and then NaOMe (0.45 eq/OAc) was added. The reaction mixture was stirred at room temperature

for 6 hours under nitrogen atmosphere. Methanol and water were added to dissolve the white precipitate formed. Dowex 50WX8-200 ion-exchange resin was added until pH=6-7 was reached. Then the solution was filtered and concentrated to give the pure compound.


32a
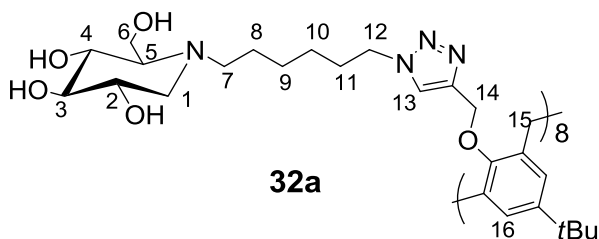
Compound 32a: 67% yield; ESI(+) MS: m/z = 3906.40; $[\alpha]_D^{33.3}$ = +13.01 (c = 0.067, MeOH); ^{1}H NMR (600 MHz, MeOD, 298 K): δ 0.96 (s, tBu, 72H), 1.26-1.29 (overlapped, H9+H10, 32H), 1.50 (br, H8, 16H), 1.73 (br, H11, 16H), 2.31 (overlapped, H5, 8H), 2.34 (overlapped, H1^a, 8H), 2.68 (m, H7^a, 8H), 2.88 (m, H7^b, 8H), 3.08 (dd, H1^b, J = 11.7 Hz, J = 5.04 Hz, 8H), 3.19 (t, H3, J = 9 Hz, 8H), 3.40 (t, H4, J = 9.2 Hz, 8H), 3.53 (m, H2, 8H), 3.87 (br, H6, 16H), 4.09 (s, H15, 16H), 4.19 (br, H12, 16H), 4.80 (br s, H14, 16H), 6.89 (s, H16, 16H), 7.96 (s, H13, 8H), 8.51 (s, OH); ^{13}C NMR (150 MHz, MeOD, 298 K): δ 25.07, 27.01, 27.48, 27.86, 28.21, 30.43, 30.55, 30.86, 31.27, 32.07, 33.16, 35.23, 36.64, 51.26,

53.86, 57.17, 58.69, 67.55, 70.16, 71.42, 80.10, 125.94, 130.98, 134.65, 145.25, 147.96, 154.07.


32b
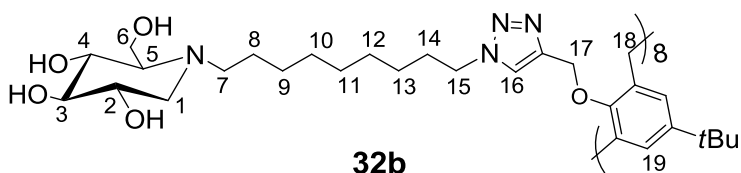
Compound 32b: 82% yield; ESI(+) MS: *m/z* = 4242.77; $[\alpha]_D^{26.9}$ = -4.15 (*c* = 0.24, MeOH); ^{1}H NMR (600 MHz, MeOD, 313 K): δ 0.95 (s, *t*Bu, 72H), 1.25 (overlapped, H9-H13, 80H), 1.57 (br, H8, 16H), 1.76 (br, H14, 16H), 2.46-2.49 (overlapped, H1^a+H5, 16H), 2.80 (m, H7^a, 8H), 3.00 (m, H7^b, 8H), 3.17 (dd, H1^b, *J* = 11.28 Hz, *J* = 4.56 Hz, 8H), 3.23 (t, H3, *J* = 9.12 Hz, 8H), 3.45 (t, H4, *J* = 9.3 Hz, 8H), 3.57 (m, H2, 8H), 3.87 (dd, H6^a, *J* = 11.88 Hz, *J* = 2.46 Hz, 8H), 3.94 (dd, H6^b, *J* = 12.06 Hz, *J* = 1.98 Hz, 8H), 4.07 (s, H18, 16H), 4.21 (br, H15, 16H), 4.81 (s, H17, 16H), 6.88 (s, H19, 16H), 7.96 (s, H16, 8H), 8.43 (br s, OH, 32H); ^{13}C NMR (600 MHz, MeOD, 313 K): δ 25.04, 27.57, 28.25, 30.04, 30.29, 30.41, 30.50, 30.56, 30.69, 30.80, 31.19, 31.30, 31.99, 33.02, 35.10, 36.53, 49.85, 51.27, 53.99, 54.74, 56.60, 58.02, 67.39, 67.50, 69.62, 70.90, 79.63, 125.78, 127.22, 134.58, 145.21, 147.82, 153.98.
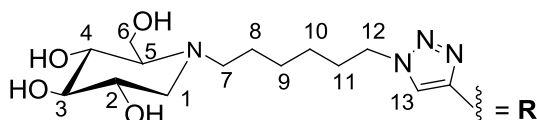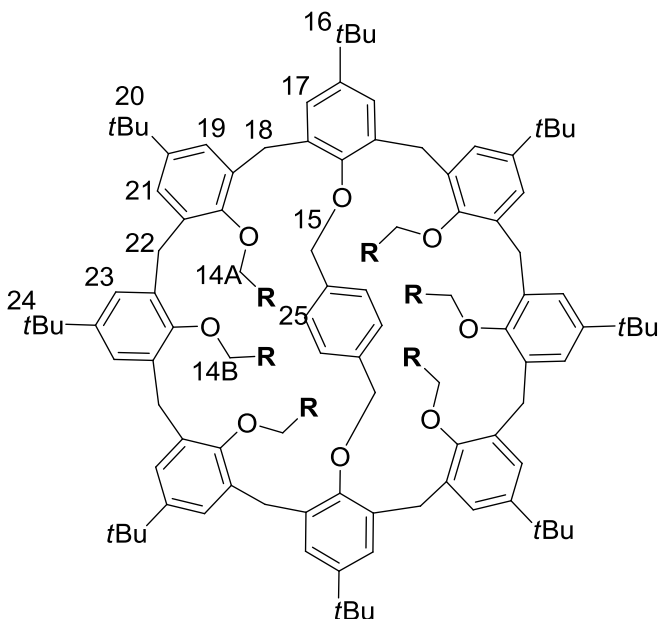
33a

Compound 33a: 67% yield; ESI(+) MS: m/z = 3356.06; $[\alpha]_D^{29}$ = -1.80 (c = 1, MeOH); ^{1}H NMR (600 MHz, MeOD, 298 K): δ 0.44 (s, tBuH16, 18H), 1.23 (s, tBuH20, 36H), 1.24-1.49 (overlapped, H8-H10 + H11A, 44H), 1.48 (s, tBuH24, 18H), 1.81 (t, H11B, J = 7.2 Hz, 4H), 2.40-2.52 (overlapped, H1A[a] + H1B[a] + H5A + H5B, 12H), 2.68-2.75 (overlapped, H7A[a] + H7B[a], 6H), 2.87-2.97 (overlapped, H7A[b] + H7B[b], 6H), 3.11-3.16 (overlapped, H1A[b] + H1B[b], 6H), 3.20-3.24 (overlapped, H3A + H3B, 6H), 3.36 (s, H15, 4H), 3.40-3.46 (overlapped, H4A + H4B, 6H), 3.52-3.58

178

(overlapped, H2A + H2B, 6H), 3.60-3.65 (overlapped, ArC*H₂*Ar, 8H), 3.82-3.94 (overlapped, H6A + H6B + H12A, 20H), 4.37-4.42 (overlapped, ArC*H₂*Ar + H12B, 8H), 4.89-4.96 (overlapped, ArC*H₂*Ar + H14B, 8H), 5.15 (br s, H14A, 8H), 5.86 (s, H17, 4H), 6.67 (s, ArH, 4H), 7.05 (d, H25, $J =$ 7.2 Hz, 4H), 7.36 (s, triazole, 4H), 7.39 (s, ArH, 4H), 7.42 (s, ArH, 4H), 8.28 (s, NH, 2H), 8.44 (br s, OH); ^{13}C NMR (150 MHz, MeOD, 298 K): δ 23.73, 24.51, 24.54, 24.75, 27.17, 27.27, 27.60, 30.31,30.46, 30.61, 30.74, 31.05, 31.13, 31.29, 31.87, 32.01, 32.22, 33.07, 34.86, 35.35, 35.36, 51.27, 51.32, 53.66, 53.72, 56.37, 56.46, 56.70, 57.54, 58.10, 66.71, 67.32, 67.37, 67.46, 69.40, 69.47, 69.72, 70.57, 70.96, 76.18, 79.48, 79.53, 79.73, 125.05, 125.29, 126.13, 128.73, 129.83, 130.30, 133.23, 133.25, 134.10, 134.87, 135.43, 137.75, 145.12, 145.14, 145.27, 147.11, 147.99, 148.10, 152.57, 153.49, 153.52, 154.82.
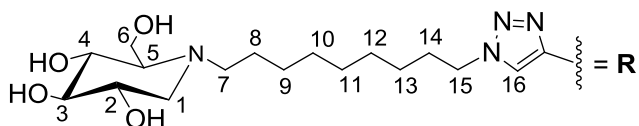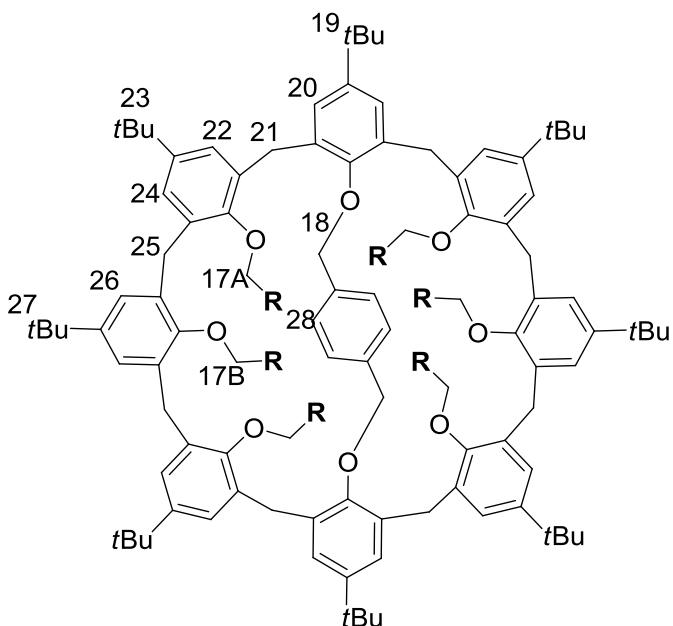
33b

Compound 33b: 80% yield; ESI(+) MS: m/z = 3608.34; $[\alpha]_D^{29.5}$ = -3.80 (c = 1, MeOH); ^{1}H NMR (600 MHz, MeOD, 298 K): δ 0.45 (s, tBuH19, 18H), 1.03-1.29 (overlapped, H9-H13, 60H), 1.22 (s, tBuH23, 36H), 1.45 (s, tBuH27, 18H), 1.48-1.56 (overlapped, H8A + H8B + H14A, 20H), 1.83 (m, H14B, 4H), 2.35-2.45 (overlapped, H1A^a + H1B^a + H5A + H5B, 12H), 2.71-2.78 (overlapped, H7A^a + H7B^a, 6H), 2.90-2.96 (overlapped, H7A^b + H7B^b, 6H), 3.09-3.14 (overlapped, H3A + H3B, 6H), 3.38 (s, H18, 4H), 3.40-3.45 (overlapped, H2A + H2B, 6H), 3.50-3.56 (overlapped, H4A + H4B +

ArCH_2Ar, 14H), 3.85-3.97 (overlapped, H6A + H6B + H15A, 20H), 4.36-4.42 (overlapped, H15B + ArCH_2Ar, 8H), 4.87-4.92 (overlapped, ArCH_2Ar + H17A[a], 8H), 5.11 (d, H17A[b], J = 12 Hz, 4H), 5.16 (s, H17B, 4H), 5.89 (s, ArH, 4H), 6.67 (s, ArH, 4H), 7.02 (s, ArH, 4H), 7.35 (s, ArH, 4H), 7.36 (s, ArH, 4H), 7.40 (s, triazole, 4H), 8.25 (s, H16B, 2H), 8.50 (br s, OH); ^{13}C NMR (150 MHz, MeOD, 298 K): δ 23.68, 25.00, 25.18, 27.43, 27.48, 28.28, 29.81, 29.97, 30.24, 30.36, 30.71, 31.13, 31.27, 31.38, 31.73, 31.86, 32.04, 32.19, 34.87, 35.26, 35.33, 51.42, 53.92, 54.76, 56.86, 57.00, 58.31, 58.57, 66.79, 67.40, 67.46, 69.88, 70.04, 71.17, 71.34, 79.85, 79.98, 125.07, 125.27, 126.02, 128.68, 129.71, 130.32, 133.30, 134.13, 134.82, 135.60, 137.92, 145.25, 147.06, 147.82, 147.89, 152.52, 153.58, 154.97.

General Procedure for the CuAAC Reaction with trivalent dendron: Alkyne, azide, CuSO$_4$·5H$_2$O (0.1 equiv. per alkyne), and sodium ascorbate (0.2 equiv. per alkyne) in DMF/H$_2$O (4:1, 2.5 to 5 mL) were successively added to a 5 mL microwave reactor vial. The resulting suspension was heated under microwave irradiation at 80 °C for 30 min, then water (10 mL) was added, and the aqueous phase was extracted with EtOAc (3x12 mL). The organic phases were combined, dried with Na$_2$SO$_4$, and concentrated in vacuo. Traces of copper salts were removed by filtration through a short pad of silica. gel eluting with CH$_3$CN/H$_2$O/NH$_4$OH (15:0.5:0.5), and the residue was then purified by flash chromatography (SiO$_2$; CH$_2$Cl$_2$/MeOH, 99:1 to 95:5) to give the desired iminosugar.

Compound 43: 66% yield; MS (ESI, deconvoluted)**:** m/z calcd for $C_{808}H_{1253}N_{120}O_{240}$ $[M + 14H]^{14+}$ 1177.7694; found 1177.7592; $[\alpha]_D^{20}$ = -3.30 (c = 1, MeOH); ^{1}H NMR (CDCl$_3$, 400 MHz): δ 7.85 (br s, 8H, H-26), 7.57 (s, 24H, H-16), 6.8 (br s, 16H, H-32), 5.10-4.99 (m, 48H, H-3 and H-4), 4.98-4.91 (m, 24H, H-2), 4.81 (br s, 5.3H, H-28), 4.51 (s, 48H, H-18), 4.41 (br s, 10H, H-25), 4.33-4.27 (t, J = 7.4 Hz, 48H, H-15), 4.14 (s, 48H, H-6), 4.03 (br s, 9.2H, H-24), 3.52-3.36 (m, 96H, H-19, H-21, H-22 and H-23), 3.21-3.15 (dd, J = 11.4, 5.0 Hz, 24H, H-1a), 2.76-2.66 (m, 24H, H-7a), 2.65-2.60 (m, 24H, H-5), 2.59-2.50 (m, 24H, H-7b), 2.35-2.28 (dd, J = 10.9, 10.5 Hz, 24H, H-1b), 2.06 (s, 72H, OAc), 2.02-1.99 (several s, 216H, OAc*3), 1.90-1.84 (m, 48H, H-14), 1.46-1.16 (m, 288H, H8 to H-13), 0.97-0.72 (m, 72H, H-35) ppm; ^{13}C-NMR (CDCl$_3$, 100 MHz): δ

171.0, 170.4, 170.1, 169.9 (C=O, acetates), 145.3 (C-17 and C-27), 122.6 (C-16 and C-26), 74.9 (C-3), 70.4-69.8 (C-21, C-22, and C-23), 69.7 (C-4), 69.6 (C-2), 69.4 (C-24), 65.2 (C-18), 61.6 (C-5), 59.7 (C-6), 53.1 (C-1), 51.9 (C-7), 50.4 (C-

183
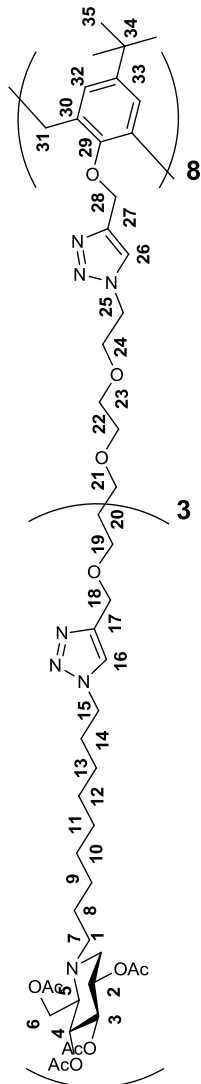
15), 50.1 (C-25), 45.5 (C-20 and C-34), 31.3 (C-35), 30.5 (C-14), 29.6, 29.2, 27.3, 26.7 (from C-9 to C-13), 24.9 (C-8), 21.0, 21.0, 20.9, 20.8 (CH$_3$-C=O, acetates).
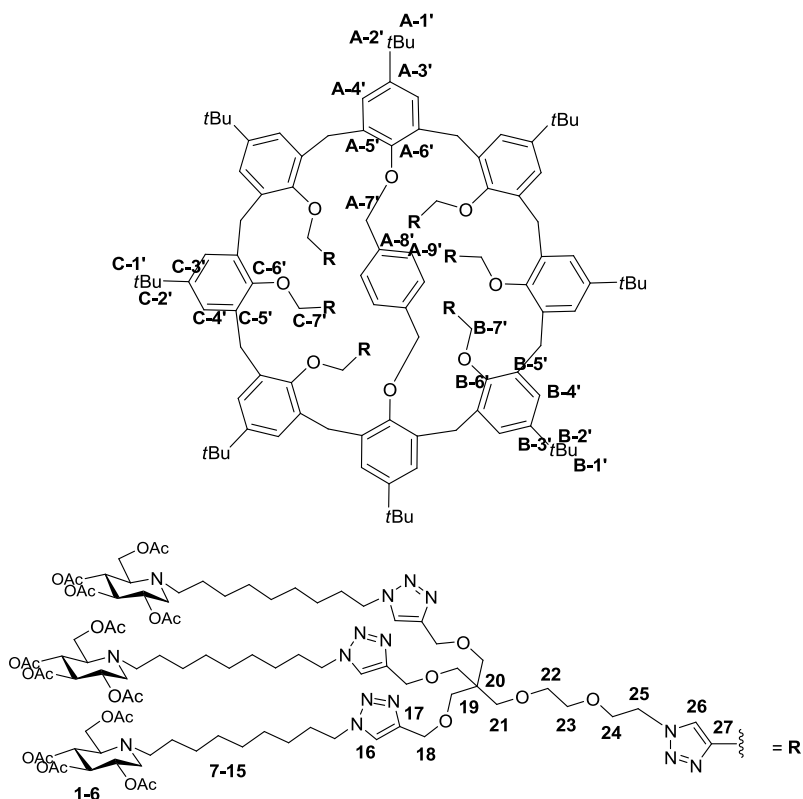

Compound 44: 48% yield; $[\alpha]_D^{20} = +4.4$ (c = 1, MeOH); MS (ESI, deconvoluted) m/z calcd for C$_{636}$H$_{978}$N$_{90}$O$_{182}$ [M + 14H]$^{14+}$ 913.9960; found 913.8864; ^{1}H NMR (CDCl$_3$, 400

MHz, 298K): δ 8.11-7.59 (m, 5.7H, H-26), 7.61-7.50 (m, 18H, H-16), 7.38-7.16 (m, 8H, ArH), 6.96-6.58 (m, 4H, ArH), 6.58 (s, 4H, ArH), 5.89-5.73 (m, 4H, A-9'), 5.16-4.99 (m, 48H, H-3, H-4, H-A,B,C-7'), 4.99-4.91 (m, 18H, H-2), 4.89-4.63 (m, 9H, H-A8, H-B8 and H-C8), 4.61-4.44 (m, 42H, H-18 and H-25a), 4.36-4.22 (m, 42H, H-15 and H-25b), 4.14 (s, 36H, H-6), 3.91-3.80 (m, 4H, H-24a), 3.78-3.63 (m, 8H, H-24b), 3.54-3.31 (m, 72H, H-19, H-21, H-22 and H-23), 3.21-3.15 (dd, J = 11.5 and 4.9 Hz, 18H, H-1a), 2.76-2.66 (m, 18H, H-7a), 265-2.60 (m, 18H, H-5), 2.59-2.49 (m, 18H, H-7b), 2.35-2.28 (t, J = 10Hz, 18H, H-1b), 2.09-2.04 (s, 54H, CH_3-C=O), 2.03-2.00 (s, 108H, CH_3-C=O), 2.01-1.98 (s, 54H, CH_3-C=O), 1.93-1.79 (m, 36H, H-14), 1.49-1.10 (m, 288H, from H-8 to H-13, A-1', B-1' and C-1') ppm; ^{13}C NMR (CDCl$_3$, 75 MHz, 298 K): δ 170.9, 170.4, 170.1, 169.8 (C=O, acetates), 162.6 (C-A3, C-B3, C-C3, C-A6, C-B7 and C-C7), 145.42, 145.37 (C-15 and C-25), 144.2 (C-A4, C-B4 and C-C4), 122.62, 122.53 (C-16 and C-26), 74.9 (C-3), 69.8 (C-4), 69.6 (C-2), 69.5 (C-19, C-21, C-22, C-23 and C-24), 68.1, 65.2 (C-18), 61.7 (C-5), 59.8 (C-6), 53.1 (C-1), 51.99, 51.95 (C-7), 50.41, 50.38 (C-15 and C-25), 45.58, 45.55 (C-20), 36.6, 34.44, 34.42 (C-A2, C-B2 and C-C2), 31.8, 31.6, 31.5, 31.1 (C-A', C-B1 and C-C1), 30.5 (C-14), 29.6, 29.2, 27.4, 26.7, 25.8 (from C-9 to C-13), 25.10, 25.05 (C-8), 20.97, 20.94, 20.85, 20.80 (CH_3-C=O, acetates).

**General procedure for the deacetylation reaction:**
Amberlite resin IRA 400 ($6n$ g/mmol of substrate; n = number of acetate groups) was added to a solution of acetylated iminosugar in a mixture of MeOH/H_2O (1:1), and the resulting solution was stirred for 4 h by using a rotary evaporator at atmospheric pressure. The resin was then removed by filtration and washed with methanol and water. The solvent was then removed from the filtrate under reduced pressure to give the desired deprotected iminosugar.

Compound 45: 89% yield; $[\alpha]_D^{20} = -2.6$(c = 1, MeOH); MS (ESI, deconvoluted) m/z calcd for $C_{616}H_{1056}N_{120}O_{144}$ $[M + 8H]^{8+}$ 1554.9796; found 1555.8798; ^1H NMR (CDCl$_3$, 400 MHz, 298K): δ 8.22-7.99 (br s, 8H, H-26), 7.97-7.82 (s, 24H, H-16), 7.19-6.59 (br s, 16H, H-32), 4.57-4.42 (m, 64H, H-18 + H-28, 48H+16H), 4.41-4.28 (m, 48H, H-15), 3.84 (s, 48H, H-6), 3.54-3.32 (m, H-2, H-4, and H-31, 48H + 16H), 3.20-3.07 (m, 24H, H-3), 3.01-2.94 (dd, J = 11.9, 5.5 Hz, 24H, H-1a), 2.83-2.71 (m, 24H, H-7a), 2.62-2.50 (m, 24H, H-7b), 2.20-2.12 (dd, J = 11.9, 11.5 Hz, 24H, H-1b), 2.12-2.07 (m, 24H, H-5), 1.94-1.79 (m, 48H, H-14), 1.55-1.38 (m, 48H, H-8), 1.39-1.17 (m, 240H, from H-9 to H-13), 0.99-0.79 (m, 72H, H-35) ppm; ^{13}C-NMR (CDCl$_3$, 100 MHz, 298K) δ 146.2 (C-17, C-27), 124.9 (C-16, C-26), 80.6 (C-3), 72.1 (C-4), 70.8 (C-2), 67.4 (C-5), 65.5 (C-18), 59.6 (C-6), 57.8 (C-1), 53.8 (C-7), 51.4 (C-15), 32.1 (C-14), 31.4, 30.6, 30.1, 28.6, 27.6 (from C-9 to C-13), 25.3 (C-8).
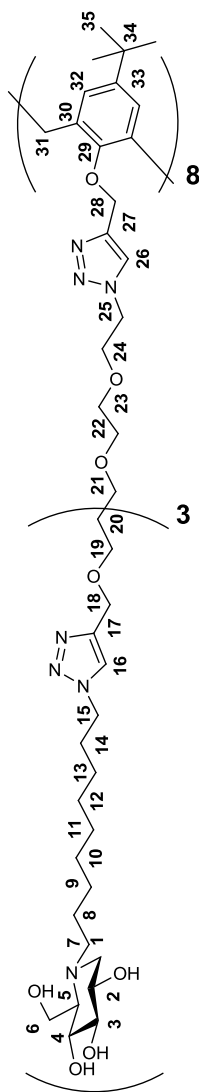
5.4 A new ligation strategy for the synthesis of glycoconjugates

The galactosyl thioacetate **53** was synthesized according to the procedure reported in literature.[105]

54
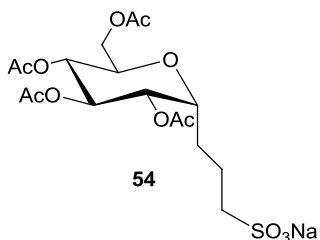
Synthesis of compound 54: Galactosyl thioacetate **53** (92 mg, 0.20 mmol) was dissolved in acetic acid (2.3 ml). Sodium acetate (272 mg, 2.0 mmol) and OXONE® (307 mg, 0.50 mmol) were added and the reaction mixture was stirred at room temperature for 6 h. The product was filtrated, washed with AcOEt and purified by flash column chromatography (CH$_2$Cl$_2$:MeOH, 4:1). 94% yield; $[\alpha]_D$ = +36.5 (c 1.0, MeOH). ^{1}H NMR (400 MHz, MeOD, 298 K): δ 5.37 (t, 1H, $J3,4$ = 9.2 Hz, H-3), 5.03 (dd, 1H, $J1,2$ = 5.8 Hz, $J_{2,3}$ = 9.5 Hz, H-2), 4.96 (t, 1H, H-4), 4.26 (dd, 1H, $J6a,6b$ = 12.2 Hz, $J6a,5$ = 5.4 Hz, H-6a), 4.20-4.15 (m, 1H, H-1), 4.11 (dd, 1H,

$J6b,5 = 2.4$ Hz, H-6b), 3.99 (ddd, 1H, $J_{4,5} = 8.0$ Hz, H-5), 2.90 (t, 1H, $J = 8.2$ Hz, -CH$_2$SO$_2$-), 2.09, 2.06, 2.04 and 2.02 (4 s, 12 H, 4 Ac), 1.82-1.68 (m, 2H, -CH$_2$-). ^{13}C NMR (75 MHz, MeOD, 298 K): δ 172.6, 171.7, 171.5, 171.4, 73.9, 72.0, 71.9, 70.4, 70.0, 63.6, 51.9, 25.2, 22.0, 20.7, 20.6; HRMS (ESI/Q-TOF) m/z for C$_{17}$H$_{25}$O$_{12}$S (M$^-$) 453.1067, found 453.1067.


55
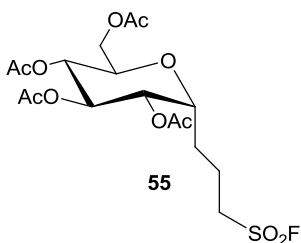
Synthesis of compound 55: Compound **54** (23.4 mg, 0.049 mmol) was dissolved in dry DMF. SOCl$_2$ (18 μl, 0.245 mmol) was added and the reaction mixture was stirred overnight under argon atmosphere. The product was concentrated and then dissolved in CH$_3$CN (0.5 ml). Potassium fluoride (6 mg, 0.10 mmol) and a catalytic amount of 18-crown-6 were added and the reaction mixture was stirred at room temperature overnight. CH$_2$Cl$_2$ was added and the mixture was filtrated. The filtrate was concentrated and the product was purified by flash column chromatography (AcOEt:Cyclohexane, 1:1).

189

52% yield; $[\alpha]_D = +42.9$ (c 1.0, CHCl$_3$). ^{1}H NMR (400 MHz, CDCl$_3$, 298 K): δ 5.26 (t, 1H, $J3,4 = 8.7$ Hz, H-3), 5.06 (dd, 1H, $J2,3 = 9.0$ Hz, $J1,2 = 5.5$ Hz, H-2), 4.92 (t, 1H, H-4), 4.24 (dd, 1H, $J6a,6b = 12.2$ Hz, $J6a,5 = 6.6$ Hz, H-6a), 4.21-4.17 (m, 1H, H-1), 4.09 (dd, 1H, $J6b,5 = 2.5$ Hz, H-6b), 3.86 (ddd, 1H, $J = 8.9$ Hz, H-5), 3.47 (m, 2H, -CH$_2$SO$_2$-), 2.09, 2.06, 2.05 and 2.04 (4 s, 12H, 4 Ac), 1.75-1.67 (m, 2H, -CH$_2$-). ^{13}C NMR (75 MHz, CDCl$_3$, 298 K): δ 170.6, 169.9, 169.5, 169.5, 71.5, 69.9, 69.8, 69.5, 68.5, 62.2, 50.1 ($J_{C-F} = 67.2$ Hz), 23.8, 20.6, 20.6, 20.6, 19.7; HRMS (ESI/Q-TOF) m/z calcd for C$_{17}$H$_{26}$FO$_{11}$S (M+H)$^+$ 457.1180, found 457.1180.

General procedure for the synthesis of sulfonamides: The reactions were performed in a sealed glass tube. Sulfonyl fluoride **55** (20 mg, 0.044 mmol) was dissolved in DMF. Then the desired amine (0.44 mmol) was added and the reaction mixture was stirred at 80 °C until full conversion of the sulfonyl fluoride (3-6 h). The solvent was removed under reduced pressure and the product was purified by flash column chromatography (AcOEt:Cyclohexane, 1:1).

56
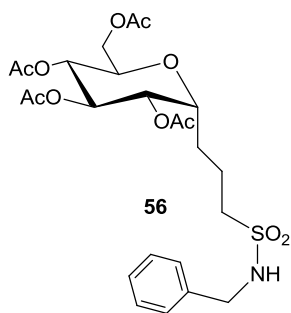
Compound 56: (90% yield); $[\alpha]_D = +33.1$ (*c* 1.0, CHCl$_3$). ^{1}H NMR (400 MHz, CDCl$_3$, 298 K): δ 7.39-7.31 (overlapped, 5H, ArH), 5.26 (t, 1H, *J*3,4 = 9.1 Hz, H-3), 5.03 (dd, 1H, *J*2,3 = 9.4 Hz, *J*1,2 = 5.7 Hz, H-2), 4.94 (t, 1H, H-4), 4.78 (t, 1H, *J* = 6.0 Hz, -NH), 4.30 (d, 2H, *J* = 6.0 Hz, -CH$_2$N), 4.22 (dd, 1H, *J*6a,6b = 12.1 Hz, *J*6a,5 = 5.7 Hz, H-6a), 4.13-4.09 (m, 1H, H-1), 4.06 (dd, 1H, *J*6b,5 = 2.9 Hz, H-6b), 3.80 (ddd, 1H, *J* = 8.8 Hz, H-5), 3.00-2.88 (m, 2H, -CH$_2$SO$_2$-), 2.08, 2.04, 2.03 and 2.02 (4 s, 12H, 4 Ac), 1.91-1.85 (m, 2H, -CH$_2$-), 1.77-1.70 (m, 1H, -CH$_2$-), 1.55-1.52 (m, 1H, -CH$_2$-). 13C NMR (75 MHz, CDCl$_3$, 298 K): δ 170.8,170.0, 169.6, 169.5, 136.9, 128.9, 128.1, 127.9, 72.0, 70.2, 70.1, 68.9, 68.8, 62.4, 52.4, 47.2, 23.8, 20.7, 20.6, 20.6, 19.69; HRMS (ESI/Q-TOF) *m/z* calcd for C$_{24}$H$_{34}$NO$_{11}$S (M+H)$^+$ 544.1853, found 544.1855.
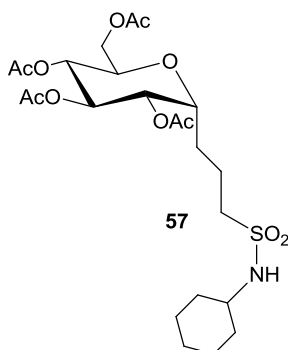
Compound 57: (97% yield); $[\alpha]_D$ = +37.2 (*c* = 0.9, CHCl$_3$). ^{1}H NMR (400 MHz, CDCl$_3$, 298 K): δ 5.27 (t, 1H, *J*3,4 = 9.0 Hz, H-3), 5.05 (dd, 1H, *J*2,3 = 9.4 Hz, *J*1,2 = 5.7 Hz, H-2), 4.94 (t, 1H, H-4), 4.23 (dd, 1H, *J*6a,6b = 12.2 Hz, *J*6a,5 = 5.7 Hz, H-6a), 4.19-4.13 (m, 1H, H-1), 4.07 (dd, 1H, *J*6b,5 = 3.0 Hz, H-6b), 3.84 (ddd, 1H, *J*6b,5 = 2.7 Hz, *J* = 5.6 Hz, *J* = 8.8 Hz, H-5), 3.30-3.21 (m, 1H, -NCH-), 3.11-2.98 (m, 2H, -CH$_2$SO$_2$-), 2.09, 2.04, 2.02 and 2.01 (4 s, 12H, 4 Ac), 1.98-1.94 (overlapped, 4H, -CH$_2$-), 1.87-1.79 (m, 1H, -CH$_2$-), 1.75-1.55 (overlapped, 5H -CH$_2$-), 1.35-1.15 (overlapped, 4H -CH$_2$-). ^{13}C NMR (75 MHz, CDCl$_3$, 298 K): δ 170.8, 170.0, 169.6, 169.5, 72.0, 70.2, 70.1, 68.9, 68.8, 62.3, 53.2, 52.8, 34.6, 25.1, 24.8, 23.9, 20.7, 20.7, 20.7, 20.6, 19.8; HRMS (ESI/Q-TOF) *m/z* calcd for C$_{23}$H$_{38}$NO$_{11}$S (M+H)$^+$ 536.2166, found 536.2170.
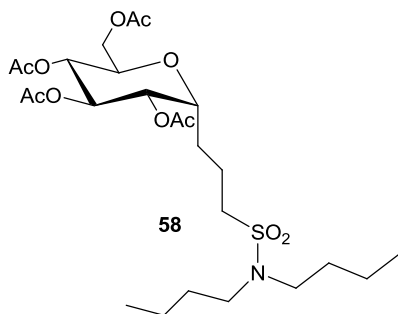
Compound 58: (45% yield); $[\alpha]_D$ = +22.3 (c = 0.9, CHCl$_3$).
^{1}H NMR (400 MHz, CDCl$_3$, 298 K): δ 5.29 (t, 1H, J3,4 = 9.1
Hz, H-3), 5.07 (dd, 1H, J2,3 = 9.5 Hz, J1,2 = 5.8 Hz, H-2),
4.97 (t, 1H, H-4), 4.24 (dd, 1H, J6a,6b = 12.2 Hz, J6a,5 = 5.6
Hz, H-6a), 4.20-4.15 (m, 1H, H-1), 4.08 (dd, 1H, J6b,5 = 2.0
Hz, H-6b), 3.84 (ddd, 1H, J = 9.0 Hz, H-5), 3.17 (t, 4H, J =
7.8 Hz, -NCH$_2$butyl-), 3.00-2.88 (m, 2H, -CH$_2$SO$_2$-), 2.11,
2.06, 2.03 and 2.02 (4 s, 12H, 4 Ac), 2.03-2.92 (overlapped,
2H, -CH$_2$-), 1.87-1.78 (m, 1H, -CH$_2$-), 1.71-1.62 (m, 1H, -
CH$_2$-), 1.60-1.52 (m, 4H, -CH$_2$butyl-), 1.28-1.20 (m, 4H, -
CH$_2$butyl-), 0.94 (t, 6H, J = 7.3 Hz, -CH$_3$butyl). ^{13}C NMR (75
MHz, CDCl$_3$, 298 K): δ 170.7, 170.0, 169.6, 169.5, 72.0,
70.2, 68.9, 69.7, 62.2, 50.9, 47.3, 31.0, 24.1, 20.7, 20.7, 20.6,
19.9, 19.5; HRMS (ESI/Q-TOF): m/z calcd for C$_{25}$H$_{44}$NO$_{11}$S
(M+H)$^+$ 566.2635, found 566.2634.